UNIVERSITÀ DEGLI STUDI DI UDINE
hic sunt futura

www.uniud.it

Corso di dottorato di ricerca in:

"Scienze Biomediche e Biotecnologiche"

in convenzione con Centro di Riferimento Oncologico di Aviano, IRCCS

Ciclo 32°

"miRNA:mRNA interplay in the malignant evolution of miniGIST to overt GIST"

Dottorando

Mondello Alessia

Supervisore

Dr.ssa Maestro Roberta

Anno 2020

Abstract

Gastrointestinal Stromal Tumor (GIST) is the most common mesenchymal tumor that occurs throughout the digestive tract and is thought to arise from the gastrointestinal (GI) pacemakers, the Interstitial Cells of Cajal (ICC).

Different from most sarcomas for which premalignant lesions are not known, premalignant GIST counterparts have been identified. These entities, named miniGIST, share with overt GIST histological and molecular features, namely the presence of oncogenic mutations affecting the tyrosine kinases KIT or PDGFRA. MiniGISTs are remarkably common (about 1/3 of unselected elderly subjects carry miniGIST in their GI tract) whilst GIST are quite rare, indicating that a very minute fraction of miniGIST actually progress to clinically relevant tumors. This indicates that KIT/PDGFRA oncogenic mutations are insufficient to convey malignancy.

The aim of this work was to address the molecular mechanisms that sustain miniGIST to overt GIST malignant evolution, focusing in particular on the role of miRNAs. By performing combined miRNA and mRNA NGS profiling on a large set of miniGISTs and overt GISTs, we identified a set of miRNAs potentially involved in the transcriptional perturbation during GIST progression. We made a step ahead by *in vitro* validating the role of hsa-miR-485-5p loss in determining the BIRC5 gene upregulation in overt GIST.

Overall, our work laid down the bases for the elucidation of the role of miRNA:mRNA interaction in the malignant evolution of GIST.

Index

1. Introduction

1.1. Soft tissue tumors: overview and molecular pathogenesis

Sarcomas are rare neoplasms of mesenchymal nature with an estimated incidence of about 60/million and representing about 1% of all malignant tumors. They are more common in children than adults and may affect bone (BS) or soft tissues (STS) at various anatomical sites (head and neck, extremities, mediastinum, abdominal cavity, retroperitoneum and pelvic cavity) (Fletcher et al., 2013).

Sarcomas are aggressive tumors, with an overall 5-year survival rate of less than 65%. The term sarcoma actually identifies a quite heterogeneous group of tumors (Fig. 1.1) (Taylor et al., 2011) including over 60 different histotypes, as defined by the World of Health Organization (WHO) (Fletcher et al., 2013).

The complexity of sarcomas makes their diagnosis challenging, and besides parameters such as morphology and immunoprofile, molecular and genetics investigations are often required. Conventionally, sarcomas are divided into two major genetic subgroups: complex karyotype and simple karyotype tumors.

Complex karyotype sarcomas, which include for instance osteosarcomas, leiomyosarcomas, myxofibrosarcoma, and undifferentiated pleomorfic sarcomas, feature heavily unbalanced genotypes, with numerous non-recurrent alterations, including complex rearrangements and copy number changes (Mariño-Enríquez and Bovée, 2016). This group of tumors has a higher frequency of gene mutations compared to simple karyotype sarcomas and this relatively high mutation load makes them potentially eligible for immunotherapies targeting neoantigens.

Simple karyotype sarcomas account for about 1/3 of all sarcomas (Mitelman et al., 2007). These tumors commonly feature recurrent and pathognomonic genetic defects in the context of a near-diploid karyotype. Since these genetic alterations are often histotype-specific, their detection may be of help in the diagnosis and in particular in the differential diagnosis of highly similar pathological entities. As such, they are defined pathognomonic alterations. Pathognomonic molecular aberrations affecting simple karyotype sarcomas include chromosomal rearrangements, as in the case of Ewing's sarcomas, myxoid liposarcomas, synovial sarcomas and alveolar rhabdomyosarcomas, all featuring chromosome translocations that give rise to the generation of fusion genes. In other cases, the pathognomonic molecular alteration is represented by a selective chromosome amplification, as in the case of dedifferentiated liposarcomas that are characterized by a 12q13-15 amplification involving HMGA2, MDM2, and CDK4 genes. Specific gene mutations may also be a genetic hallmark for certain subtypes of simple karyotype sarcomas. Gastrointestinal stromal tumors, with their KIT or PDGFRA oncogenic mutations, or epithelioid sarcomas, typified by inactivating SMARCB1 mutations, typically fall into this category of sarcomas.

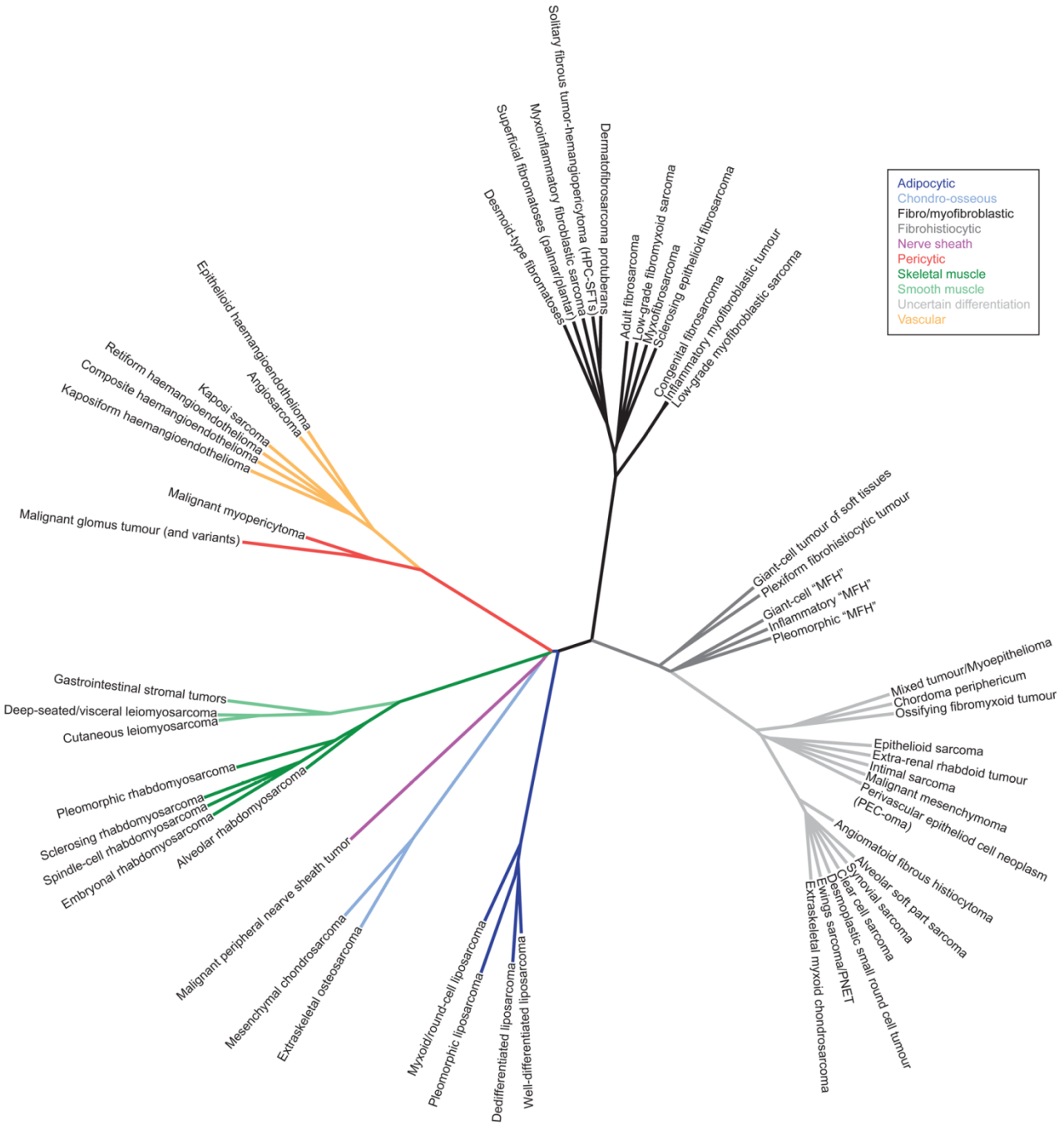

Figure 1.1 Unrooted phylogeny of Soft Tissue Sarcoma (STS). This taxonomy tree shows the ~60 sarcoma subtypes defined by the WHO 2013. The classification is based on lineage of differentiation, prognosis and gene driver alteration represented as primary, secondary and tertiary branches, respectively. From Taylor *et al.,* 2011**.**

1.2. Gastrointestinal Stromal Tumors

Gastrointestinal Stromal Tumors (GISTs) are simple karyotype sarcomas. They account for approximately 20% of the soft tissue tumors, with an annual incidence of about 10 per million population (Von Mehren and Joensuu, 2018).

GISTs, which are the most common mesenchymal tumor of the digestive tract, occur throughout the GI region, mainly in the stomach, followed by small bowel, rectum, esophagus and other sites (omentum, mesentery, and retroperitoneum) (Casella et al., 2012; Miettinen et al., 2002).

GISTs were identified as tumor entities only in 1995 by Miettinen and coworkers who described these tumors as separate from mimics such as typical leiomyomas, leiomyosarcomas or schwannomas (Miettinen et al., 1995). In their study, Miettinen and colleagues demonstrated that these atypical tumors were almost immunonegative for conventional muscle cell markers (desmin, alpha-smooth muscle actin), s-100 protein and epithelial marker (CD31) but were positive for CD34, the myeloid progenitor cell antigen. Some years later, Kindblom and coworkers reported that the so-called GISTs expressed the c-KIT tyrosine kinase (CD117) (Kindblom et al., 1998).

Since then, GISTs are overall defined as KIT-expressing mesenchymal tumors and the immunohistochemistry evaluation of c-KIT (CD117) has become a gold standard for GIST diagnosis, although a small percentage of GIST (about 5%) is c-KIT negative (Tzen, 2005).

The current immunohistochemical panel for GIST diagnosis includes CD117 (c-KIT), CD34 (myeloid progenitor cell antigen), DOG1 (anoctamin-1), VIM (vimentin), SMA (smooth muscle actin) and desmin, which are typical muscle cell markers, and S-100 (neural marker). Staining for PDGFRA (platelet-derived growth factor receptor A) and PKCΘ (protein kinase C theta) may be of some utility, especially in the CD117-negative fraction of GIST (González-Cámpora et al., 2011).

1.2.1. Clinical and pathological features

Gastrointestinal stromal tumors can occur throughout the digestive tract. Most often, they arise in the stomach (60%), followed by small intestine (30-35%), rectum (4%), colon and appendix (1-2%), esophagus (<1%) and more rarely in extra GI sites (Miettinen and Lasota, 2006). The vast majority of intestinal GISTs arise in the jejunum and in the ileum (30%), whereas a smaller fraction emerges in the duodenum and in the colon (4-5%). Rectal GISTs are infrequent, accounting for less than 5% of all GISTs (Fletcher et al., 2013; Miettinen and Lasota, 2006).

Gastric GISTs tend to arise earlier respect to intestinal GISTs, which have a peak at seventies. There is no sex predominance for adult tumors. A minute fraction of GISTs occurs in childhood, with a slight prevalence in females, and often in the context of syndromic conditions (Fletcher et al., 2013).

The symptoms of GISTs vary from vague abdominal pain, bleeding, hemorrhage, anemia, or bowel obstruction. Tumor rupture may also occur causing tumor spreading in the abdominal cavity and neighbor organs (Fletcher et al., 2013).

GISTs are heterogeneous in size, from tiny intramural lesions to bulky mass, and may be found as single or multiple lesions. In the stomach they are usually nodular, well-confined, sometimes bosselated, but not truly encapsulated. Larger tumors become necrotic, hemorrhagic, or cystic-degenerated. In the intestine, they may cause adhesion between bowel loops (Fletcher et al., 2013).

Microscopically, GISTs appear typically as spindle-cell tumors. Cells look elongated, with ovoid nuclei and fibrillary eosinophilic cytoplasm sometimes vacuolated. If GISTs are predominantly

spindle-shaped, GISTs with epithelioid features may also be detected especially in the stomach (Fletcher et al., 2013; Miettinen and Lasota, 2006).

The stroma may be sclerosed, hyalinized, or even calcified, sometimes with rich-hyaluronic acid or myxoid connective tissue components. The degree of cellularity changes greatly within and between tumors (Cooper et al., 1992; Fletcher et al., 2013).

Noteworthy, correlations between morphological and molecular features have been identified and the morphological pattern could be predictive of GIST genetics (Fig. 1.2) (Chetty and Serra, 2016). More in detail, the majority of GISTs with spindle-cell morphology are KIT-mutant or harbor alterations in RAS pathway genes. Conversely, the majority of GISTs with epithelioid morphology carry mutations in PDGFRA or are defective for the mitochondrial succinate dehydrogenase complex (SDH). Mutations affecting any components of the SDH complex (SDH-A, -B, -C or -D genes) result in complex destabilization and degradation. Thus, a negative immunohistochemical staining for any SDH protein (most commonly SDHB) is used as a readout for SDH complex deficiency (Casali et al., 2018).

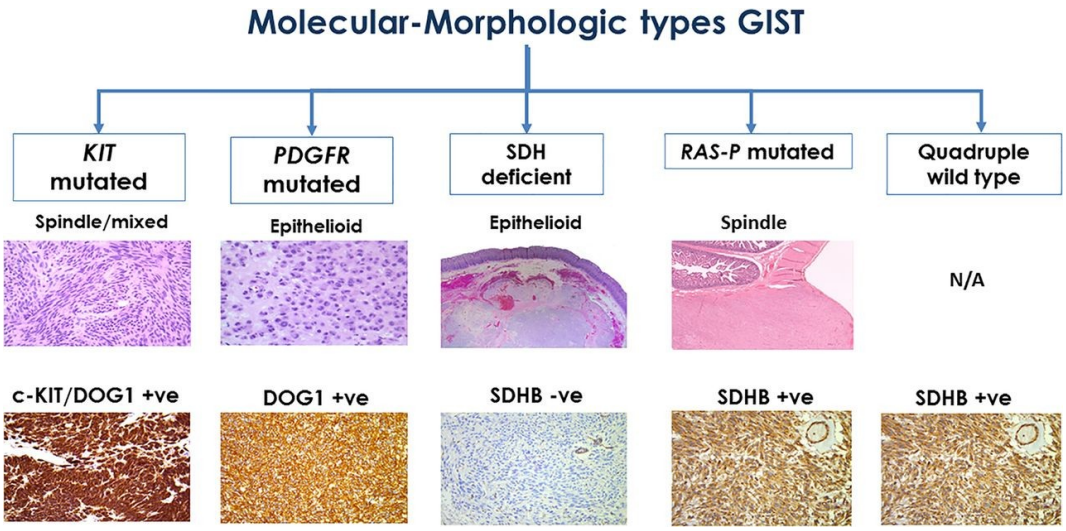

Figure 1.2 Correlations between molecular and morphological features in GIST. From Chetty and Serra, 2016

GISTs enter into differential diagnosis with diverse malignancies with myogenic and neuronal features: true smooth muscle and nerve sheath tumors predominantly, but also inflammatory fibroid polyps and spindle cells proliferation, such as inflammatory myofibroblastic tumors, solitary fibrous tumors and desmoids fibromatosis (Fletcher et al., 2013; Hirota, 2018). Moreover, epithelial GISTs should be distinguished from other epithelioid cell tumors such as perivascular epithelioid cell tumors (PEComas) and neuroendocrine tumors (NETs) (Fig. 1.3) (Hirota, 2018).

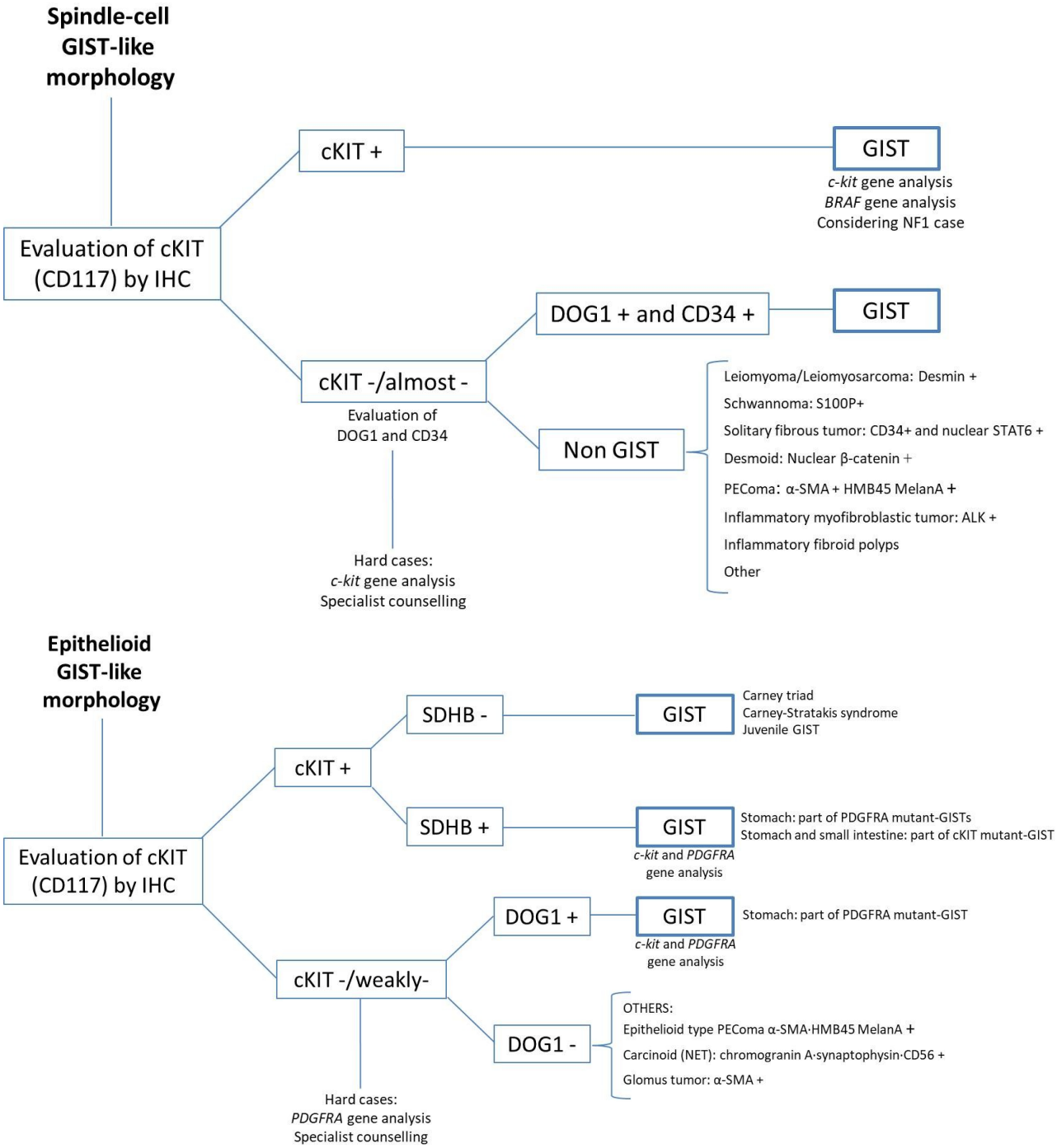

Figure 1.3 Workflow of differential diagnosis of GIST. ALK: anaplastic lymphoma kinase; STAT: signal transducer and activator of transcription; α-SMA: α-smooth muscle actin; SDHB: succinate dehydrogenase complex iron sulfur subunit B. Adapted from Hirota, 2018.

Immunohistochemistry and morphology are the most helpful instrument for a correct diagnosis: even if other tumors in the digestive tract could be positive for c-KIT, the concomitant expression of CD34 and DOG1 reveal the true nature of the lesion (Fig. 1.3) (Fletcher et al., 2013). Additional molecular analysis supports clinicians in treatment management and may contribute to risk stratification (Rossi et al., 2015).

The vast majority of GIST is sporadic. However, syndromic conditions may include GIST as manifestation. First of all, rare familial GIST due to hereditary KIT or PDGFRA mutations have been reported (Postow and Robson, 2012). About 30 cases of familial GIST have been reported so far.

Familial GISTs tend to be smaller in size and multiple in number. Moreover, familial GIST patients tend to develop cutaneous hyperpigmentation and abnormalities in the mast cells (also KIT positive cells), such as urticaria pigmentosa or systemic disease (Antonescu, 2006). Other GIST predisposing conditions include Carney's triad (GISTs, extra-adrenal paragangliomas, pulmonary chondroma), and Carney-Stratakis dyad (GISTs, paragangliomas), both associated to defect in the SDH complex genes (Corless et al., 2011). Neurofibromatosis type 1, due to NF1 mutations, is also a GIST predisposing condition (Miettinen et al., 2005).

1.2.2. Molecular oncology

Gastrointestinal stromal tumors are simple karyotype sarcoma, best characterized as receptor tyrosine kinase-driven tumors. Activating mutations in c-KIT oncogene were first reported in 1998 by Hirota and colleagues, sanctioning the beginning of the "molecular era" of GIST (Hirota, 1998). Some years later, Heinrich and coworker identified activating PDGFRA (platelet-derived growth factor receptor alpha) mutations in GIST landscape (Heinrich et al., 2003a).

KIT and PDGFRA belong to the type III of the receptor tyrosine kinase (RTK) family, which also includes platelet-derived growth factor receptor beta (PDGFRB), colony-stimulating factor 1 receptor (CSF1R) and FMS-like tyrosine kinase 3 (FLT3). Given the close similarity between KIT and PDGFRA, the downstream signaling pathways are *bona fide* shared by the two RTK. Indeed, KIT and PDGFRA mutations, which account for about 80-85% of all mutations in GISTs, are essentially mutually exclusive in these tumors (Heinrich et al., 2003a; Schaefer et al., 2017). While KIT mutations are detected both in the gastric and in the intestinal lesions, PDGFRA mutations are essentially confined to the gastric site (Lasota et al., 2008).

Physiologically, upon the binding to the natural ligand (SCF, stem cell factor), c-KIT homodimerizes, undergoes phosphorylation and hence triggers the activation of the downstream signaling (Corless et al., 2011). Oncogenic mutations in the RTKs result in the constitutive activation of the kinase.

The most common KIT mutations (Fig. 1.4) detected in GIST involve the juxtamembrane domain (encoded by exon 11) and cause the disruption of the auto-inhibition of the kinase, leading to its activation in the absence of the ligand (Li K. et al., 2017). KIT exon 11 mutations occur in approximately 70% of cases. They can be point mutations, in-frame deletions or insertions. Deletions involving codons 557 and/or 558 are reported to convey worse prognosis than the KIT exon 11 point mutations, as patients have a higher rate of recurrence (Corless et al., 2011; Lasota et al., 1999).

Mutations in the extracellular domain encoded by exon 9 in KIT are also common (about 10%) and favor receptor dimerization (Bannon et al., 2017; Corless et al., 2011). The major type of change in KIT exon 9 is the duplication of amino acids 502 and 503. Mutations in exon 9 are predominantly reported in intestinal GISTs, whereas only a small fraction of gastric tumors is KIT exon 9 mutant (Corless et al., 2011).

Other primary alterations occurring in the KIT gene involve exon 13, 17 and extremely rarely exon 8 (Li K. et al., 2017). Exon 13 encodes for the ATP-binding pocket. The K642E substitution is the principal alteration found in this genomic region. Exon 17 encodes the kinase activation loop and point mutations in codons 820, 822, 823 are the most commonly reported ones. Alterations in exon 13 are most frequently found in gastric GISTs with spindle-cell morphology, but occasionally also in epithelioid or mixed-shaped tumors, whereas mutations affecting exon 17 are reported mainly in the small bowel GISTs that have spindle-cell histology. Exon 8 encodes part of the extracellular domain and mutations at this site are quite rare and detected so far in the small bowel or in extragastrointestinal GISTs that frequently metastasize (Ito et al., 2014; Lasota et al., 2008).

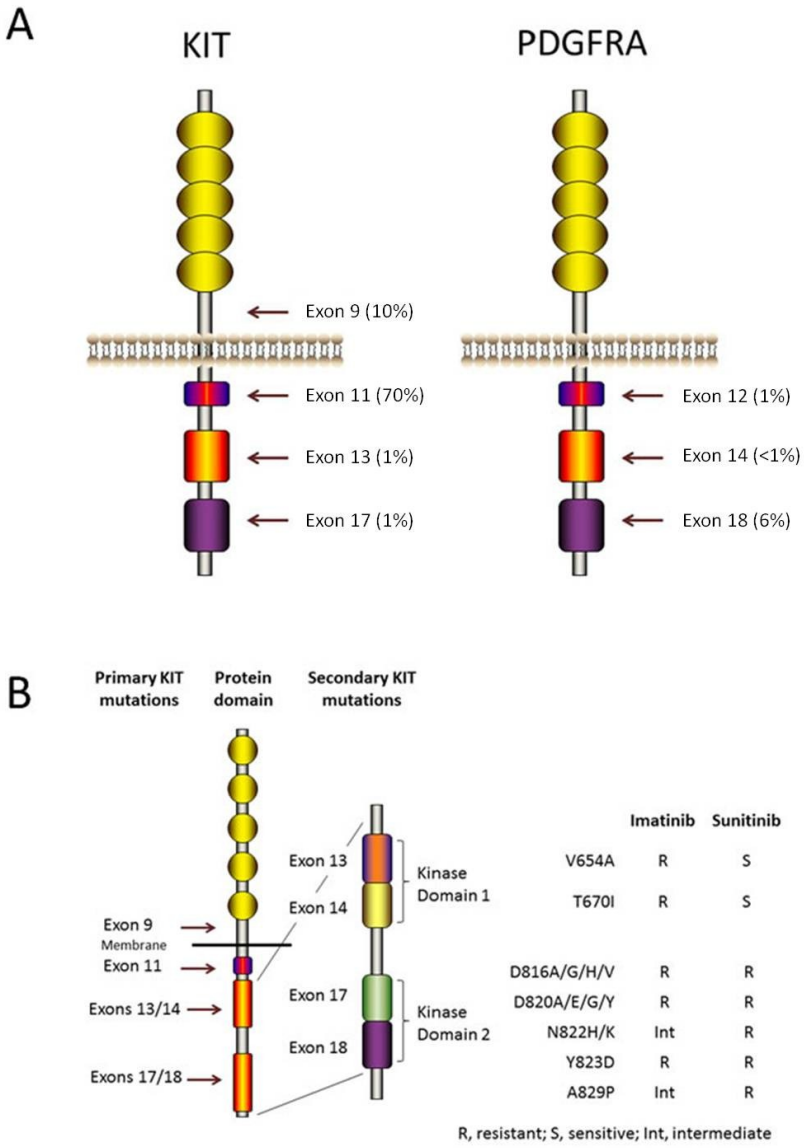

Figure 1.4 KIT and PDGFRA tyrosine kinase receptors share topology and type of mutations. A) Mutations in KIT and PDGFRA are essentially mutually exclusive in GIST and affect the juxtamembrane domain (KIT exon 11; PDGFRA exon 12), the ATP-binding domain (KIT exon 13; PDGFRA exon 14) and the activation loop (KIT exon 17; PDGFRA exon 18). **B)** Primary and secondary KIT mutations and their sensitivity to the RTK inhibitors Imatinib and Sunitinib. Adapted from Li *et al.*, 2017a.

PDGFRA alterations, typically detected in gastric GIST (Lasota et al., 2008), account for about 8% of all GIST mutations. They commonly involve exon 18, encoding for the activation loop. The D842V point mutation accounts for the vast majority of alterations in exon 18 (Lasota et al., 2008). Other mutations involve exon 12 (encoding the juxtamembrane domain), and exon 14 (encoding the ATP-binding domain) (Bannon et al., 2017).

About 15% of GISTs are devoid of canonical KIT or PDGFRA mutations and are therefore considered RTK wild type tumors. They are essentially indistinguishable from KIT- or PDGFRA-mutant GISTs, displaying the same morphology and immunohistochemical profile. In particular, about 5% of RTK wild type GIST harbors mutations in BRAF, HRAS/NRAS (Rossi et al., 2015; Schaefer et al., 2017) or in the SDH complex genes. The V600E BRAF mutation, common in papillary thyroid carcinoma and melanoma, is the only BRAF alteration detected in GIST (Agaimy et al., 2009).

Defects in the Succinate Dehydrogenase (SDH) genes complex are also reported in GISTs and are associated with syndromic conditions (Carney's triad and Carney-Stratakis). SDH acts as a tumor suppressor and its defects include inactivating mutations as well as promoter methylation (Killian et al., 2013, 2014). SDH is one of the five complexes belonging to the mitochondrial respiratory chain and takes part in the Krebs cycle and electron transport of the oxidative phosphorylation. The complex has a tetrameric structure, in which the two hydrophilic subunits that have catalytic activity (SDHA and SDHB) are anchored to the mitochondrial membrane thanks to the SDHC and SDHD hydrophobic subunits. Alterations in any of the components of the SDH complex result in complex subunits instability that can be detected by immunohistochemistry as loss of staining.

The mechanism whereby SDH inactivation leads to GIST development is poorly understood. It seems that the elevated concentration of succinate, an SDH metabolite, inactivates the prolyl hydroxylase that regulates the levels of HIF1α. This results in the activation of HIF1α downstream targets VEGF and IGF2, which sustain GIST growth (Corless et al., 2011).

We have recently reported that about 60% of all RTK-wild type GIST harbor NF1 inactivating mutations (Gasparotto et al., 2017; Rossi et al., 2017). NF1 (Neurofibromin-1) is considered a tumor suppressor gene that controls the conversion of GTP-bound active state to the GDP-bound inactive state of Ras. Thus, the inactivation of NF1 causes the hyperactivation of Ras signaling cascade (Niinuma et al., 2018). NF1 is involved in the Neurofibromatosis type I disorder, a syndromic condition with extreme variability in symptoms, ranging from mild signs (*cafè-au-lait* spots, freckles and Lisch nodules in eyes), to more severe manifestations including disfiguring neurofibromas, optical gliomas and bone defects. Noteworthy, this autosomal dominant disease predisposes patients to diverse malignancies, including GISTs (Jett and Friedman, 2010).

NF1-mutant GISTs arise mainly in the intestine, frequently as multiple lesions. These GISTs may be sporadic, due to somatic NF1 mutations, or syndromic, due to constitutional NF1 alterations of which the patient may be unaware. Thus, we suggested that in the presence of an RTK-wild type GIST a syndromic condition should always be considered as often underdiagnosed (Gasparotto et al., 2017).

Recently, few GIST cases were reported to carry NTRK3 activation as a result of an ETV6-NTRK3 gene fusion. The presence of this fusion in GIST was first described by Brenca *et al.* (Brenca

et al., 2016). The fusion retains the SAM domain of the ETV6 transcription factor and the tyrosine kinase domain of the NTRK3 receptor (Brenca et al., 2016; Shi et al., 2016). The discovery of the ETV6-NTRK3 alteration in GIST disclosed new therapeutic opportunities for patients harboring this fusion (Drilon et al., 2018). Other fusion products reported in GISTs include FGFR1 with various partners, and PRKAR1B-BRAF (Charo et al., 2018; Shi et al., 2016).

In the end, less than 5% of wild type GISTs is currently considered "driver gene unknown". The different types of mutations impact on clinicopathological features, prognosis and treatment (see 1.2.7 section).

1.2.3. Cell of origin

Gastrointestinal Stromal Tumors are thought to arise from the Interstitial Cells of Cajal (ICCs), the gut pacemaker cells responsible for peristaltic contractions (Robinson et al., 2000). ICCs were first described by the neuroanatomist Santiago Ramon Y Cajal in 1911 as intestinal ganglionic cells that he named intestinal ganglia (Cajal, 1911). These cells were defined as nerve cells, dispersed within the circular smooth muscle layer of the intestine. Subsequently, intestinal ganglion cells have been identified also in the stomach and in a variety of other organs, as pancreas, mammary gland, heart, blood vessel wall, urinary and genital tracts (Pasternak et al., 2016).

ICCs show some common features with neural crest-derived cells (neurons and ganglia) as well as with cells of mesenchymal origin (i.e. fibroblasts, smooth muscle cells). Lecoin and colleagues demonstrated that ICCs derive from the embryonic mesenchyme and that their growth is independent of neuroectoderm and enteric neurons, with which ICCs later establish an intricate network (Lecoin et al., 1996).

Morphologically, Cajal cells are elongated, with a fusiform body and processes sprouting and branching from it. They have a very large, oval nucleus with one or more nucleoli, and peripherally arranged heterochromatin. The cytoplasm contains numerous mitochondria, well-developed Golgi apparatus, lysosomes and a network of intermediate filaments made of microtubules, vimentin, thin filaments and caveolae (Sanders et al., 2014).

Electrophysiology studies have shown that ICCs create slow waves of peristalsis by inducing a depolarization potential. This spontaneous generation of depolarization in ICCs is made possible by the periodic release of calcium (Ca^{2+}) from the endoplasmic reticulum. This, in turn, regulates the concentration of inositol 1,4,5 triphosphate (IP_3) that activates mitochondrial Ca^{2+} intake. This cyclic process generates potential energy responsible for the transmission of the excitation to the neighbor smooth muscle cells (Pasternak et al., 2016). As previously described, Cajal cells establish a thick network with the neighbor enteric neurons and smooth muscle cells. In order to keep the connections with neural cells, ICCs have several receptors for tachykinins (NK1R) on their surface (Vannucchi, 1999). Moreover, ICCs have their own nitric oxide (NO) synthase, which induces the production of NO. The presence of NO, a gas that easily diffuses across biological membranes, may play a dual role both in the relaxation of the gut smooth muscle cells and in the amplification of the nitrergic neurotransmission sustained by enteric neurons (Sanders, 1996; Ward et al., 1998).

Several studies have highlighted that ICCs show specialized features depending on location. Specifically, ICCs can be divided into four groups (Komuro, 2006; Sanders et al., 1999):

- ICC-SM, located along the submucosal (SM) surface of the circular muscle bundles in the colon;
- ICC-MY, located within the intramuscular space between the circular and the longitudinal muscle layers, the myenteric region, of the stomach (ICC-MY_{ST}), small intestine (ICC-MY_{SI}) and colon (ICC-MY_{C});
- ICC-IM, the intramuscular ICCs of the esophagus sphincter (ICC-IM_{ES}), stomach (ICC-IM_{ST}) and colon (ICC-IM_{C});
- ICC-DMP, located within the deep muscular plexus (DMP) region of the small intestine.

The four ICCs subtypes do not differ simply for localization and macroscopic features, but also for gene expression pattern. In their work, Chen *et al.* demonstrated that murine small intestine ICC-MY and ICC-DMP have different gene expression signature that underlined different functions, with enrichment in metabolic and Ca^{2+} transport genes in ICC-MY, and neurotransmission-related genes in ICC-DMP (Chen et al., 2007).

As mentioned above, ICCs are c-KIT immunopositive cells and rely on the c-KIT signaling pathway for their growth (Hulzinga et al., 1995). The natural c-KIT ligand is the Steel Factor (Kit Ligand- KL- or Stem Cell Factor –SCF), a glycoprotein of 30 kDa. The binding between KL and c-KIT receptor causes the dimerization of two neighbor RTKs, cross phosphorylation of tyrosines and recruitment of downstream signaling molecules. The blockage of c-KIT signaling is disruptive for ICCs, as it induces transdifferentiation of ICCs into smooth muscle cells, impairing their development (Torihashi et al., 1999). Homozygous null mutant mice for c-KIT die in utero from anemia, while heterozygous null mice have an impaired GI motility (Ward et al., 1994).

ICCs are considered the precursor of GIST due to common morphology and immunophenotype, as cytoplasm with abundant mitochondria, tubular cisternae of smooth endoplasmic reticulum, abundant Golgi apparatus, filaments and microtubules. Moreover, ICCs are the only cells in the digestive tract that show as GIST CD117 (c-KIT) and CD34 dual positivity (Hirota, 1998; Kindblom et al., 1998). Finally, mouse models for a KIT mutation typically detected in GIST (V558Δ) show hyperplasia of ICCs and eventually die for a condition that mimics human GIST (Chen et al., 2002; Kwon et al., 2009; Sommer et al., 2003).

1.2.4. Risk classification

The revised Union for International Cancer Control for tumor, node and metastasis classification of malignant tumors (UICC TNM 8) defines the main prognostic criteria in GISTs (Casali et al., 2018). In details, tumor size, site and mitotic activity, defined as the number of mitosis per 50 High Power Field (HPF, 40x), are the main parameters for the assessment of GIST risk (Fig. 1.5), that has been originally proposed by the Armed Force Institute of Pathology (AFIP) in 2006 (Miettinen and Lasota, 2006).

	Tumor parameters		% of patients with progressive disease during long-term follow up and characterization of risk for metastasis			
Group	Size	Mitotic rate	Gastric GISTs	Jejunal and ileal GISTs	Duodenal GISTs	Rectal GISTs
1	≤2 cm	≤5 per 50 HPFs	0 none	0 none	0 none	0 none
2	>2 ≤ 5 cm	≤5 per 50 HPFs	1.9 very low	4.3 low	8.3 low	8.5% low
3a	>5 ≤ 10 cm	≤5 per 50 HPFs	3.6 low	24 moderate		
3b	>10 cm	≤5 per 50 HPFs	12 moderate	52 high	34 high‡	57† high‡
4	≤2 cm	>5 per 50 HPFs	0†	50†	§	54 high
5	>2 ≤ 5 cm	>5 per 50 HPFs	16 moderate	73 high	50 high	52 high
6a	>5 ≤ 10 cm	>5 per 50 HPFs	55 high	85 high		
6b	>10 cm	>5 per 50 HPFs	86 high	90 high	86 high‡	71 high‡

Figure 1.5 Prognostic factors for GIST risk assessment. HPF: HIGH Power Field. †Category with small numbers of cases. ‡Groups 3a and 3b or 6a and 6b are pooled in duodenal and rectal GISTs due to small number of cases. §No tumors with these features were present in the study. From Miettinen and Lasota, 2006.

These criteria take into account that GISTs of the same size and mitotic index (MI) if located in the stomach follow a more indolent clinical course compared to intestinal GISTs. Tumor rupture is considered an additional prognostic factor associated with poor outcome, both happening during or after surgery (Casali et al., 2018).

Mutational status has not been formally incorporated in any standardized risk classification, even if several reports indicate that different genotypes have a distinct natural history and peculiar clinical course. In their report, Rossi and colleagues proposed that the stratification of patients based on molecular profiling may complement the canonical AFIP risk assessment, especially for those GIST with intermediate-risk (Rossi et al., 2015). In particular, the authors described three different prognostic groups of naïve tumors according to mutation status: the first one includes PDGFRA exon 12, BRAF and KIT exon 13, with best overall survival; the second group, including KIT/PDGFRA/BRAF wild type GISTs, KIT exon 17, PDGFRA exon 14, PDGFRA exon 18 D842V, with intermediate-risk; the latter group had the worst prognosis and included KIT exon 9, KIT exon 11, PDGFRA exon 18 non-D842V (Fig. 1.6).

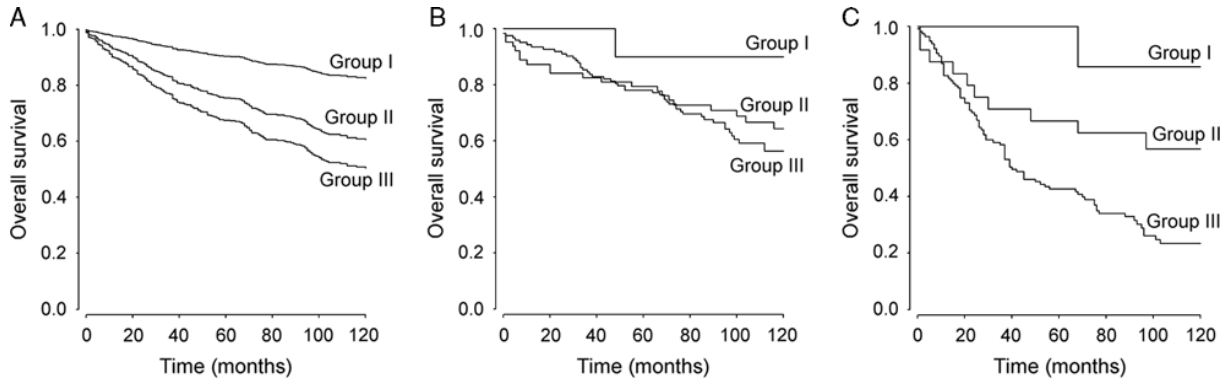

Figure 1.6 Stratification of patients according to molecular characterization. A) Kaplan-Meier curves of overall survival (OS), calculated by multivariable Cox regression statistics. **B)** Molecular signature-based OS stratification of patients who were classified as low-moderate risk according to AFIP criteria. **C)** Molecular signature-based OS stratification of patients who were classified as high risk accordingly to AFIP criteria. Group I: BRAF exon 15, KIT exon 13, PDGFRA exon 12 GISTs; Group II: KIT/PDGFRA/BRAF wild type, KIT exon 17, PDGFRA exon 14, PDGFRA exon 18-D842V; Group III: KIT exon 9, KIT exon 11, PDGFRA exon 18 non-D842V. From Rossi *et al.*, 2015.

Other genomic-based methods for GIST risk assessment have been proposed. The CINSARC score is a predictor of metastasis, that can be applied to GIST as well as to other types of sarcomas (Chibon et al., 2010). This CINSARC score relies on the signature of 67 genes, involved in the maintenance of chromosomal integrity and mitotic checkpoints (Chibon et al., 2010). Also the expression of AURKA, one of the top-ranked genes in the CINSARC signature, seems to provide a reliable prognostic assessment (Lagarde et al., 2012).

Finally, a measurement of aneuploidy as assessed by the Genomic Index (GI), could be another valuable prognostic factor for the stratification of intermediate GIST patients (Lartigue et al., 2015; Rudolph et al., 1998).

1.2.5. GIST of small size: miniGIST

In the AFIP risk criteria, GISTs smaller than 2 cm in diameter are considered no risk lesions. Besides being small, these lesions are mitotically inactive, which accounts for their limited tumorigenic potential.

MiniGISTs are common lesions being detected in about 1/3 of elderly individuals (Agaimy et al., 2007). They are usually found incidentally during surgical or endoscopic procedures and are most commonly recorded in the stomach than in the small intestine (Fletcher et al., 2013; Rossi et al., 2010).

MiniGISTs share with overt GISTs the canonical driver mutations (Rossi et al., 2010) indicating that KIT or PDGFRA alterations are not *per sé* sufficient to trigger GIST development. MiniGIST is considered the premalignant counterpart of an overt GIST, a malignant evolution occurring in less than 0.1% of miniGIST (Schaefer et al., 2017). Thus, other molecular aberrations must co-occur with driver mutations for a miniGIST to progress (Agaimy et al., 2007).

1.2.6. Chromosomal alterations during GIST progression

Increasing evidence suggests that chromosome changes play an important role in GIST malignant evolution. It has been estimated that GISTs have an average of 2.6 to 7.5 chromosome aberrations/case depending on their grading (El-Rifai et al., 2000). In particular, El-Rifai and colleagues demonstrated that about 2/3 of GISTs have total or partial monosomy of chromosome 14q, and about 50% display losses in 22q. Alterations in 1p and 15q are also frequent in GISTs and often coexist, especially in high-grade GISTs.

Debiec-Rychter *et al.* confirmed that losses of 14q and 22q were detected both in low mitotic index-GISTs and malignant GISTs, suggesting that these are early events in ICC transformation. Losses of chromosomes 1, 7, 9 and 15 were instead likely gained during progression (Debiec-Rychter et al., 2001).

Loss of 14q seems more common in gastric GISTs than in intestinal GIST where chromosome 22q loss seems to prevail. Moreover, intestinal tumors tend to undergo 1p and 15q losses (Chen et al., 2004; Gunawan et al., 2004; Wozniak et al., 2007).

What are the molecular targets of these chromosome imbalances is still largely unknown. Protein coding genes, e.g. MAX (MYC associated factor X) mapping to 14q23.3, have been suggested to act as tumor suppressors in GIST pathogenesis. The role of miRNA located in these regions is poorly defined.

To summarize (Fig. 1.7), chromosomal instability is a frequent event in GIST development and progression. Losses are the most common alteration detected in low-grade GIST, whereas gains are typically correlated with higher risk GISTs. Loss in 14q is an early event in the tumorigenesis and is more frequently observed in the gastric tumors, which are often associated with a better outcome. Losses of chromosomes 1p and 15q are features of intestinal GISTs that have more aggressive behavior. Moreover, chromosomes 7 and 9 losses emerge as genomic aberration in GIST with higher malignant potential (Yang et al., 2008).

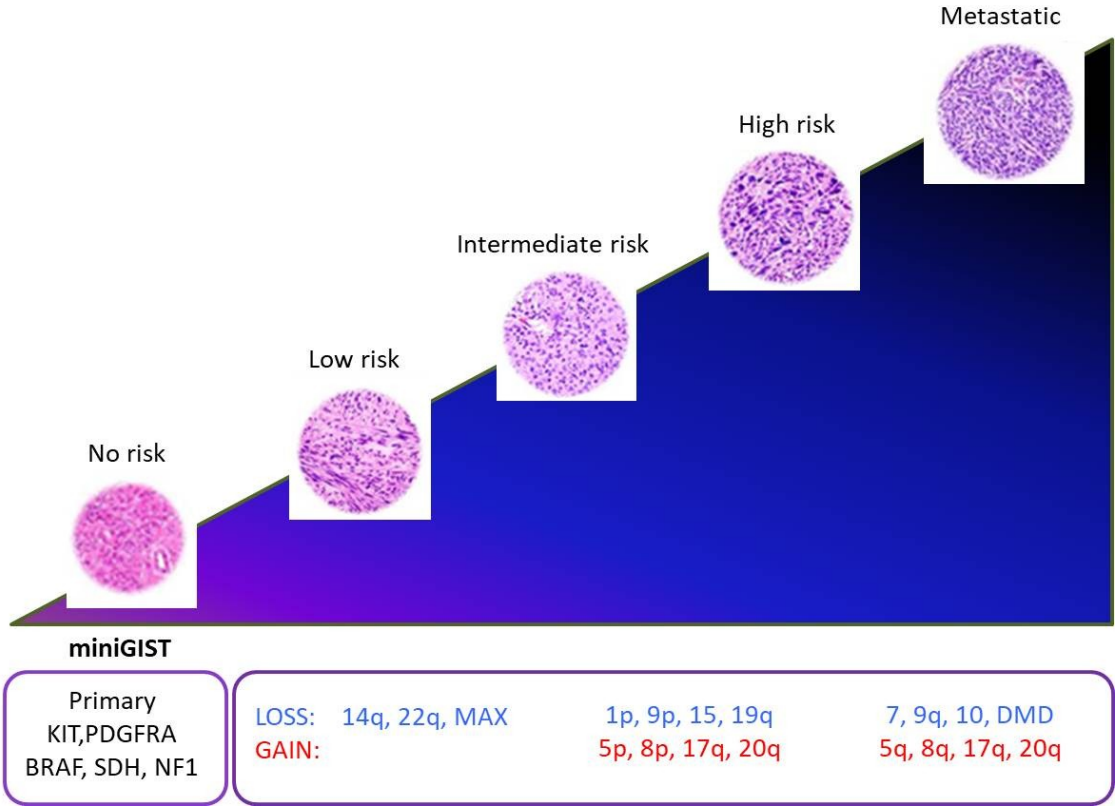

Figure 1.7 Major genomic alterations during GIST progression. Primary mutation in KIT/PDGFRA/BRAF/SDH/NF1 is considered a trigger oncogenic event, responsible for ICC hyperplasia and development of miniGIST. Chromosome losses in 14q and 22q are reported as early events in low-risk GIST. Accumulation of additional genomic imbalances (gain and loss) characterizes the progression of GIST. MAX: Myc associated factor X (14q23.3); DMD: dystrophin (Xp21.2-p21.1). Adapted from Li *et al* 2017a*.,* and Schaefer *et.al.* 2017.

1.2.7. Treatment approaches to GIST

The standard approach for localized but clinically overt GIST is surgery, with no dissection of clinically negative lymph nodes (Casali et al., 2018). *Vice versa* given the low probability of evolution for most miniGIST endoscopic assessment and follow-up are chosen (Casali et al., 2018). An exception is represented by rectal tumors, that are removed after endorectal ultrasound assessment or pelvic magnetic resonance regardless of tumor size and mitotic rate, as lesions in this site have a higher progression risk and a worse prognosis compared to tumors with other locations (Casali et al., 2018).

Until year 2000, few treatment options were available for advanced GIST patients that could not undergo surgery, with a response rate to conventional chemotherapy of less than 5% and a median survival of 18 months (Corless et al., 2011). The "molecular era" of GIST began in 1998 when Hirota *et al.* demonstrated that KIT mutation participated in GIST oncogenesis (Hirota, 1998). In the same years, Imatinib was developed as a receptor tyrosine kinase inhibitor (TKI) for the treatment of BCR-ABL positive chronic myeloid leukemia (CML) (Druker et al., 1996). Based on the structural similarity between ABL and c-KIT RTKs, Imatinib was probed on a patient with advanced GISTs (Demetri et al., 2002; Heinrich et al., 2000; Joensuu et al., 2001). The drug showed an impressive efficacy toward the disease, which within few weeks of treatment became metabolically inactive as revealed by [18F]fluorodeoxyglucose PET (positron emission tomography) loss of uptake (Fig. 1.8). This result unveiled a new therapeutic avenue for GIST.

Imatinib inhibits KIT directly by acting as an ATP competitive antagonist for the ATP-binding pocket (Druker et al., 1996). The advent of Imatinib in the clinical arena set the ground of the so-called targeted therapy and GIST become the paradigm of targeted therapy-treated solid tumors and one of the most encouraging examples. As Imatinib was introduced in the clinical practice for treating GIST, the median overall survival for advanced GIST patients increased from 18 to over 50 months (standard dose: 400mg/day) (Casali et al., 2018).

In the case of relapse, nowadays clinicians may rely on a portfolio of different TKIs. Second-line Sunitinib and third-line Regorafenib, as well as additional TKIs as Dasatinib, Nilotinib and Pazopanib, are now used for patients that become resistant to first-line Imatinib or that are insensitive to the treatment (Casali et al., 2018).

Primary resistance to Imatinib is observed in about 10-15% of primary GISTs and is most often associated with PDGFRA D842V mutation. This mutation favors the active conformation of the kinase preventing the correct and full binding of the inhibitor to the site of action. Also non-KIT/non-PDGFRA mutant GIST (23%) are poorly responsive to Imatinib (Corless et al., 2011; Heinrich et al., 2003b). The KIT exon 9 mutations (16%) are less Imatinib sensitive compared to KIT exon 11 mutations but dose escalation (800mg/daily instead of 400mg/daily) has proven to circumvent this resistance (Corless et al., 2011; Gastrointestinal Stromal Tumor Meta-Analysis Group (MetaGIST), 2010).

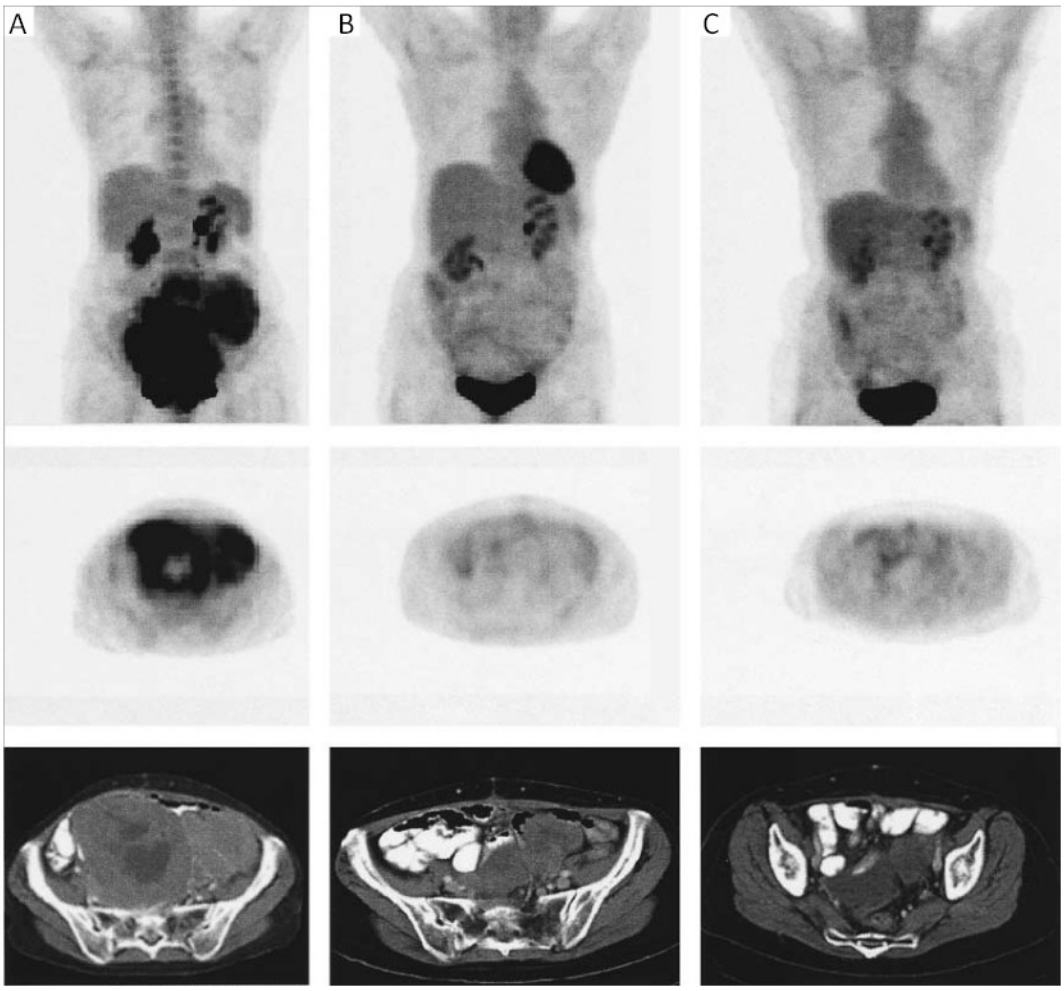

Figure 1.8 F18-fluoro-deoxyglucose positron emission tomography (F18-FDG-PET) response during Imatinib treatment. Images are from the same GIST patient **A)** before, **B)** after 1 month and **C)** after 16 months of continuous treatment with Imatinib. Images of every time point represent a PET scan of the body (top), an axial PET scan of the tumor slice (middle) and the corresponding CT scan at the same level (bottom). From Demetri et al., 2002.

Secondary resistance occurs after initial response to Imatinib. Most patients develop secondary resistance as a result of the gain of resistant mutations. These mutations occur mainly in KIT exon 13-14, encoding the ATP-binding domain, and/or exon 17-18, encoding for the activation loop. These mutations interfere with drug binding and with the stabilization of the active conformation of the kinase (Corless et al., 2011). Another mechanism of resistance is represented by the loss of KIT expression that underlines the loss of KIT dependency (Debiec-Rychter et al., 2005).

Several clinical trials are currently ongoing to circumvent TKI resistance (Fig. 1.9) (https://clinicaltrials.gov) (October 1, 2019). One of the most promising TKI is Avapritinib (also known as BLU-285), a highly selective TKI with particular activity against resistant mutations, including the PDGFRA D842V. A clinical benefit rate of 40-70% in heavily treated GIST patients was observed with a tumor reduction in 60% of cases, as reported in the phase I NAVIGATOR and in the phase III VOYAGER trials (Bauer et al., 2018; Heinrich et al., 2018).

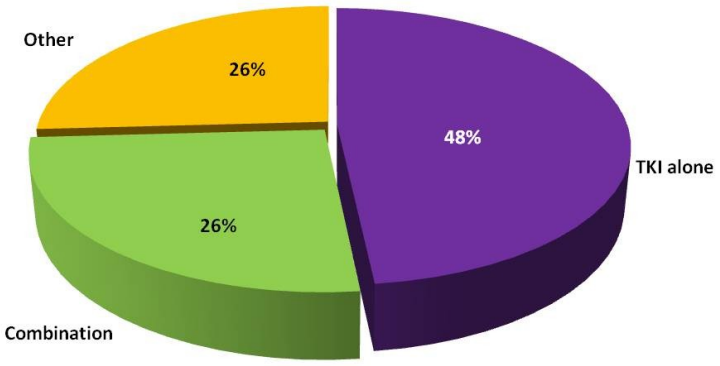

Figure 1.9 Schematic representation of active/open clinical trials for GIST. TKI: tyrosine kinase inhibitor, alone as monotherapy; Combination: TKI and other non-TKI agents; Other: clinical trials with non-TKI molecules (e.g. immunotherapy) (October 1, 2019).

Other promising approaches for the treatment of GIST included the use of humanized monoclonal antibodies (mAbs) that display various mechanism of action, among which the direct inhibition of the target or the mediation of immune response with the regulation of T-cell function (Sankhala, 2017; Scott et al., 2012). Unfortunately, despite initial encouraging results (Wagner et al., 2017), the anti-PDGFRA mAb Olaratumab, failed to reach the primary endpoints in phase III study (American Association for Cancer Research, 2019) and has been therefore withdrawn (ASCO Annual Meeting, 2019).

The vast majority of RTK-wild type GISTs rely on a hyperactive MAPK pathway due to mutations in BRAF, HRAS or NF1. These patients could benefit from MAPK or MEK inhibitors (Jessen et al., 2013).

Finally, the detection of the ETV6-NTRK3 fusion product in GISTs (Brenca et al., 2016) has disclosed unprecedented therapeutic opportunities for GIST with this genotype. In fact, the ETV6-NTRK3 fusion protein is particularly sensitive to an NTRK inhibitor, Larotrectinib, which has demonstrated impressive activity in NTRK fusion-positive tumors, including GISTs (Drilon et al., 2018). Interestingly, Larotrectinib is the first FDA approved drug that has been designated “tumor-agnostic”, as it can be prescribed just based on tumor genetics, irrespective of histology (Huang and Feng, 2019).

1.3. The role of miRNAs in human cancer

miRNAs (also known as microRNAs) are small non-coding RNA molecules, 20-25 nucleotides (nt) long, that have an important role in gene regulation. The RNA interference (RNAi) was first discovered in the Nineties by Lee and colleagues, who reported that the lin-4 RNA from *Caenorhabditis Elegans*, although non-coding, was able to regulate gene expression during developmental timing (Lee et al., 1993). Some years later, exogenous double-strand RNAs (dsRNAs) were shown to be able to dampen gene expression in a target-specific manner through a mechanism called RNA interference (Fire et al., 1998; Mello and Conte, 2004).

In general, non-coding RNAs (ncRNAs) can be distinguished by length (small: 18-200 nt; long: >200 nt) or by function (housekeeping or regulatory). Housekeeping ncRNAs include transfer-RNA (tRNAs) and ribosomal-RNA (rRNAs). Regulatory ncRNAs include miRNA, which exert mainly transcriptional and post-transcriptional inhibition on target protein-coding genes; small-interference RNAs (siRNAs), which act as the defenders of genome integrity in response to foreign or invasive nucleic acids as viruses, transposons and transgenes; PIWI-interacting RNAs (piRNAs), which can induce silencing of germline transposons; small nucleolar RNAs and their partner small nucleolar ribonucleoprotein (snoRNAs and snoRNPs), which are implicated in chemical modifications of rRNA; finally, the recently discovered transfer RNA-derived RNA fragments (tRFs), which can act in a miRNA-like fashion (Romano et al., 2017). These functional classes of ncRNAs are distinguished predominantly *per* size (Romano et al., 2017) and represent less than 1% of total RNA by mass (Fig. 1.10) (Palazzo and Lee, 2015).

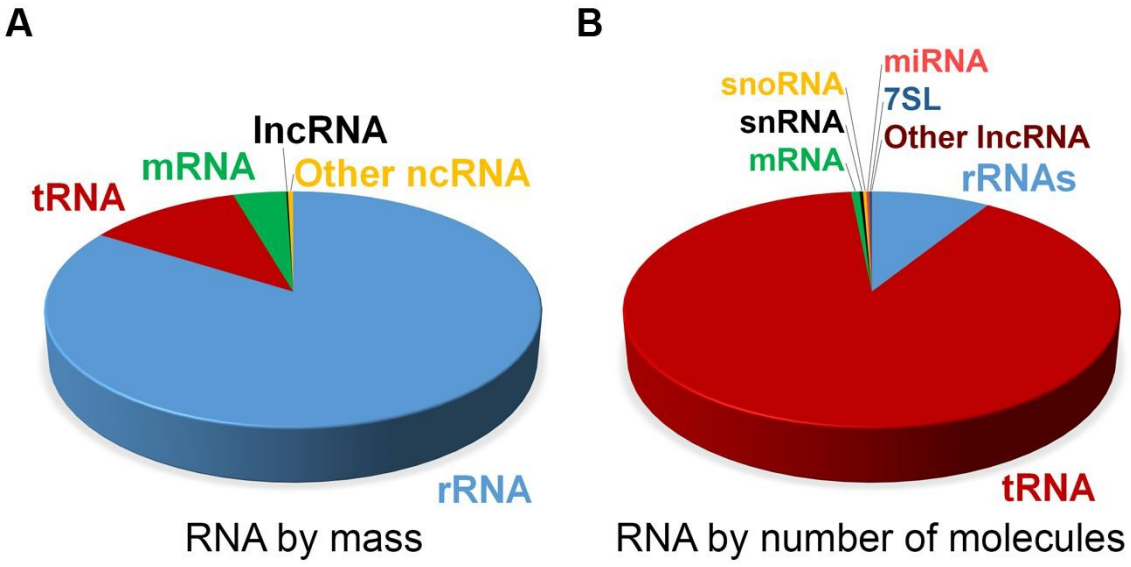

Figure 1.10 Estimation of the different RNA species in a typical mammalian cell by A) total mass or B) the absolute number of molecules. From Palazzo and Lee, 2015.

In the present work, we focused on the miRNA class of non-coding RNAs. miRNAs are highly conserved small ncRNAs in eukaryotes. The official reference database of miRNAs is miRBase and includes 38589 entries in its latest version (October 2018, version 22.1), with 1917 stem-loop

sequences annotated as human miRNAs precursors, a number that increases over time (Kozomara et al., 2019).

1.3.1. miRNA biogenesis and mechanism of interference

The biogenesis of a mature, functionally active miRNA (Fig. 1.11) begins in the nucleus, where a miRNA locus either as separate units or embedded within the introns of protein-coding genes is transcribed by the RNA polymerase II as a primary double-stranded hairpin transcript (at least 1000nt long) called pri-miRNA (Bartel, 2004; Ruby et al., 2007). The pri-miRNA is then cleaved to a 65-70nt long molecule, called pre-miRNA, by the microprocessor complex formed by the RNase enzyme DROSHA and the dsRNA binding protein DGCR8 (DiGeorge syndrome Critical Region 8). Once DROSHA trims the transcript and releases the pre-miRNA, the pre-miRNA is subsequently exported by the transport facilitators, Exportin-5 (XPO5) and RanGTP in the cytoplasm (Bohnsack, 2004; Ha and Kim, 2014). Here the pre-miRNA is cut down to an RNA duplex of appropriate size (22-30 nt) by the endoribonuclease DICER (Bernstein et al., 2001). The small RNA duplex originated from DICER cleavage is subsequently loaded onto Argonaute protein (AGO) to form the effector complex called RISC (RNA-Induced Silencing Complex). Therefore the minimal RISC loading complex (RLC) includes dsRNA, DICER, AGO and proteins that facilitate the complex formation, the double-stranded RNA binding proteins (dsRBPs, such as TRBP) (Carthew and Sontheimer, 2009).

The RISC loading coincides with the strand selection of the mature miRNA: one strand of the duplex maintains the binding to AGO to direct silencing (miRNA guide strand) whereas the other strand is discarded (miRNA passenger strand). The selection of the guide strand is mainly determined by thermodynamic stability and to the presence of mismatches (U-bias and C-bias) in the position 9 and 10 of the strands (Meijer et al., 2014; Okamura et al., 2009).

Once the guide strand selection has occurred and the passenger strand dissociated from the complex, the silencing machinery is ready. To perform cellular surveillance, the guide strand miRNA binds those single-stranded mRNAs that have near-perfect or perfect complementarity in their sequence with the miRNA seed sequence. The seed sequence of the guide strand miRNA is the region of the mature miRNA that is involved in the binding and comprises nucleotides in positions 2-8 of the mature miRNA (Carthew and Sontheimer, 2009).

Noteworthy, even if the vast majority of miRNAs have been observed to exert inhibitory function on gene expression by interfering with the stability or/and translation of the target mRNA, phenomena of gene expression enhancement have also been reported (Catalanotto et al., 2016; Valinezhad Orang et al., 2014).

Canonically, miRNA genes are located inside the introns of protein-coding genes, or in non-coding regions, but some miRNA genes have been found in exons. miRNA transcripts may be monocistronic or polycistronic, depending on the presence of multiple miRNA duplexes in the pri-miRNA (Saini et al., 2007). In many species, including *Homo Sapiens*, several miRNA loci arose from gene duplication. miRNAs encoded by the same locus are considered a cluster of miRNAs and the pri-miRNA is generally polycistronic (Saini et al., 2007). Moreover, miRNAs that share the seed sequence form a miRNA family (Ha and Kim, 2014).

miRNAs represent a redundant and highly interconnected mechanism of gene regulation, as multiple miRNAs may target the same mRNA and different mRNAs could be targeted by the same miRNA. For at least 60% of cellular mRNA, a miRNA-mediated regulation has been documented (Jansson and Lund, 2012).

This general observation implies that miRNAs orchestrate a fine-tuning of cellular transcriptome and any deregulation in miRNA expression is likely to result in a domino effect.

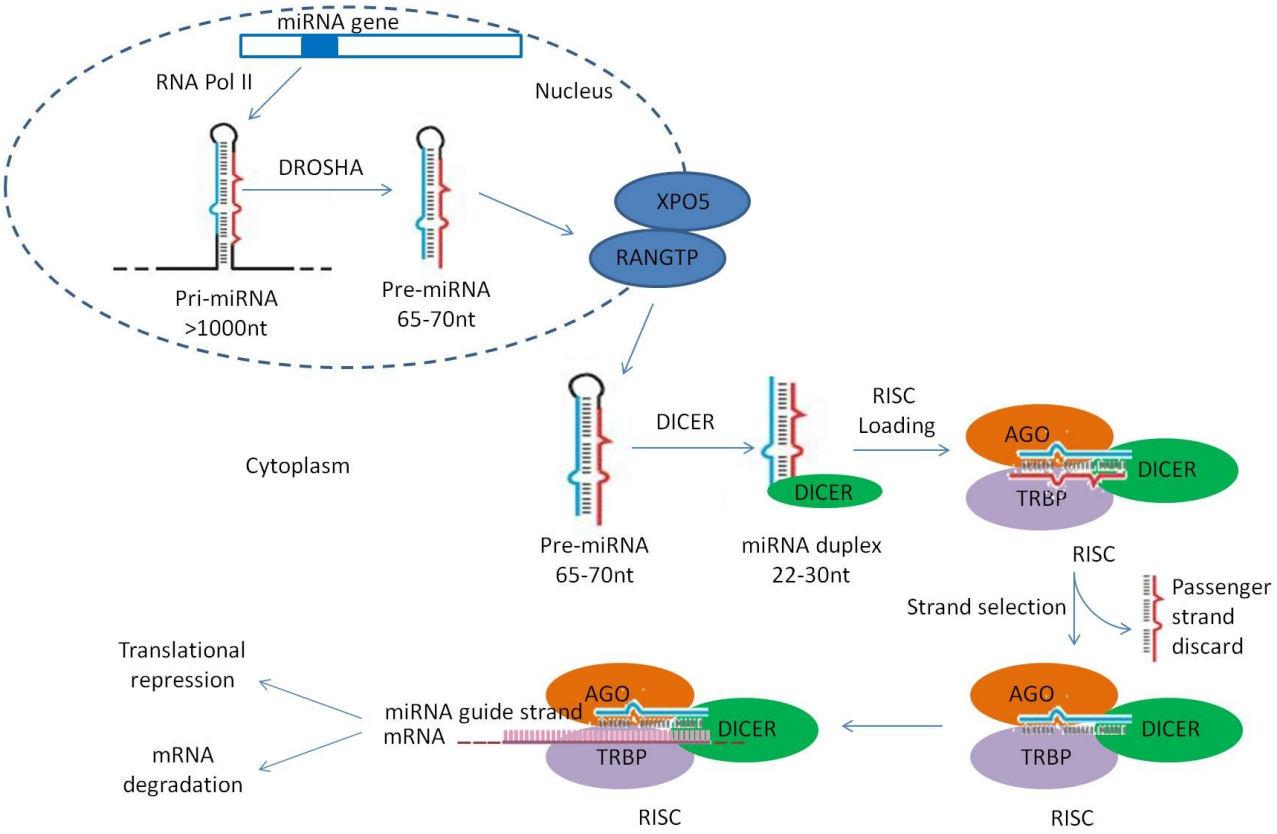

Figure 1.11 The biogenesis of a mature miRNA and the mRNA silencing. miRNA biogenesis starts in the nucleus with the transcription of the miRNA gene by the RNA polymerase II enzyme, which generates the pri-miRNA hairpin. The pri-miRNA is then cleaved by the DROSHA in a 65-70 nt long fragment, the pre-miRNA, that is subsequently exported into the cytoplasm by Exportin5 (XPO5) and RanGTP. The pre-miRNA is processed by DICER to form a shorter duplex (22-30 nt) that is subsequently loaded into the RISC complex formed by the duplex, DICER, Argonaute and TRBP. Here the selection of the miRNA guide strand occurs, and the passenger strand is discarded from the RISC. At the same time, coding gene transcript with perfect/near-perfect complementarity to the seed of the miRNA guide strand is incorporated in the RISC and bound by the miRNA, leading to the translational repression or mRNA degradation. Adapted from Ruby *et al.,* 2007.

1.3.2. miRNAs in cancer

As previously described, miRNAs are implicated in a variety of biological processes, including proliferation, cell cycle, apoptosis, differentiation, migration and metabolism, central processes in cancer development (Alvarez-Garcia, 2005). Moreover, as single miRNA may target up to hundred mRNAs, aberrant miRNAs expression may affect a multitude of transcripts and profoundly influence cancer-related signaling pathways.

miRNAs are classified as oncomiRs if they target tumor suppressor mRNAs, and tumor suppressor miRNAs if they bind predominantly oncogene transcripts. However, miRNA function may be tissue-dependent and vary in relation to the genetic context (Guo et al., 2015). For example, miR-29 behaves as an oncomiR in breast cancer and as a tumor suppressor in lung cancer (Fabbri et al., 2007; Gebeshuber et al., 2009).

Most cancer-related miRNAs described so far are thought to act as tumor suppressor. Both intrinsic and extrinsic mechanisms of miRNA failure exist (Fig. 1.12). Genetic and epigenetic alterations at miRNA loci seem to be the most prevalent mechanisms of miRNA inactivation as about 50% of miRNAs is located at fragile sites and cancer susceptible loci (Fig. 1.13) (Calin et al., 2004; Lujambio et al., 2007; Weber et al., 2007). Mutations that alter the seed sequence ablate target repression by tumor-suppressive miRNAs. It should be pointed out that mutations may also contribute to the tumorigenic properties of oncomiRs by conferring new target specificity (Mayr et al., 2007; Mishra et al., 2008).

Defects in genes involved in miRNA biogenesis represent the extrinsic mechanisms of variation in miRNA expression level. Deregulation of the key enzymes DROSHA and DICER have been reported in several tumors (Dedes et al., 2011; Kumar et al., 2009; Merritt et al., 2008; Torres et al., 2011).

Another mechanism of miRNA failure is represented by alterations of the mRNA target. Mutations of the target mRNA affecting the seed consensus sequence result in the alleviation of miRNA control. On the other hand, mutations anywhere in the mRNA sequence may alter its folding thus preventing mRNA:miRNA duplex formation (Jansson and Lund, 2012; Mayr et al., 2007). Finally, the use of alternative splicing or the reduced 3’ UTR commonly detected in transformed cells (Mayr and Bartel, 2009), may also alter miRNA targeting.

Another important mechanism of the escape from miRNA regulation is the presence of ncRNAs as decoy. This class of ncRNAs is characterized by miRNA recognition elements (MREs) that make them compete with canonical targets for miRNA binding, hence the name competitive endogenous RNAs (ceRNAs). Moreover, some pseudogenes and genes have been shown to work as sponges towards miRNAs (Poliseno et al., 2010).

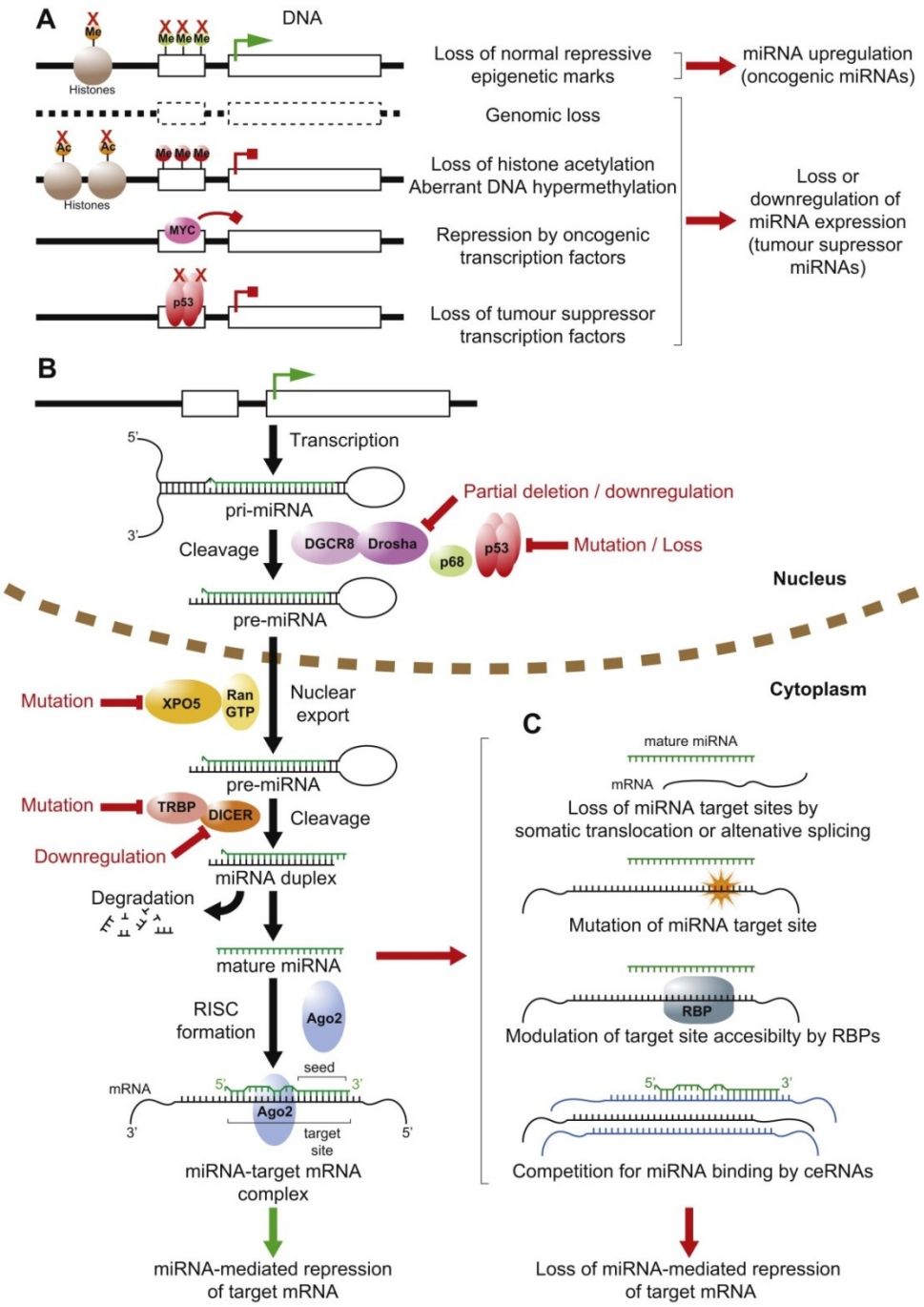

Figure 1.12 Mechanisms for miRNA deregulation in cancer. Schematic representation of the major genetic, epigenetic and transcriptional mechanisms responsible for miRNA altered activity in cancer. From Jansson and Lund, 2012.

The first evidence that miRNA could be important players in the tumorigenesis was provided by Calin and colleagues (Calin et al., 2002). In searching for tumor suppressor genes in 13q14, a chromosome region frequently deleted in B-cell chronic lymphocytic leukemia (B-CLL), they found that this region did not harbor protein-coding genes but short non-coding RNAs. Their functional characterization led the identification of the first two miRNAs, miR-15 and miR-16, which act as tumor suppressor miRNAs. Lately, Costinean and coworkers in 2006 found that miR-155 and its

host gene BIC are involved in B cell lymphoma disease (Costinean et al., 2006). Since then, many efforts have been made in order to elucidate the role of miRNA in cancer as they are valuable molecules that can even distinguish between tumor and normal cells and between different cancer subtypes and stages (Iorio and Croce, 2012). Furthermore, due to their small size and permanence in tissue and biofluids, they should be considered in diagnostics and prognostics.

Chromosome	Location (defining markers)	Size, Mb	miR	Hystotype	Known OG/TS
3p21.1–21.2-D	ARP-DRR1	7	*let-7g/miR-135–1*	Lung, breast cancer	—
3p21.3(AP20)-D	GOLGA4-VILL	0.75	*miR-26a*	Epithelial cancer	—
3p23–21.31(MDR2)-D	D3S1768-D3S1767	12.32	*miR-26a; miR-138–1*	Nasopharyngeal cancer	—
5q32-D	ADRB2-ATX1	2.92	*miR-145/miR-143*	Myelodysplastic syndrome	—
9q22.3-D	D9S280-D9S1809	1.46	*miR-24–1/mir-27b/miR-23b; let-7a-1/let-7f-1/let-7d*	Urothelial cancer	PTC, FANCC
9q33-D	D9S1826-D9S158	0.4	*miR-123*	NSCLC	—
11q23-q24-D	D11S927-D11S1347	1.994	*miR-34a-1/miR-34a-2*	Breast, lung cancer	PPP2R1B
11q23-q24-D	D11S1345-D11S1328	1.725	*miR-125b-1/let-7a-2/miR-100*	Breast, lung, ovary, cervix cancer	—
13q14.3-D	D13S272-D13S25	0.54	*miR-15a/miR-16a*	B-CLL	—
13q32–33-A	stSG15303-stSG31624	7.15	*miR-17/miR-18/miR-19a/miR-20/ miR-19b-1/miR-92–1*	Follicular lymphoma	—
17p13.3-D	D17S1866-D17S1574	1.899	*miR-22; miR-132; miR-212*	HCC	—
17p13.3-D	ENO3-TP53	2.275	*miR-195*	Lung cancer	TP53
17q22-t(8;17)	miR-142s/c-MYC		*miR-142s; miR-142as*	Prolymphocytic leukemia	c-MYC
17q23-A	CLTC-PPM1D	0.97	*miR-21*	Neuroblastoma	—
20q13-A	FLJ33887-ZNF217	0.55	*miR-297–3*	Colon cancer	—
21q11.1-D	D21S1911-ANA	2.84	*miR-99a/let-7c/miR-125b*	Lung cancer	—

Figure 1.13 miRNA located in minimal deleted regions, minimal amplified regions and translocated regions involved in human cancer. OG: oncogene; TS: tumor suppressor; D: deleted region; A: amplified region; NSCLC: non-small-cell lung cancer; HCC: hepatocellular carcinoma. Adapted from Calin *et al.,* 2004.

An extensive bulk of literature reports that the miRNA repertoire is a stable and unique feature of diseases, and the use of miRNAs as non-invasive and bioavailable markers could enter clinical practice. miRNAs could give a lot of information about the type of disease, the stage and even the response to surgery and pharmacological treatments (Sabarimurugan et al., 2019).

Novel drug delivery strategies are under investigation in order to ensure to small, chemical-modified, miRNA-like molecules the properly achievement of tumor site, for anticancer therapy. At present, many clinical trials that test miRNAs as therapeutic options have been launched (http://clinicaltrials.gov), but many of them have to face toxicity and adverse effects. Despite that, they seem to be promising in cancer gene-targeted therapy (Simonson and Das, 2015).

1.3.3. miRNAs in Gastrointestinal Stromal Tumors

Since the discovery of their involvement in cancer, miRNAs grabbed the attention of researchers also in the sarcoma and GIST field, with the majority of study being performed by using microarray (Haller et al., 2010; Kelly et al., 2013; Pantaleo et al., 2016).

One of the first studies that analyzed the miRNA signature in GIST was performed by Subramanian and colleagues in 2008. In this study, authors compared miRNA expression in GIST vs. four other sarcoma subtypes and observed in the former the overrepresentation of 15 miRNAs (among which: miR-140, miR-143, miR-145, miR-125a, miR-29b, miR-29c and miR-30c) and the

downregulation of 9 miRNAs (as miR-368, miR-133b, miR-133a and other) thus suggesting a GIST-specific signature (Subramanian et al., 2008).

A GIST-specific miRNA signature was also reported by Gyvyte and coworkers by comparing the miRNome of GIST vs. adjacent normal tissue (Gyvyte et al., 2017). They found 110 differentially expressed miRNAs in GIST vs. adjacent normal tissue; on these, 34 were up and 76 were downregulated, in line with previous reports indicating that miRNAs are more often lost in cancer (Calin et al., 2004; Jansson and Lund, 2012). These miRNAs were reported to be implicated in cytokine-cytokine interaction, cell cycle, ERBB, p53, MAPK, mTOR, JAK/STAT and Insulin signaling pathways and included miR-200 family members, miR-192/215, miR-133a-3p, miR-133b, miR-375, miR-483-5p, miR-509-3p and miR-675-3p (Gyvyte et al., 2017).

Haller and colleagues reported that the miRNA signature of GIST is affected by primary tumor location, with miR-504 and miR-598 more expressed in gastric tumors and miR-210, miR-220c, miR-329, miR-370 and miR-409-3p more expressed in intestinal GISTs. Moreover, they reported that miR-330 was overexpressed in KIT-mutant tumors, whilst miR-629, miR-652 and miR-766 were found to be overexpressed in PDGFRA mutant GISTs (Haller et al., 2010).

Choi and colleagues identified 4 distinct patterns of miRNA expression in GIST, according to site, tumor grade and chromosome imbalances. Intriguingly, 14q loss represented one separate cluster containing miRNA downregulated in high-risk tumors. These miRNAs are mainly involved in the control of genes belonging to mitogen-activated protein kinase (MAPK) and cell cycle pathways, thus accounting for their implication in aggressive tumors (Choi et al., 2010).

The implication of 14q loss in miRNA expression was further investigated by Kelly and coworkers (Kelly et al., 2013). The 14q region is typically paternally imprinted. Thus, the loss of chromosome material in 14q showed a different impact on miRNA expression depending on whether the maternal (active) or the paternal (inactive) region is lost during GIST progression. Furthermore, authors reported that gene targets of the miRNAs mapping to 14q included genes with key function in GIST pathogenesis, such as KIT, PDGFRA IGF1R, MAPK1, KRAS BCL6, CCND2, HDAC6, NF-YBs (Kelly et al., 2013).

2. Aim

In the present work, we wanted to shed light on the role of miRNA:mRNA interplay in the malignant evolution of miniGIST to overt GIST.

As previously mentioned, miniGISTs are *bona fide* considered benign precursors of GISTs, with which they share location, cytology, immunophenotype and most of all, canonical driver gene mutations. The working hypothesis of this thesis is that miRNA expression plays a role in the conversion of a miniGIST into a malignant lesion.

To this end, we sought to provide a comprehensive transcriptional profiling (miRNA and mRNA) of a set of miniGISTs and overt GISTs and to identify and eventually validate miRNA:mRNA regulatory networks involved in miniGISTs to overt GISTs evolution.

3. Results

3.1. Tumor series

A cohort of 88 primary untreated tumors was the ground for this study. The series included 32 miniGISTs and 56 overt GISTs. The most relevant clinicopathological features are reported in Table 3.1. The series included 54 cases with mutations in KIT, 17 in PDGFRA, 3 in BRAF, 8 in NF1 and 6 tumors that were negative for known GIST-related mutations and were therefore considered "driver unknown". As a side note, the identification of NF1 as a driver gene in GIST has been also the object of study during my Ph.D. course and has yielded two publications (attachment) (Gasparotto et al., 2017; Rossi et al., 2017).

Table 3.1: Clinicopathological features of the 88 cases included in this study.

Cohort:88 cases		**Overt GIST ≥ 2cm**	**MiniGIST <2 cm**
		56	32
Site			
	Gastric	30*	19
	Intestinal	26	13
Mutation			
	KIT	37	17
	PDGFRA	9	8
	BRAF	2	1
	NF1	6	2
	Unknown	2	4
Mitotic Index			
	≤ 5 HPF	29	32
	> 5HPF	24	-
	NA	3	-

*: includes 1 esophageal GIST; HPF: High Power Field (40x); NA: Not Assessed.

In order to identify miRNAs that could account for gene deregulation during miniGIST to overt GIST evolution, we performed RNA-Seq and miRNA-Seq profiling on 77 (25 miniGISTs; 52 overt GISTs) and 68 cases (31 miniGISTs; 37 overt GISTs), respectively. The two series overlapped for 57 cases (24 miniGISTs; 33 overt GISTs), while for 20 and 11 cases data were available for RNA-Seq or miRNA-Seq only. The profiled cohorts were representative of the major tumor variables impacting on GIST pathobiology, namely size, site, type of driver mutations and mitotic index (Tab. 3.2).

Table 3.2: Clinicopathological features of cases profiled by RNA-Seq (left) and miRNA-Seq (right).

RNA profiling 77 cases		Overt GIST ≥ 2cm	Mini GIST <2 cm
		52	25
Site			
	Gastric	28*	15
	Intestinal	24	10
Mutation			
	KIT	34	13
	PDGFRA	9	6
	BRAF	2	1
	NF1	5	2
	Unknown	2	3
Mitotic Index			
	≤ 5 HPF	28	25
	> 5HPF	23	-
	NA	1	-

miRNA profiling 68 cases		Overt GIST ≥ 2cm	Mini GIST <2 cm
		37	31
Site			
	Gastric	20	19
	Intestinal	17	12
Mutation			
	KIT	24	16
	PDGFRA	7	8
	BRAF	2	1
	NF1	4	2
	Unknown	-	4
Mitotic Index			
	≤ 5 HPF	21	31
	> 5HPF	13	-
	NA	3	-

*: includes 1 esophageal GIST; HPF: High Power Field (40x); NA: Not Assessed.

3.2. Whole series: transcriptome and miRNome profiling

The transcriptome profiling (RNA-seq) was carried out on 77 cases, 25 miniGISTs and 52 overt GISTs. The median number of reads was 64 million (range 25-280).

Principal Component Analysis (PCA) of the whole series clearly indicated a net separation according to tumor site, for both overt and miniGIST (Fig. 3.1A-B). No clear separation was instead observed for tumor class (miniGIST vs. overt GIST), even when gastric and intestinal sites were analyzed separately (Fig. 3.1C-D). Interestingly, the type of driver mutation represented an element of separation along PC1 for both miniGIST and overt GIST of the gastric site (Fig 3.1E) (KIT vs. PDGFRA). A similar trend was observed also in the intestine where non-KIT mutant tumors tended to co-cluster (Fig. 3.1F). The comparison of the transcriptome of overt GISTs vs. miniGISTs identified 2296 genes as differentially expressed (DEG), 1382 overexpressed and 914 underexpressed (cutoffs: abs.$\log_2$FC≥0.6; p-value≤0.05). For about half of these genes, the p-adj was less than 0.1.

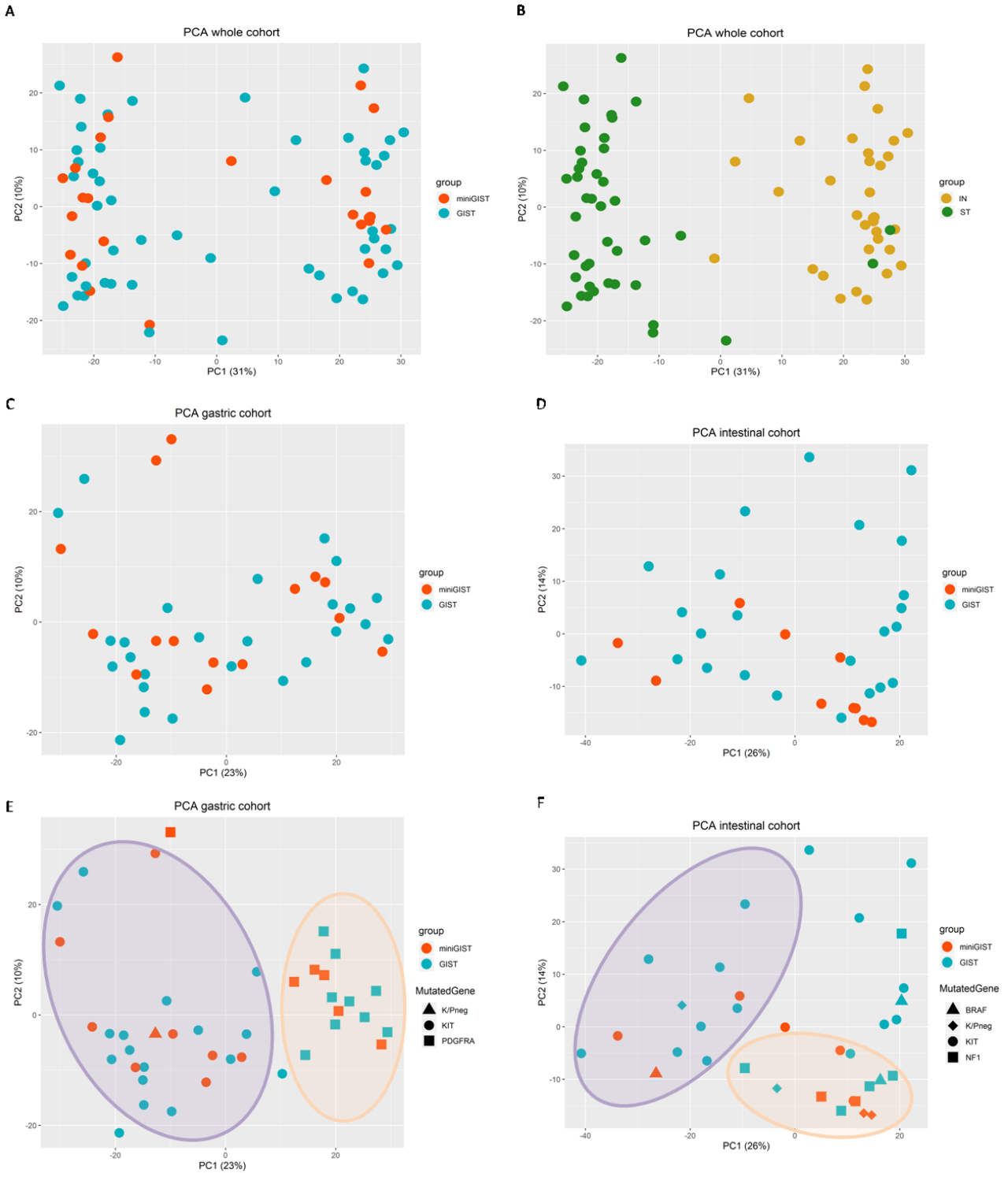

Figure 3.1 Principal component analysis (PCA) of the transcriptome. PCA of 77 cases profiled by RNA-Sequencing labeled by **A)** condition (blue: overt GIST; red: miniGIST) or **B)** site (green: stomach; yellow: intestine). PCA of gastric (C, E) and intestinal (D, F) cohorts labeled by condition; the different shape points represent the mutated gene. The group of cases with KIT or non-KIT mutations are indicated by purple and salmon ellipses, respectively. PCAs were built on the top 500 genes with higher variance. K/P neg: tumors devoid of KIT or PDGFRA mutations.

Functional enrichment analyses of DEGs (overt GIST vs. miniGIST comparison) were performed by using Ingenuity Pathways Analysis (IPA) and Gene Set Enrichment Analysis (GSEA).

Several statistically enriched pathways were identified by both IPA and GSEA (Fig. 3.2), with an important involvement of the immune system and metabolism among positive enriched pathways (enriched in overt GIST), and axon guidance and terms related to muscle contraction among negative enriched pathways (enriched in miniGIST).

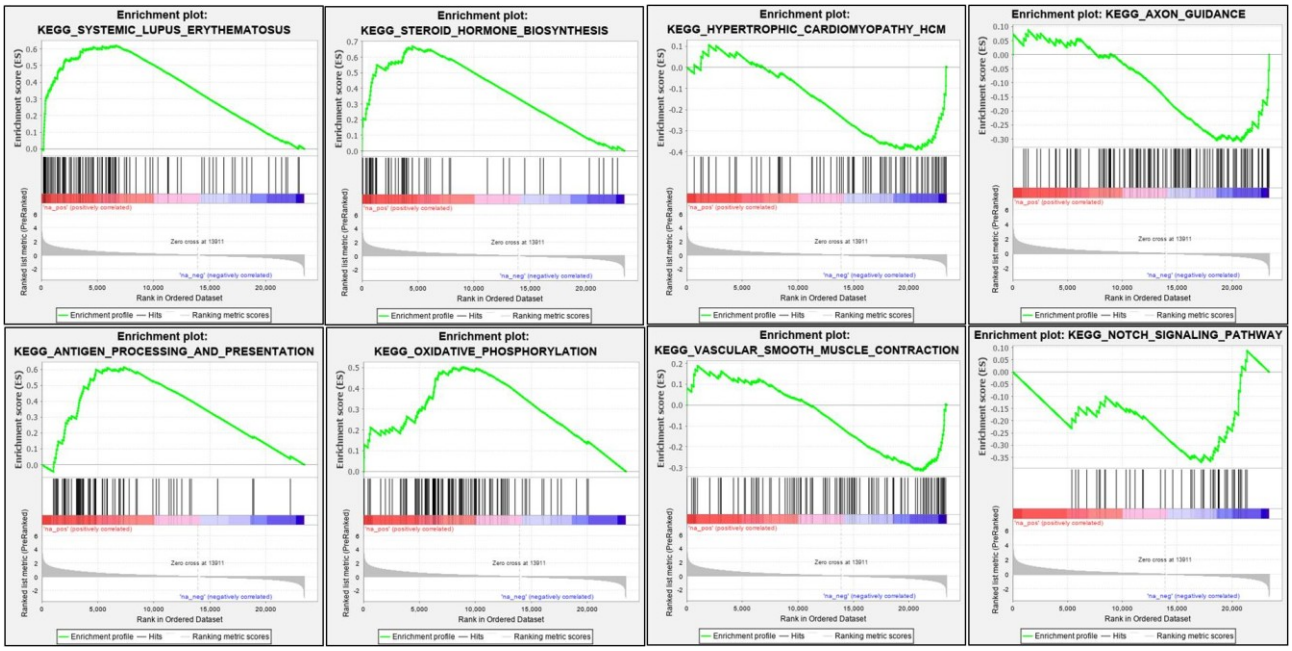

Figure 3.2: GSEA results showing the most relevant KEGG terms enriched in overt GIST vs. miniGIST (whole cohort). Each plot represents positive enrichments (ES >0, left panels) and negative enrichments (ES <0, right panels) in the DEGs of overt GIST vs. miniGIST contrast. Enrichment Score (ES) is indicated on the left.

A subset of 68 cases was then profiled for miRNA expression. Sample reads ranged from 0.6 to 3.8 million reads (median 2.1). Differently from transcriptome, the miRNome better captured differences between miniGISTs and overt GISTs, especially in the gastric site (Fig. 3.3A, C-D). Moreover, as observed for the transcriptome, tumor location, as well as mutation driver, had an important impact on miRNome profile (Fig. 3.3B, E-F). Specifically, in the gastric cohort KIT- and PDGFRA-mutant tumors separated along PC2 and a trend of separation along PC2 was also observed in the intestinal cohort for KIT vs. non-KIT tumors (Fig 3.3E, F).

In the differential expression analysis, over a hundred (109) of differentially expressed miRNAs (DEmiRs) were detected in the overt GIST vs. miniGIST contrast, 82 over- and 27 under-expressed (cutoffs: abs.$\log_2$FC≥0.6; p-value≤0.05).

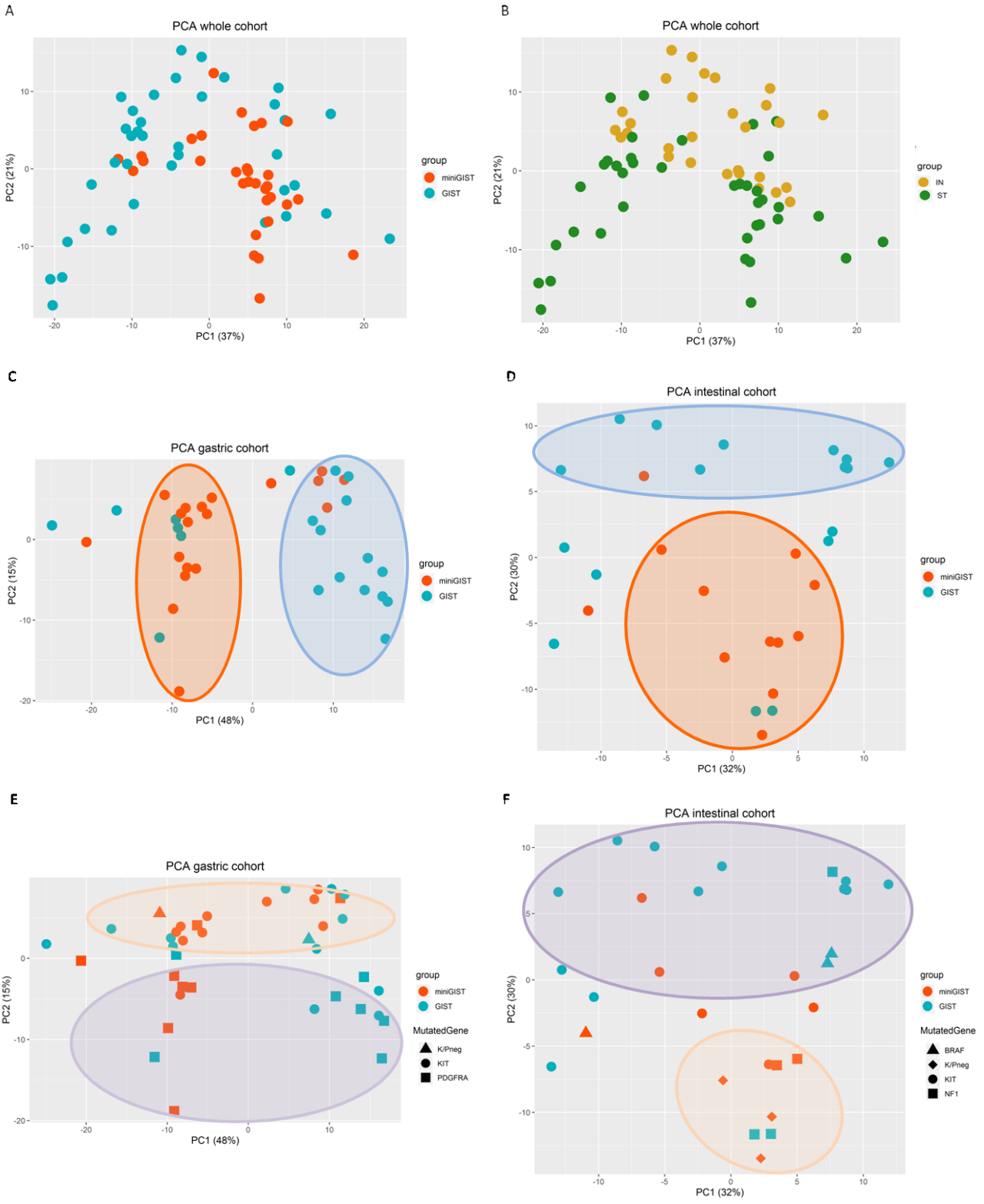

Figure 3.3 Principal component analysis (PCA) of the miRNome. PCA of the 68 cases profiled by miRNA-Sequencing labeled by **A)** condition (blue: overt GIST; red: miniGIST) and **B)** site (green: stomach; yellow: intestine). PCA of gastric (C, E) and intestinal (D, F) cohorts labeled by condition; the different shape points represent the mutated gene. miniGIST and GIST group of cases are indicated by red and blue ellipses, respectively (C-D); the group of cases with KIT or non-KIT mutations are indicated by purple and salmon ellipses, respectively (E-F). PCAs were built on the top 100 miRNAs with higher variance. K/P neg: tumors devoid of KIT or PDGFRA mutations.

Functional enrichment analyses of DEmiRs, performed with miRPath v.3 and PathDIP, highlighted that the miRNAs possibly implicated in the miniGIST to overt GIST transition are predicted to target genes related to many cancer-related pathways (Tab. 3.3).

Table 3.3 DEmiRs of the whole cohort: top 10 most significantly enriched KEGG pathways.

KEGG pathway	p-value	#Predicted genes	#DEmiRs
Fatty acid biosynthesis	6.85E-13	6	4
Mucin type O-Glycan biosynthesis	7.68E-13	16	11
Proteoglycans in cancer	1.14E-08	147	69
Renal cell carcinoma	1.29E-06	57	58
Pancreatic cancer	1.35E-06	38	16
Glioma	1.47E-06	35	16
TGF-beta signaling pathway	1.19E-05	61	54
Axon guidance	1.19E-05	92	54
N-Glycan biosynthesis	1.40E-05	38	44
Neurotrophin signaling pathway	1.40E-05	95	67

#Predicted genes: number of genes predicted to be targeted by DEmiRs according to the DIANA tool (microT-CDS v 5.0). #DEmiRs: number of DEmiRs associated with the indicated pathway. The enrichment was performed by using the union genes method.

By interrogating the chromosomal position dataset for the DEmiRs, we observed that several of the DEmiRs enriched in the overt GIST mapped to chromosome 1 and chromosome X, whereas many of the underexpressed DEmiRs in the same contrast mapped to chromosome 14 and chromosome 6 (Tab. 3.4).

Table 3.4 DEmiRs of the whole cohort: chromosome enrichment results

Chromosomal location	Enrichment	p-value	# Observed DEmiRs
Chromosome 1	enriched	0.0493	7
Chromosome 14	depleted	0.0001	8
Chromosome 6	depleted	0.0448	4
Chromosome X	enriched	2.40E-06	27

Results of chromosomal mapping enrichment of the DEmiRs identified as differentially expressed in overt GIST vs. miniGIST of the whole cohort. Enriched: chromosomal location enriched in the overt GIST category; depleted: chromosomal location enriched in the miniGIST category.

Although clearly GIST share common pathways of transformation irrespective of tumor location, as indicated by the involvement of the same gene drivers (e.g. KIT mutations) or chromosome alterations (e.g. 14q loss) in both sites, our data suggest that GIST pathogenesis possibly relies also on site-specific molecular routes.

Based on these results, we sought to address the mechanisms of malignant evolution of GIST both as a whole (site-shared alterations) as well as per site.

3.3. Gastric GISTs: transcriptome and miRNome profiling

The transcriptome of overt GISTs compared to that of miniGISTs of the stomach identified 1905 DEGs, 1055 up and 850 down (cutoffs: abs.log_2FC≥0.6; p-value≤0.05) For about half of these genes the p-adj was ≤0.1.

Functional enrichment analyses corroborated the important involvement of the immune system during the transition from miniGIST to overt GISTs. The Hedgehog pathway, typically provided of immune exclusion activity, was instead called as overrepresented in miniGIST (Fig. 3.4).

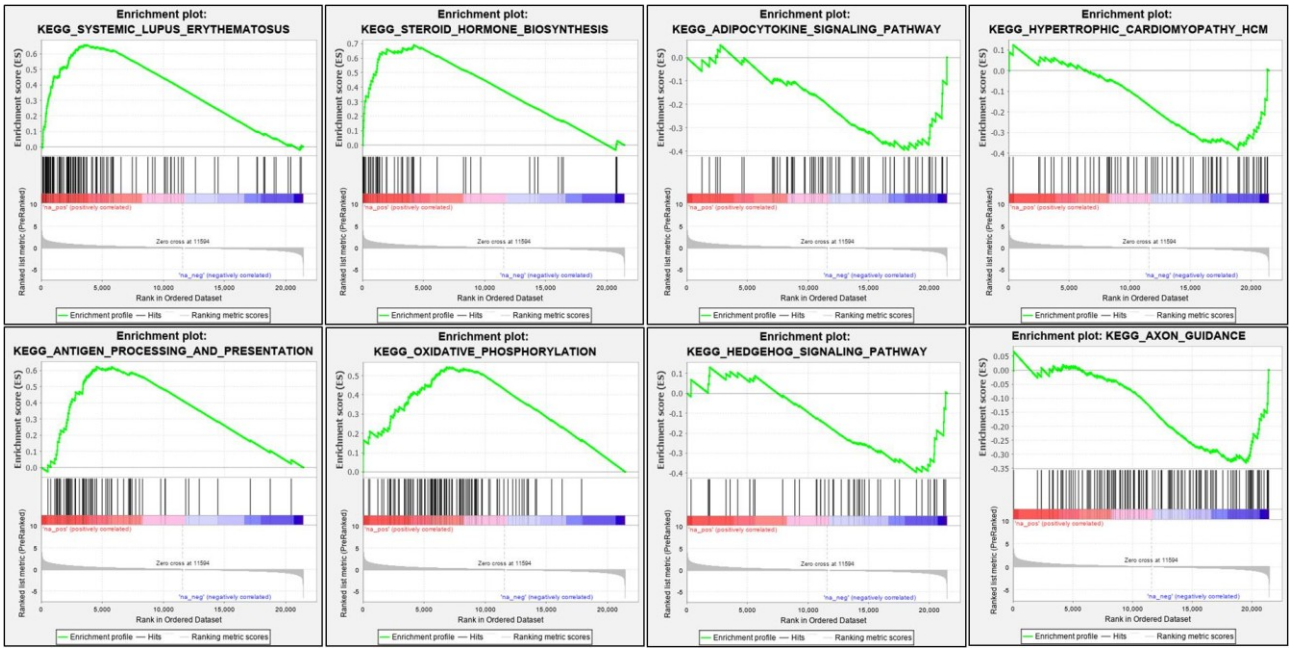

Figure 3.4 GSEA results showing the most relevant KEGG terms enriched in overt GIST vs. miniGIST (gastric cohort). Each plot represents positive enrichments (ES >0, upper panel) and negative enrichments (ES <0, bottom panel) of the gastric DEGs of overt GIST vs. miniGIST contrast. Enrichment Score (ES) is indicated on the left.

The comparison of the miRNome of the overt GISTs vs. miniGISTs identified 70 DEmiRs, 49 up and 21 down in overt GIST.

Functional enrichment analysis results are similar in the miRPath v.3 and PathDIP tools. 45 most statistically significant (p-value<0.01) enriched pathways were found by miRPath tool (Tab. 3.5).

Table 3.5 Gastric GIST DEmiRs: top 10 most significantly enriched KEGG pathways

KEGG pathway	p-value	#Predicted Genes	#DEmiRs
Proteoglycans in cancer	9.80E-12	149	59
Adherens junction	5.25E-08	60	53
ErbB signaling pathway	7.11E-07	71	54
Axon guidance	7.87E-07	90	50
Hippo signaling pathway	1.94E-06	108	50
TGF-beta signaling pathway	2.08E-06	60	46
Rap1 signaling pathway	1.81E-05	149	57
Renal cell carcinoma	1.91E-05	54	47
Fatty acid biosynthesis	2.11E-05	8	16
Pancreatic cancer	2.11E-05	51	46

#Predicted genes: number of genes predicted to be targeted by DEmiRs according to the DIANA tool (microT-CDS). #DEmiRs: number of DEmiRs associated with the indicated pathway. The enrichment was performed by using the union genes method.

Chromosomal enrichment of DEmiRs of the gastric cohort was performed by using MIEAA (miRNA Enrichment Analysis and Annotation). A positive enrichment of chromosomes 1 and X and a negative enrichment of chromosome 14 were observed for overt GIST vs. miniGIST among over- and underexpressed miRNAs, respectively (Tab. 3.6).

Table 3.6 Gastric GIST DEmiRs: chromosome enrichment results

Chromosomal location	Enrichment	p-value	# Observed DEmiRs
Chromosome 1	enriched	0.0144	5
Chromosome 14	depleted	0.0072	5
Chromosome X	enriched	3.50E-07	21

Results of chromosomal mapping enrichment of the DEmiRs identified as differentially expressed in overt GIST vs. miniGIST of the gastric cohort. Enriched: chromosomal location enriched in the overt GIST category; depleted: chromosomal location enriched in the miniGIST category.

3.4. Intestinal GISTs: transcriptome and miRNome profiling

As for the gastric subset, transcriptome and miRNome profiling of the intestinal cohort were analyzed. The transcriptome of overt GISTs compared to that of miniGISTs yielded the identification of 2125 DEGs, of which 1140 up and 985 down in the overt tumors (cutoffs: abs.$\log_2$FC≥0.6, p≤0.05). For about 1/3 of these genes, the p-adj was ≤0.1.

IPA and GSEA functional enrichment analyses highlighted immune response and cell cycle-related pathways as particularly enriched in the overt GIST category (Fig. 3.5).

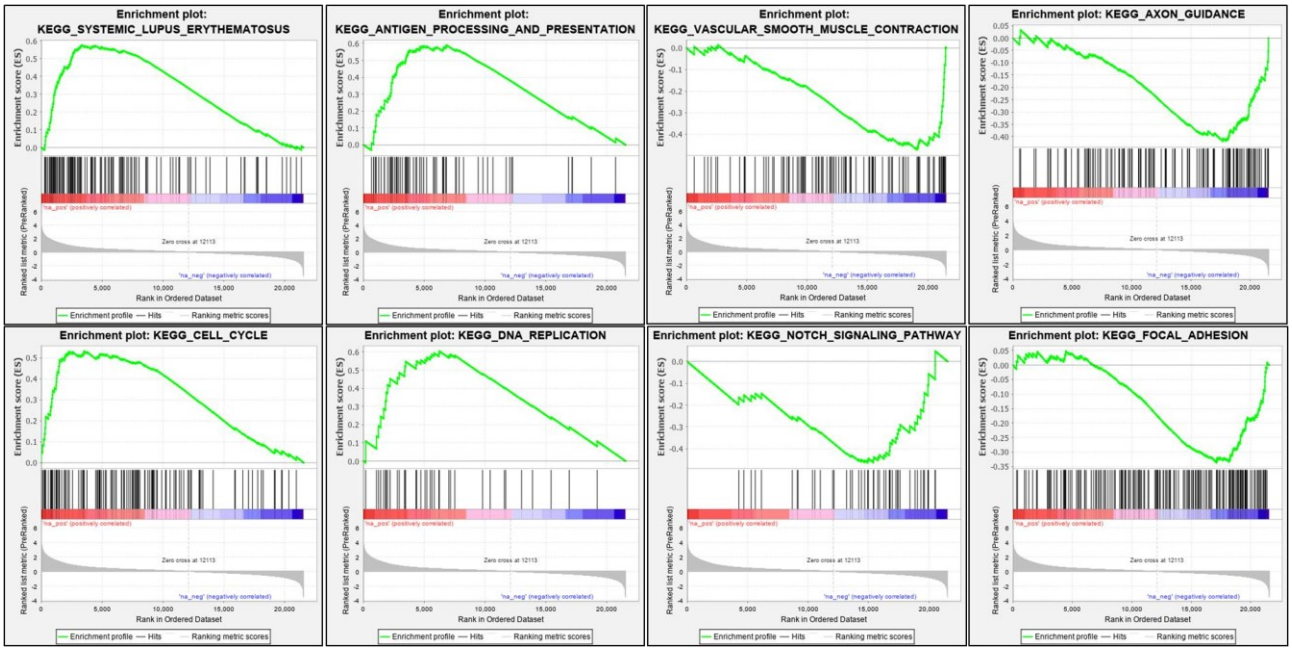

Figure 3.5 GSEA results showing the most relevant KEGG terms enriched in overt GIST vs. miniGIST (intestinal cohort). Each plot represents positive enrichments (ES >0, left panels) and negative enrichments (ES <0, right panels) of intestinal DEGs in the overt GIST vs. miniGIST contrast. Enrichment Score (ES) is indicated on the left.

By the same token of the gastric subset, the comparison of overt GISTs vs. miniGISTs miRNome identified 74 DEmiRs (49 up and 25 down in overt GISTs). Functional enrichment analysis results are reported in Table 3.7.

Table 3.7 Intestinal GIST DEmiRs: top 10 most significantly enriched KEGG pathways

KEGG pathway	p-value	#Predicted genes	#DEmiRs
Proteoglycans in cancer	1.57E-12	149	65
Mucin type O-Glycan biosynthesis	1.86E-09	22	29
ErbB signaling pathway	2.34E-08	73	63
Hippo signaling pathway	9.69E-08	114	58
Pathways in cancer	1.86E-07	274	69
Fatty acid biosynthesis	1.87E-07	11	20
Axon guidance	4.77E-07	93	56
Signaling pathways regulating pluripotency of stem cells	5.61E-07	106	62
Glioma	1.08E-06	51	52
Pancreatic cancer	2.82E-06	53	54

#Predicted genes: number of genes predicted to be targeted by DEmiRs according to the DIANA tool (microT-CDS). #DEmiRs: number of DEmiRs associated with the indicated pathway. The enrichment was performed by using the union genes method.

By interrogating chromosomal position datasets in MIEAA, beside a positive enrichment of chromosome 11 among overexpressed DEmiRs in overt GIST, there was a negative enrichment of chromosomes 14 and 7 among underexpressed DEmiRs in overt GIST vs. miniGIST comparison (Tab. 3.8).

Table 3.8 Intestinal GIST DEmiRs: chromosome enrichment results.

Chromosomal location	Enrichment	p-value	# Observed DEmiRs
Chromosome 11	enriched	0.0423	9
Chromosome 14	depleted	0.0025	3
Chromosome 7	depleted	0.0065	4

Results of chromosomal mapping enrichment of the DEmiRs identified as differentially expressed in overt GIST vs. miniGIST of the intestinal cohort. Enriched: chromosomal location enriched in the overt GIST category; depleted: chromosomal location enriched in the miniGIST category.

3.5. miRNA validation on NanoString platform

To strengthen our miRNA-Seq profiling data we sought to orthogonally validate the results obtained with NGS by using a digital hybridization-based method. To this end, a subset of cases was profiled on the NanoString platform. Twenty-three samples for which we had enough material were analyzed along with the control cell line SK-BR-3 for which miRNA-Seq data were publicly available (see material and methods section for additional information).

3.5.1. Setting of the NanoString validation system

In contrast to NGS profiling, which covers the whole dataset of annotated miRNAs (1917 miRNAs), the NanoString Human v3 panel allows the analysis of only 773 uniquely identified miRNAs. In house NanoString profiling of the SK-BR-3 cell line identified 267/773 miRNAs as expressed above the threshold. These miRNAs were compared to the publicly available SK-BR-3 NGS miRNome. To this end, the FastQ file of the SK-BR-3 cell line was downloaded from the European Nucleotide Archive repository (SRX273666) and processed with GX. Reads were trimmed and aligned to mature miRNA reference sequences (miRBase v.22.1). 793 miRNAs were detected by NGS as having a number of counts per miRNA sequence greater than 5. Of these, 191 miRNAs were detected positive also by the NanoString platform (72% of NanoString positive hits).

Overall, there was a very good agreement in the detection and in the quantification of positive miRNAs in the SK-BR-3 sample by the two platforms (rho: 0.62; p-value: $8.56E^{-22}$) (Fig. 3.6).

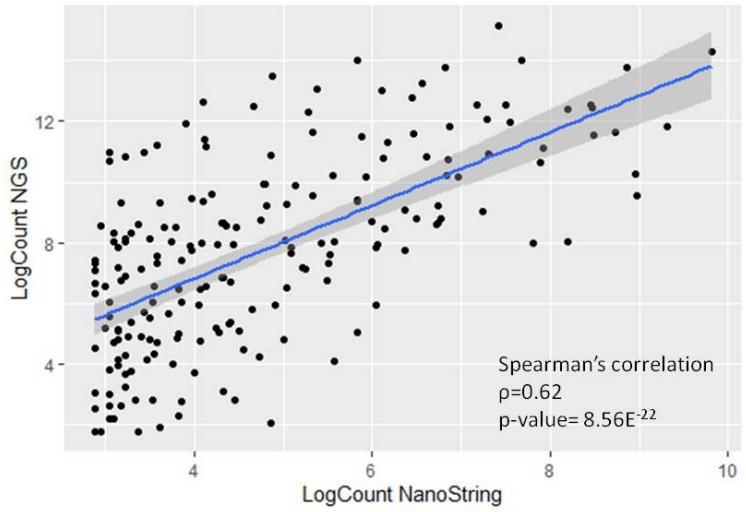

Figure 3.6 Scatter plot representing the Spearman's correlation between NanoString and NGS counts of the miRNAs scoring positive with both platforms.

3.5.2. NanoString validation of DEmiRs

The validation cohort for gastric miRNAs was composed of 12 cases (6 miniGISTs and 6 overt GISTs), 7 KIT and 5 PDGFRA mutated samples. The RCC files obtained from the Digital Analyzer were evaluated by the nSolver 4.0 software for quality controls.

As a first step, a correlation analysis of the counts obtained by the two platforms was performed using the same criteria as used for the control SK-BR-3 cell line. 208 positive miRNAs were recognized by the two platforms, accounting for 60.8% of the 342 positive miRNAs identified by NGS and 65.8% of the 316 positive miRNA identified by NanoString. Spearman's correlation of the 208 positive miRNAs was 0.63 (range per sample 0.53-0.82) ($p<0.0001$).

The validation cohort for intestinal miRNAs was composed of 11 cases (5 miniGISTs and 6 overt GISTs), 6 KIT and 5 non-KIT samples (of these, one overt GIST sample was excluded from the analysis as it failed the ligation check). In this subset, 210 positive miRNAs were identified, accounting for 63.6% of the 330 positive miRNAs in the NGS system and for 54.0% of the 389 positive miRNAs in the NanoString platform. Spearman's correlation of the positive miRNA counts obtained by the two platforms yielded a rho value of 0.61 (range 0.53-0.80) with statistically significance (p-value<0.0001).

Given the different biochemistries and dynamic ranges of the two approaches, the outcomes of NGS and NanoString cannot be compared in a linear manner. Yet, 59% (34/58) miRNAs with a number of counts >5, identified as DE by the NGS approach and included also in the NanoString dataset were coherently identified as DE also by Nanostring (14/20 in the gastric site and 20/38 in the intestinal site) (Tab. 3.9).

Table 3.9 List of the DEmiRs identified in the gastric (left) and in the intestinal (right) sites by NGS and confirmed with NanoString.

DEmiRs	Log_2FC	Chr	Other
hsa-miR-10b-5p	↑	2q31.1	
hsa-miR-196b-5p	↑	7p15.2	
hsa-miR-675-5p	↑	11p15.5	
hsa-miR-148b-3p	↑	12q13.13	
hsa-miR-3613-5p	↑	13q14.2	
hsa-miR-451a	↑	17q11.2	
hsa-miR-301a-3p	↑	17q22	
hsa-miR-424-5p	↑	Xq26.3	
hsa-miR-509-3-5p	↑	Xq27.3	
hsa-miR-514a-3p	↑	Xq27.3	
hsa-miR-891a-5p	↑	Xq27.3	
hsa-miR-382-5p	↓	14q32.31	
hsa-miR-485-5p	↓	14q32.31	
hsa-miR-133a-3p	↓	18q11.2	20q13.33

DEmiRs	Log_2FC	Chr	Other
hsa-miR-194-5p	↑	1q41	
hsa-miR-31-5p	↑	9p21.3	
hsa-miR-146b-5p	↑	10q24.32	
hsa-miR-210-3p	↑	11p15.5	
hsa-miR-483-3p	↑	11p15.5	
hsa-miR-675-5p	↑	11p15.5	
hsa-miR-192-5p	↑	11q13.1	
hsa-miR-21-5p	↑	17q23.1	
hsa-miR-221-3p	↑	Xp11.3	
hsa-miR-28-3p	↓	3q28	
hsa-miR-1271-5p	↓	5q35.2	
hsa-miR-490-3p	↓	7q33	
hsa-miR-23b-3p	↓	9q22.32	
hsa-miR-199b-5p	↓	9q34.11	
hsa-miR-409-5p	↓	14q32.31	
hsa-miR-324-3p	↓	17p13.1	
hsa-miR-497-5p	↓	17p13.1	
hsa-miR-133a-3p	↓	18q11.2	20q13.33
hsa-miR-99b-5p	↓	19q13.41	
hsa-miR-99a-5p	↓	21q21.1	

Chr: chromosomal location of miRNA gene; Other: miRNA gene location of other putative hairpin precursor that gives birth to the same mature miRNA. hsa-miR-514a-3p may be encoded by three distinct genes all mapping to Xq27.3.

In summary, although compared to NGS the NanoString technology clearly has a more limited breath (some miRNAs of potential pathogenic significance in GIST were not covered by NanoString) and is known to perform poorly in the detection of low-abundance miRNA (Knutsen et al., 2013), the results obtained by this platform comparison allowed us to identify a robust set of miRNA validated by both approach.

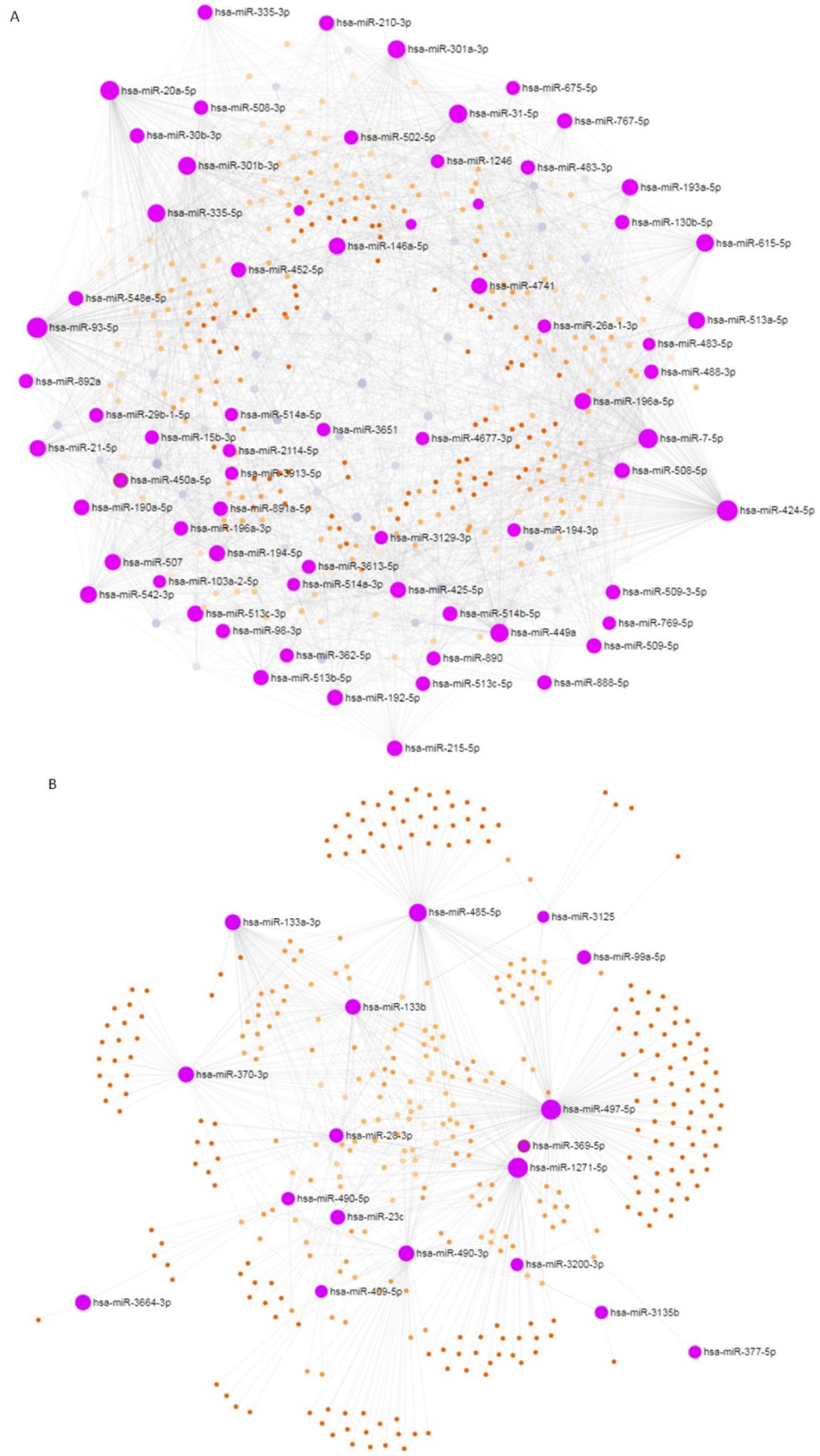

Figure 3.7 mirDIP network analysis illustrating the predicted interactions between DEmiRs and DEGs in the whole cohort. The figure is meant at providing a glimpse of the degree of interconnection between differentially expressed miRNAs and differentially expressed genes. Network analysis of **A)** negative DEGs:positive DEmiRs

interactions (2271 interactions) and **B)** positive DEGs:negative DEmiRs interactions (664 interactions). Purple dots represent DEmiRs; orange and grey dots represent DEGs. The gray edge represent the interaction between the DEmiR and the target DEG. Color and size of the orange and gray dots reflects the degree of the connection between DEmiRs and DEGs and between DEGs and DEGs.

3.6. miRNA target prediction analyses

Target prediction analyses were performed by using the mirDIP 4.1 software, developed by Igor Jurisica, a collaborator of us (Tokar et al., 2018). This tool relies on 30 different sources for miRNAs target prediction databases and identifies the most reliable targets based on the calculation of an integrative score. In addition, mirDIP performs miRNA:mRNA bidirectional search by allowing the upload of both DEmiRs and DEGs of the series in analysis.

Considering that miRNA are best known to affect mRNA biology by promoting their degradation, we sought to focus our attention on the "inverse pair" target predictions, namely genes whose direction in the DE analysis is opposite to that of the cognate miRNAs in the miRNA DE analysis. In other words, we searched for genes whose up/downregulation in overt GIST vs. miniGIST contrast could be justified by reduced/increased expression of a cognate miRNA. In order to get more confident results, we set as cutoffs "high" and "very high" scores of predictions and confirmation by at least two different databases.

In the whole cohort, 2935 target:miRNA predicted interactions were found to satisfy these criteria, among which 664 interactions for gene up:miRNA down and 2271 for gene down:miRNA up (Fig. 3.7). Overall, these predictions covered 81% of DEmiRs (88/109) and, more interestingly, 46% of DEGs (731/1592).

Analyses performed *per* gastric and intestinal sites identified 1656 and 2449 target:miRNA interactions, respectively. Of these, 189 and 715 were predicted to be gene up:miRNA down, and 1467 and 1734 gene down:miRNA up, respectively (Fig. 3.8 and 3.9).

Overall, these predicted interactions covered over 75% of DEmiRs (54/70 of the stomach and 66/74 of the intestine), and over 40% of DEGs (400/996 in the stomach and 572/836 in the intestine).

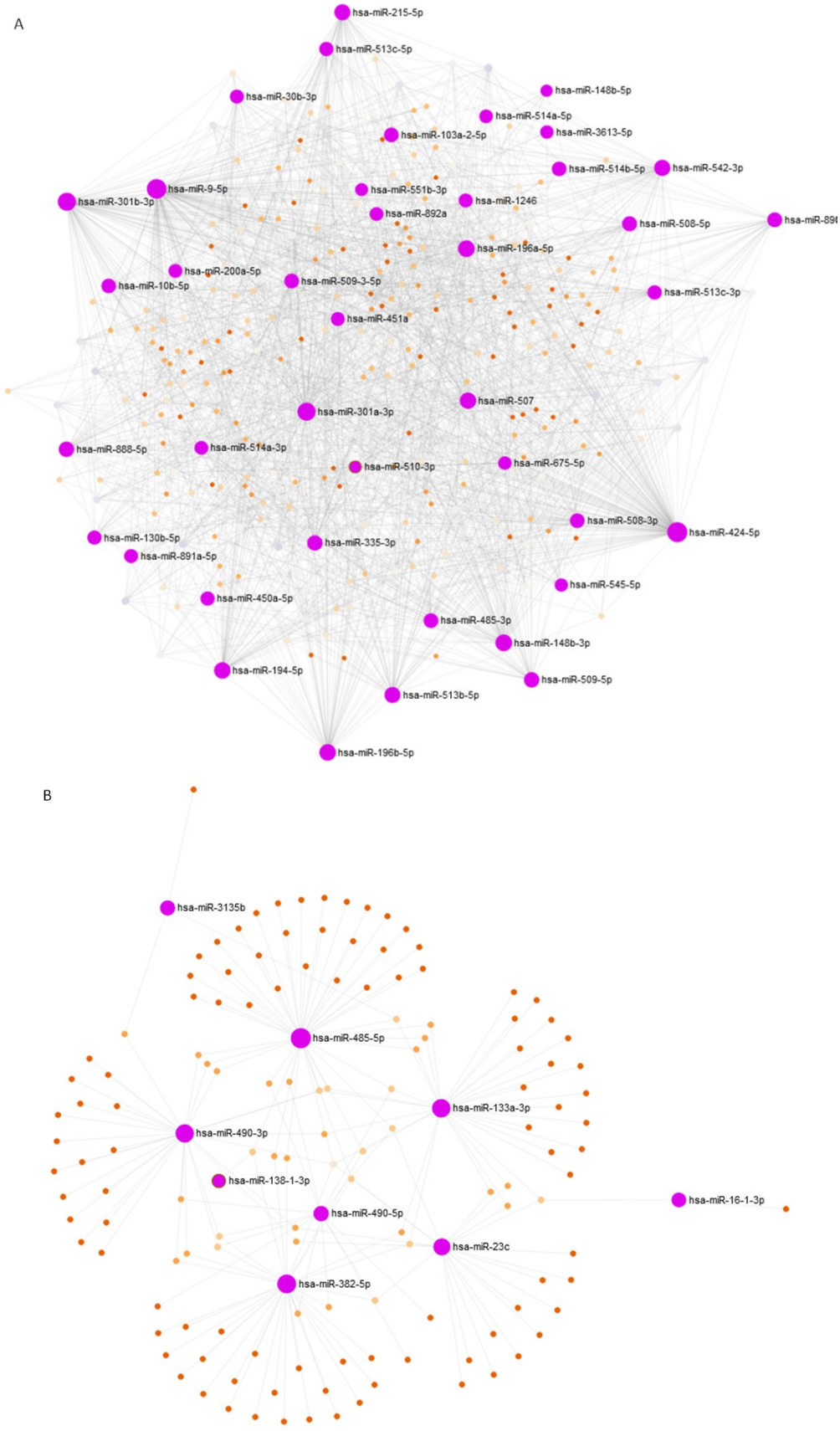

Figure 3.8 mirDIP network analysis illustrating the predicted interactions between DEmiRs and DEGs of the gastric cohort. Network analysis of **A)** negative DEGs:positive DEmiRs interactions (1467 interactions) and **B)** positive DEGs:negative DEmiRs interactions (189 interactions).

Figure 3.9: mirDIP network analysis illustrating the predicted interactions between DEmiRs and DEGs of the intestinal cohort. Network analysis of **A)** negative DEGs:positive DEmiRs interactions (1734 interactions) and **B)** positive DEGs:negative DEmiRs interactions (715 interactions).

3.7. Validation of the approach

hsa-miR-485-5p is a site-shared tumor suppressor miRNA that targets BIRC5

The gathering of all these data was the premise for the identification of miRNA:mRNA pairs involved in GIST malignant evolution. As a first step in this direction, we sought to focus on the DEmiRs located in chromosome regions notoriously involved in GIST pathogenesis and shared by both anatomical sites.

Partial to complete loss of chromosome 14q is frequently detected in both gastric and intestinal GIST (El-Rifai et al., 2000). On these grounds, we focused on the miRNAs downregulated in the overt GIST vs. miniGIST contrast and located in this chromosome region. Seven miRNAs with such features were identified: hsa-miR-369-5p, hsa-miR-370-3p, hsa-miR-377-5p, hsa-miR-409-5p, hsa-miR-485-5p, hsa-miR-494-5p and hsa-miR-889-5p. With the exception of the last two miRNAs, the first five miRNAs were overall potentially responsible for the upregulation of 146 genes.

Among these DEmiRs identified in 14q, hsa-miR-485-5p stand out as the most significantly downregulated in overt GISTs (Log_2FC: -1.47; p-value: 0.0024) (Fig. 3.10A). hsa-miR-485-5p has been reported to act as a tumor suppressor in the progression of other cancers but its role in GIST is still undefined (Chen et al., 2015; Kang et al., 2015; Sun et al., 2015).

hsa-miR-485-5p was predicted to target 95 genes identified as DE in our series. Among these genes, we sought to focus on BIRC5 (Survivin). This gene was not only overexpressed in overt GIST vs. miniGIST of our series (Fig. 3.10B), but it has been recently associated with GIST pathogenesis (Chen et al., 2011; Falkenhorst et al., 2016; Yun et al., 2018). In our cohort, the expression values of the hsa-miR-485-5p and the BIRC5 were inversely correlated with rho value of -0.26 (Fig. 3.10C).

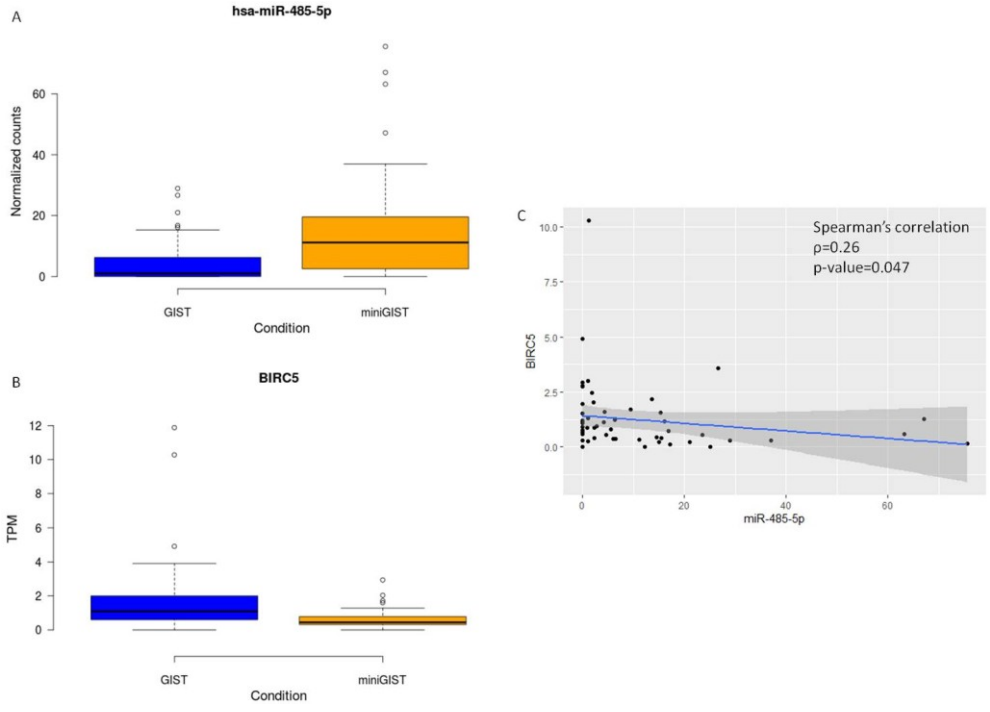

Figure 3.10 Inverse expression of hsa-miR-485-5p and BIRC5. Box plots showing the expression values of **A)** the miRNA and **B)** the gene in GIST and miniGIST groups. **C)** Correlation between the hsa-miR-485-5p and BIRC5 gene expression in the 57 cases that were profiled for both miRNome and transcriptome (matched data).

The predicted binding site of hsa-miR-485-5p lies on the 3'UTR of BIRC5 (pos: 2008-2017, NM_001168.2, BIRC5, transcript variant 1) (Fig. 3.11A). To investigate the effect of hsa-miR-485-5p on endogenous BIRC5, the human fibrosarcoma HT1080 cells were transiently transfected with the hsa-miR-485-5p mimic. Upon ectopic hsa-miR-485-5p expression, a significant reduction of BIRC5, both at the mRNA and the protein level, was observed (Fig. 3.11B-C).

To understand if this effect was determined by the direct binding of miR-485-5p to the BIRC5 3'UTR, we cloned the 3'UTR seed sequence of BIRC5 in a pMIR-eGFP reporter vector. This plasmid was derived from the pMIR-Report^{TM} plasmid by replacing the firefly Luciferase reporter gene with eGFP. This modification was necessary due to the fact that the Luciferase reporter sequence was targeted by our negative control miRNA. Both the 3'UTR wild type and a miR-485-5p binding-defective mutant seed sequence were cloned. The mutant seed sequence was generated in a way to avoid nucleotide perfect complementarity and the G:U imperfect pairing. Cells were then stably transfected with pMIR-eGFP containing the wild type or mutant 3'UTR of BIRC5 and single-cell cloned, in order to ensure a homogeneous expression of the reporter gene. Engineered cells were then transiently transfected with hsa-miR-485-5p mimic and the expression of the eGFP reporter gene was measured by quantitative real-time PCR and Western Blot. hsa-miR-485-5p efficiently affected the expression of the wild type-seed reporter gene while had no relevant effect on the expression of the reporter gene containing mutant hsa-miR-485-5p seed (Fig. 3.11D-E). These findings corroborate the hypothesis of a direct targeting of BIRC5 by hsa-miR-485-5p and suggest that loss of chromosome 14q may contribute to BIRC5 upregulation during GIST progression via hsa-miR-485-5p loss of expression.

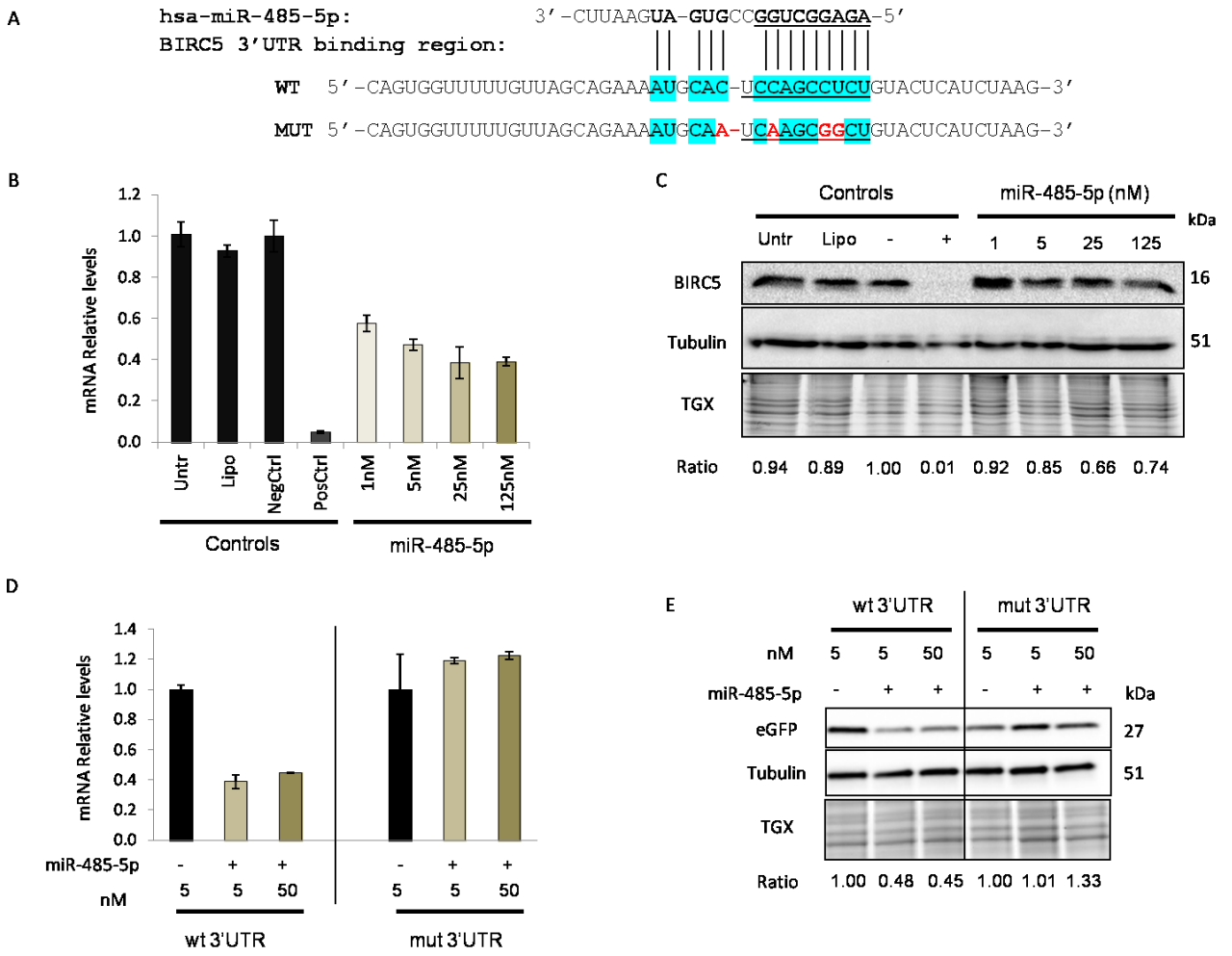

Figure 3.11 hsa-miR-485-5p negatively affects the expression of BIRC5 by binding the 3'UTR. A) Alignment of BIRC5 3'UTR with the hsa-miR-485-5p sequence as provided by microRNA.org. Nucleotides involved in the binding are highlighted in light blue. The sequence of miRNA:mRNA binding is underlined. Nucleotides that have been mutagenized to disrupt the seed between miRNA and 3'UTR are marked in red. **B)** Decrease of BIRC5 mRNA levels in HT1080 cell line upon ectopic delivery of increasing concentration (from 1 to 125 nM) of hsa-miR-485-5p mimic. hsa-miR-542-3p mimic (25 nM) was included as a positive control, as its interaction with BIRC5 is reported in the literature (Althoff et al., 2015). An irrelevant miRNA-like synthetic sequence was used as negative control. **C)** Immunoblots showing the reduction of the BIRC5 protein in the hsa-miR-485-5p mimic transfected cells. TGX gel staining is shown to correct for protein loading. The numbers under the panel indicate BIRC5/(TGX lane) ratio. **D-E)** Reduction of the reporter gene (eGFP) expression (mRNA in D and protein in E) in cells stably expressing the wild type 3'UTR BIRC5 plasmid after transfection with the has-miR-485-5p mimic (5 nM, 50 nM). No significant variation was observed in cells engineered to express the mutant 3'UTR BIRC5 plasmid. TGX gel staining is shown to correct for protein loading.The numbers under the panel indicate eGFP/(TGX lane) ratio. Untr: untransfected; Lipo: cells transfected with lipofectamine only; NegCtrl/"-": Negative Control #1; PosCtrl/"+": positive control (mirVana mimic hsa-miR-542-3p); wt: wild type; mut: mutant.

.

4.Discussion

The work described in this thesis is the piece of a larger project aimed at defining the molecular pathways of transformation of gastrointestinal stromal tumors (GISTs). This project has yielded the identification of NF1 as a key driver tumor suppressor gene in the fraction of GIST devoid of canonical KIT/PDGFRA mutations. The results of this part of the project, to which I contributed, have been reported in these two papers:

1) "Quadruple-negative GIST is a sentinel for unrecognized Neurofibromatosis Type 1 syndrome." Gasparotto D[1], Rossi S[2], Polano M[1], Tamborini E[3], Lorenzetto E[1], Sbaraglia M[2], **Mondello A[1]**, Massani M[4], Lamon S[5], Bracci R[6], Mandolesi A[6], Frate E[7], Stanzial F[8], Agaj J[9], Mazzoleni G[10], Pilotti S[3], Gronchi A[11], Dei Tos AP[2], Maestro R[12]. Clin Cancer Res. 2017 Jan 1;23(1):273-282. DOI: 10.1158/1078-0432.CCR-16-0152. Epub 2016 Jul 7

2) "Neurofibromin C terminus-specific antibody (clone NFC) is a valuable tool for the identification of NF1-inactivated GISTs." Rossi S[1], Gasparotto D[2], Cacciatore M[1], Sbaraglia M[1], **Mondello A[2]**, Polano M[2], Mandolesi A[3], Gronchi A[4], Reuss DE[5,6], von Deimling A[5,6], Maestro R[2], Dei Tos AP[1,7]. Mod Pathol. 2018 Jan;31(1):160-168. DOI: 10.1038/modpathol.2017.105. Epub 2017 Sep 1.

This thesis focuses essentially on the part of the project that deals with the definition of the molecular determinants of GIST malignant progression. The development of a GIST is thought to be preceded by the growth of a premalignant tumor lesion called miniGIST. While GISTs are typically rare, miniGISTs, which share with overt GIST the presence of canonical driver mutations (mostly KIT or PDGFRA), are quite common, being detectable in up to 1/3 of adult individuals (Agaimy et al., 2007). This suggests that these premalignant precursors evolve to GIST only in a minute fraction of cases.

As a first step to clarify the molecular mechanisms that sustain miniGIST to overt GIST malignant evolution we sought to focus on the role of miRNA in transcriptional deregulation. To this end, we performed NGS profiling and compared miRNome and transcriptome profiles of a large set of cases representative of both conditions (miniGIST and overt GIST).

As an introductory section of the discussion, I wish to highlight some technological aspects of this study that I consider represent an added value to our approach. Specifically, while NGS-based transcriptome profiling has become standard in the last years, miRNome profiling in GIST still heavily relies on microarray or qRT-PCR-based technologies (Haller et al., 2010; Kelly et al., 2013; Subramanian et al., 2008). Over these methods, NGS-based miRNA profiling offers a number of advantages. In particular, being a digital approach, NGS features a higher sensitivity and a wider linear range of detection over array-based assays; NGS is less prone to sequence bias and hence shows higher accuracy in distinguishing very similar miRNAs sequences (e.g. clustered miRNAs or isomiRs); finally, NGS allows for the identification of novel, un-annotated miRNAs (Pritchard et al., 2012).

Also, the choice of validating positive hits through an orthogonal high-throughput digital approach (NanoString) I consider to be a plus, as it represents a sample and time-saving approach (compared to single hit validation) yielding at the same time an absolute quantification.

This study highlighted a relevant impact of tumor location and type of driver mutation on gene and miRNA expression profile, with a tendency for gastric vs. intestinal tumors and for KIT vs. non-KIT tumors to cluster separately. Previous reports have described the influence of these factors on GIST gene expression profile (Antonescu et al., 2004; Haller et al., 2007, 2010). Our work complements these observations by pinpointing that this dichotomy occurs very early, being detectable also in miniGIST.

Surprisingly, compared to the site of origin and type of mutation driver, the nature of the lesion (benign vs. malignant) seems to affect the global transcriptome at a lesser degree. Instead, elements of separation for miniGIST and overt GIST, especially for the tumors of the gastric site, emerged from the analysis of the miRNome. Although preliminary, these results suggest that the deregulation of miRNAs could play a significant role as a trigger in the malignant progression of miniGIST.

Differential expression analyses highlighted an important involvement of cell cycle, metabolism and immune system in overt GIST, suggesting that miniGIST evolution is paralleled by a metabolic rewiring and gain of immunogenicity of the tumor. *Vice versa*, KEGG terms related to axon guidance, myogenic differentiation, and Notch signaling turned out to be overrepresented in miniGIST, supporting a progressive loss of myogenic/neural features during GIST progression.

The myogenic DMD (dystrophin) gene, recently claimed to play a tumor-suppressive function in GIST (Wang et al., 2014), was significantly downregulated in overt GIST vs. miniGIST contrast, supporting the notion that GIST evolution is paralleled by an attenuation of a myogenic differentiation program.

The Notch signaling has been reported to provide either oncogenic or tumor-suppressive signals, depending on the context. Also in sarcomas, the Notch pathway seems to play a Janus-faced role, with pro-tumorigenic or anti-tumorigenic activity in different sarcoma subtypes (Ban et al., 2014; Conti et al., 2016). In the context of neural cells, Notch loss has been shown to synergize with receptor tyrosine kinase signaling, namely PDGF (Giachino et al., 2015). The cell of origin of GIST, interstitial cells of Cajal, are a very peculiar cell type with pacemaker functions and mixed neuronal and myoid features (Sanders et al., 2014). Thus, it is tempting to speculate that inhibition of Notch signaling may sustain the malignant progression of receptor tyrosine kinase (KIT or PDGFRA)-driven miniGIST.

Notch establishes a close connection with the Hedgehog (HH) pathway (Chatterjee and Sil, 2019), which turned out to be overrepresented in the miniGIST of the stomach. HH signaling has been reported to induce immune exclusion (Hanna et al., 2019). Thus, the activation of this pathway might create a permissive, immune-tolerant milieu conductive to oncogenesis. Moreover, a recent work described a mouse model in which HH activation results in the induction of GIST-like tumors in which activation of PDGFRA signaling facilitates tumorigenesis (Pelczar et al., 2013). Thus, the activation of the HH pathway could represent an early trigger of the transformation of gastric Cajal cells.

Focusing on the miRNome, differential expression and functional annotation analyses revealed that the miRNAs identified as correlated to miniGIST to overt GIST evolution were widely

involved in cancer-related pathways. More importantly, the integration of transcriptome and miRNome profiling allowed the identification of alleged miRNA:mRNA pairs. Intriguingly, over 40% of the transcripts detected as differentially expressed were putatively targeted by differentially expressed miRNAs. This result is in line with literature data according to which about half of the transcriptome is regulated by miRNAs (Bartel, 2009; Jansson and Lund, 2012).

Several miRNAs detected as differentially expressed mapped to chromosome regions previously associated with GIST pathogenesis. Namely, about 1/3 of miRNA whose expression was reduced in overt GIST compared to miniGIST mapped to chromosome 14q, notoriously lost in GIST (El-Rifai et al., 2000). This result corroborates the relevance of this chromosome region in GIST progression and adds weight to the hypothesis that chromosome imbalances mirror the presence not only of coding genes but also miRNAs implicated in GIST malignant evolution. Intriguingly, some of the miRNAs mapping to this region and indentified by our study as differentially expressed in overt GIST vs. miniGIST comparison had been previously suggested to be potentially implicated in GIST pathogenesis. In particular, miRNA located in 14q and lost in miniGIST to overt GIST evolution, such as hsa-miR-369-5p, hsa-miR-409-5p and hsa-miR-494-5p, whose mRNA targets are involved in cell cycle and MAPK pathways (IGF1R, MAPK1, CDK6 and HDAC genes) had been shown to be negatively associated to high-risk tumors (Choi et al., 2010). Moreover, miRNAs that we identified as differentially expressed in overt GIST vs. miniGIST comparison, among which hsa-miR-133a-3p, hsa-miR-133b, hsa-miR-301a-3p, hsa-miR-483-5p and hsa-miR-490-3p, had been previously found as differentially expressed in GIST vs. GIST adjacent normal tissue contrast (Gyvyte et al., 2017).

As a first step toward validation of the DEmiRs identified as possibly implicated in GIST progression and mapping to 14q, we focused on hsa-miR-485-5p (14q32.31). The differential expression of this miRNA was also corroborated by NanoString profiling. hsa-miR-485-5p has been predicted to target, among others, the BIRC5 gene, a member of the Inhibitor of Apoptosis (IAP) protein family. BIRC5 was among the genes that we identified as differentially expressed in overt GIST vs. miniGIST and a role for BIRC5 in KIT regulation has been recently suggested (Yun et al., 2018).

The BIRC5-encoded protein, aka survivin, is considered a multitasking factor implicated not only in cell survival but also in cell division and in microtubule assembly (Altieri, 2015; Wheatley and Altieri, 2019). Specifically, BIRC5 participates in the chromosome passage protein complex (CPC) involved in chromosome alignment and segregation during mitosis. BIRC5 is highly expressed during fetal development but is physiologically repressed in normal adult tissues. Augmented expression of BIRC5 is reported for a broad range of human malignancies, where it has been linked to tumor aggressiveness, chromosomal instability, angiogenesis and resistance to therapies (Altieri, 2015; Hingorani et al., 2013; Hirano et al., 2015; Li S. et al., 2017; Wang et al., 2018; Zhou et al., 2018).

Here, we report that BIRC5 overexpression in overt GIST is mediated, at least in part, by a miR-485-5p-mediated regulation. Specifically, we provided evidence that ectopic expression of hsa-miR-485-5p negatively affects BIRC5 mRNA levels in a dose-dependent manner. Moreover,

reporter assays indicated that this effect relies on an intact miR-485-5p binding site on BIRC5 3'UTR, supporting a direct targeting of the messenger. Intriguingly, we observed a trend toward reduced cell survival after miR-485-5p delivery in HT-1080 human fibrosarcoma cells, although this result needs further experimental validations. Taken together, our data suggest that BIRC5 overexpression may contribute to miniGIST to overt GIST evolution as a result of the loss of a chromosome region (14q) harboring a key epigenetic negative regulator (miR-485-5p).

Clearly, the hsa-miR-485-5p:BIRC5 axis here described represents just the tip of an iceberg, i.e. a convoluted regulatory network that connects miRNAs and coding genes and that sustains tumor progression. Our integrated analysis of gene expression and miRNA-mediated epigenetic regulation just laid down the basis for unrevealing the role of miRNAs as triggering players of miniGIST to overt GIST evolution. The untangling of these networks will be the object of further investigations.

5. Materials and methods

5.1 Case series

Samples were retrieved from the Department of Pathology and Molecular Genetics of Treviso General Hospital (TV, Italy) and from the Centro di Riferimento Oncologico di Aviano (CRO IRCCS) (Aviano, PN Italy) biobanks. Specimens were collected between 1993 and 2018 and were almost all formalin-fixed paraffin-embedded (FFPE), with the exception of 13 cases that were fresh frozen (FF). Of 91 cases collected, five yielded poor quality RNA-Seq libraries and were then excluded from transcriptome analysis.

5.2 RNA extraction

FFPE tissues were dewaxed by using the Qiagen deparaffinization solution. Total RNA was then recovered by using the Ambion RecoverAll Nucleic Acid isolation kit, according to the manufacturer's instructions (ThermoFisher Scientific). For FF tissues RNA extraction was performed by using EZ1 biorobot (Qiagen) and the EZ1 RNA Tissue Mini kit (Qiagen).

RNA was quantified by a fluorimetric method on the Qubit instrument (Qubit RNA Assay Kit, Invitrogen). The RNA quality was assessed by Agilent 2200 TapeStation electrophoresis (RNA Assay Kit, Agilent Technologies).

RNA from cell lines was extracted by using Qiagen miRNeasy Mini Kit (Qiagen), and the RNA yield was measured by using the NanoDrop1000D spectrophotometer (ThermoFisher Scientific).

5.3 RNA profiling and data processing

RNA (250 to 1000 ng) was used to prepare TruSeq stranded total RNA libraries, according to Illumina guidelines (https://emea.support.illumina.com/documentation.html) (Illumina). Briefly, RNA was treated with RiboZero Deplete and Fragment RNA reagents, then double-stranded cDNAs were synthesized. After adenylation of the 3' end and adapter indices ligation, the libraries were then amplified and quality and quantity assessed. Next libraries were diluted to the same concentration and pooled, to a final overall concentration of 2 nM. Size, purity and concentration of the final pools were evaluated by using the Agilent 2200 TapeStation instrument with TapeStation High Sensitivity D1000 kit (Agilent Technologies) and Qubit fluorometer with the Qubit DNA High Sensitivity assay (Invitrogen). Validated pools were finally run on an Illumina HiSeq 1500 instrument, by using the HiSeq Rapid PE Cluster kit v2 (50 cycles) (Illumina).

FastQ files obtained from the sequencing were uploaded onto the Illumina BaseSpace Hub, trimmed, aligned and quantified by using STAR (Dobin et al., 2013) and Salmon (Patro et al., 2017) algorithms. DEseq2 pipeline (Love et al., 2014) on R (version 3.6) was used for the identification of differentially expressed genes. PCAs were built by using the top 500 genes with the highest variance. The reference genome used for all the analyses was the Genome Reference Consortium Human Built 37 (GRCh37, hg19).

5.4 miRNA profiling and data processing

miRNA profiling was performed by using two different technologies: Next Generation Sequencing (NGS) on an Illumina MiSeq platform for discovery and NanoString probe hybridization for validation. Only a subset of cases profiled with NGS was selected for NanoString validation.

5.4.1 miRNA profiling by sequencing (NGS)

RNA (300 to 1500 ng) was used as input for ribosomal RNA (rRNA) depletion performed with the RiboZero rRNA removal kit (Human/Mouse/Rat) (Illumina). The depleted RNA was then used for miRNA library preparation with the TruSeq smallRNA Library preparation kit (Illumina) (https://emea.support.illumina.com/documentation.html). according to the manufacturer's instructions Briefly, adapters were ligated to the 3' and 5' end of rRNA-depleted RNA. Then libraries are reverse transcribed, indexed and amplified. Afterward, cDNA libraries with unique indexes were pooled, size-fractionated by gel electrophoresis on a 6% Novex TBE gel (Life technologies), and purified by gel excision (range 160-145bp corresponding to 22 nt and 30 nt long miRNAs). After ethanol precipitation and resuspension, size, purity and concentration of the final pools were evaluated by using the Agilent 2200 TapeStation instrument with TapeStation High Sensitivity D1000 kit (Agilent Technologies) and Qubit fluorometer with the Qubit DNA High Sensitivity assay (Invitrogen). Validated pooled libraries were sequenced on a MiSeq Illumina platform, by using the MiSeq Reagent kit v3 (150 cycles) (Illumina).

Data obtained from miRNA sequencing were subsequently analyzed by using the CLC Genomic Workbench 12 (GX) tool from Qiagen Bioinformatics (http://www.qiagenbioinformatics.com).

The standard workflow for smallRNA included adapter trimming, alignment to the reference (miRBase version 22.1) and differential expression analysis. PCAs for miRNA were built by using the top 100 miRNAs with the highest variance.

miRNA expression profiling of the SK-BR-3 cell line was available on the European Nucleotide Archive repository of the European Bioinformatics Institute (accession number: SRX273666). These data were provided by Knutsen and colleagues (Knutsen et al., 2013). The corresponding FastQ was analyzed by using the CLC Biomedical Genomics Workbench tool. Reads were trimmed and aligned to mature miRNA reference sequence (miRBase version 22.1) for the comparison with the NanoString technology.

5.4.2 miRNA profiling by hybridization (NanoString)

A subset of samples of the discovery cohort was chosen for orthogonal validation with the NanoString assay. Cases were selected on the basis of availability and quality of RNA.

For quality check, we assessed the RNA integrity (% of RNA>300 bp) with the Agilent TapeStation instrument; contamination from DNA and proteins (ratio of absorbance A260/A280

and A260/A230) was determined with a NanoDrop1000D spectrophotometer (ThermoFisher Scientific).

A small amount of total RNA (100 ng) of selected samples was processed for miRNA NanoString profiling on a nCounter instrument (Human v3 miRNA Expression Assay, NanoString Technologies). Shortly, 100ng of total RNA was ligated with a miRTag in order to elongate the RNA fragment and then hybridized overnight with miRNA sequence-specific probes. Afterward, magnetic-bead-based purification and electrophoresis steps were carried out on a Prep-Station. Finally, the Digital Analyzer instrument counted the number of probes and associates each detected barcode to the sequence-specific associated miRNA, thus providing an absolute miRNA quantification.

NanoString data obtained from the Digital Analyzer were analyzed by using nSolver 4.0 software (https://www.nanostring.com/products/analysis-software/nsolver) for runs quality control and quantification. The NanoStringDiff Bioconductor R package was used for differential expression analysis (Wang et al., 2016).

5.5 Tertiary bioinformatics data analysis

Differentially expressed genes (DEGs) and differentially expressed miRNAs (DEmiRs) were interrogated for functional analyses and miRNA target prediction.

Functional enrichment analyses of DEGs were performed by using Ingenuity Pathway Analysis (IPA®) (Qiagen Bioinformatics, www.qiagenbioinformatics.com), and Gene Set Enrichment Analysis (GSEA) from Broad Institute (pre-ranked analysis), using the KEGG (Kyoto Encyclopedia of Genes and Genome) dataset (Mootha et al., 2003; Subramanian et al., 2005). Analyses were performed by using genes with p-value≤0.05 (GSEA) and genes with abs.$\log_2$FC≥0.6 and p-value≤0.05 (IPA).

miRNA functional enrichment analyses were performed by using mirPath v.3 (Vlachos et al., 2015) and PathDIP (Rahmati et al., 2017) for KEGG pathways analyses. miRNA enrichment analysis and annotation (MIEAA) was interrogated for chromosomal enrichment (Backes et al., 2016) DEmiRs with abs.$\log_2$FC≥0.6 and p-value≤0.05 were used for these analyses. Target prediction of DEmiRs among DEGs (abs.$\log_2$FC≥0.6 and p-adj≤0.1) were performed using mirDIP version 4.1 (Tokar et al., 2018). “High” and “very high” scores for prediction and call from at least 2 sources were set as cutoffs.

NetworkAnalyst was used to build the network among DEmiRs and predicted targets among DEGs (Zhou et al., 2019).

5.6 Cell cultures and reagents

The human fibrosarcoma HT1080 (ATCC: CCL-121) cell line was cultured in Dulbecco’s Modified Eagle’s Medium (DMEM) (Gibco, ThermoFisher Scientific) plus 10% Fetal Bovine Serum (FBS) (Gibco, ThermoFisher Scientific). The human breast cancer SK-BR-3 (ATCC: HTB-30) cell line

was cultured in Minimum Essential Medium-α (MEM-A) (Gibco, ThermoFisher Scientific) with 10% FBS. Cells were maintained at 37°C with 5% CO_2.

Transfection was carried out with Lipofectamine RNAiMax (Life Technologies), mirVana Mimics and Negative Control #1 (ThermoFisher Scientific) at scalar concentrations. Cells (lipofectamine only, negative control #1, miRNA mimics) were harvested 48 hours post transfection.

The full sequence of wild type 3' UTR of BIRC5 was cloned into the pMIR-Report system (primer sequences, forward: TCTATCGAACTAGTTTCAAATTAGATGTTCAACTGTGCTC; reverse: TAGGATCTAAGCTTAGTGAAGTATCCATTTACAGACTGACAC).

A mutant 3'UTR for the seed sequence of hsa-miR-485-5p was created by using the following primers: forward: GGTTTTTGTTAGCAGAAAATGCAATCAAGCGGCTGTACTCATCTAAGC; reverse: GCTTAGATGAGTACAGCCGCTTGATTGCATTTTCTGCTAACAAAAACC. The Luciferase reporter gene was excised with BamHI and XhoI restriction enzymes to be replaced by the eGFP sequence derived from pLPC-eGFP. All plasmid sequences were verified by Sanger sequencing. Stable expression of pMIR-eGFP reporter vectors (wild type and mutant) in HT1080 was achieved by using Puromicin antibiotic selection (0.5 μg/mL) (Sigma Aldrich). Single-cell clones were expanded and selected for having comparable eGFP expression levels. These cell models were transfected with mirVana Mimics and Negative Control #1 (ThermoFisher Scientific) at 5nM and 50nM and the reporter expression was assessed at 48 hours post transfection.

5.7 Quantitative Real-Time PCR and Western Blot

RNA was extracted from cells, and then 0.5-1 ug of RNA were retro-transcribed to cDNA using the Superscript III reverse transcriptase (Invitrogen), according to standard protocol. Real-Time PCR (qRT-PCR), carried out with the SsoFast EvaGreen Supermix (BioRad), was performed by using a 1:10 dilution of the cDNA. Primer sequences are listed in Table 5.1.

Relative expression levels were normalized to the mean values of two housekeeping genes (B2M and GAPDH) by using the comparative Ct (ΔΔCt) method and the Bio-Rad CFX manager software.

Table 5.1: Primers used in qRT-PCR.

	Forward	Reverse
BIRC5	CGGAGCGGATGGCCGA	ATGGGGTCGTCATCTGGCTCC
eGFP (used for 3'UTR reporter assays)	CAAGGACGACGGCAACTACAA	GTAGTTGTACTCCAGCTTGTGCC
B2M	TGCTGTCTCCATGGTTTGATGTAT	TCTCTGCTCCCCACCTCTAAGT
GAPDH	GAAGGTGAAGGTCGGAGT	GAAGATGGTGATGGGATTTC

B2M: β-2 microglobulin, GAPDH: glyceraldehyde 3-phosphate dehydrogenase

For protein analyses, cells were lysed in RIPA Buffer (Santa Cruz), supplemented with complete protease inhibitors cocktails (Roche Diagnostic GmbH), pefabloc (Roche Diagnostics), sodium orthovanadate and sodium fluoride (Sigma Aldrich).

Protein lysates were resolved by SDS-PAGE on TGX stain-free gels (BioRad) and were transferred onto nitrocellulose membranes (Sartorius Stedim Biotech GmbH). Membranes were incubated with primary antibodies overnight at 4°C; after washing in TBST (137 mM NaCl, 10 mM Tris HCl pH 7.5, Tween 0.1%), blots were incubated with the proper secondary antibody for 90 minutes at room temperature. Antibodies used were the follows: anti-BIRC5 (1:1000) (Abcam), anti-eGFP (1:1000) (Covance), anti-Tubulin (1:10000) (Sigma Aldrich), anti-mouse (1:1000) (Abcam), anti-rabbit (1:1000) (Santa Cruz).

Detection was carried out with the Western Lightning Plus-ECL reagent (Perkin Elmer). Protein expression analyses were performed with a Chemidoc Imaging System (BioRad) and the Image-Lab software was used for image analysis.

6. References

Agaimy, A., Wünsch, P.H., Hofstaedter, F., Blaszyk, H., Rümmele, P., Gaumann, A., Dietmaier, W., and Hartmann, A. (2007). Minute gastric sclerosing stromal tumors (GIST tumorlets) are common in adults and frequently show c-KIT mutations. Am. J. Surg. Pathol. *31*, 113–120.

Agaimy, A., Terracciano, L.M., Dirnhofer, S., Tornillo, L., Foerster, A., Hartmann, A., and Bihl, M.P. (2009). V600E BRAF mutations are alternative early molecular events in a subset of KIT/PDGFRA wild-type gastrointestinal stromal tumours. J. Clin. Pathol. *62*, 613–616.

Althoff, K., Lindner, S., Odersky, A., Mestdagh, P., Beckers, A., Karczewski, S., Molenaar, J.J., Bohrer, A., Knauer, S., Speleman, F., et al. (2015). miR-542-3p exerts tumor suppressive functions in neuroblastoma by downregulating Survivin: miR-542-3p in neuroblastoma. Int. J. Cancer *136*, 1308–1320.

Altieri, D.C. (2015). Survivin – The inconvenient IAP. Semin. Cell Dev. Biol. *39*, 91–96.

Alvarez-Garcia, I. (2005). MicroRNA functions in animal development and human disease. Development *132*, 4653–4662.

American Association for Cancer Research (2019). Olaratumab for STS Disappoints in Phase III. Cancer Discov. *9*, 312.2-313.

Antonescu, C.R. (2006). Gastrointestinal stromal tumor (GIST) pathogenesis, familial GIST, and animal models. Semin. Diagn. Pathol. *23*, 63–69.

Antonescu, C.R., Viale, A., Sarran, L., Tschernyavsky, S.J., Gonen, M., Segal, N.H., Maki, R.G., Socci, N.D., DeMatteo, R.P., and Besmer, P. (2004). Gene Expression in Gastrointestinal Stromal Tumors Is Distinguished by KIT Genotype and Anatomic Site. Clin. Cancer Res. *10*, 3282–3290.

ASCO Annual Meeting (2019). ANNOUNCE prompts questions over the Accelerated Approval process. Nat. Rev. Clin. Oncol. *16*, 459–459.

Backes, C., Khaleeq, Q.T., Meese, E., and Keller, A. (2016). miEAA: microRNA enrichment analysis and annotation. Nucleic Acids Res. *44*, W110–W116.

Ban, J., Aryee, D.N.T., Fourtouna, A., van der Ent, W., Kauer, M., Niedan, S., Machado, I., Rodriguez-Galindo, C., Tirado, O.M., Schwentner, R., et al. (2014). Suppression of Deacetylase SIRT1 Mediates Tumor-Suppressive NOTCH Response and Offers a Novel Treatment Option in Metastatic Ewing Sarcoma. Cancer Res. *74*, 6578–6588.

Bannon, A.E., Klug, L.R., Corless, C.L., and Heinrich, M.C. (2017). Using molecular diagnostic testing to personalize the treatment of patients with gastrointestinal stromal tumors. Expert Rev. Mol. Diagn. *17*, 445–457.

Bartel, D.P. (2004). MicroRNAs. Cell *116*, 281–297.

Bartel, D.P. (2009). MicroRNAs: Target Recognition and Regulatory Functions. Cell *136*, 215–233.

Bauer, S., George, S., Kang, Y.-K., Tap, W.D., Zhou, T., Picazio, N., Boral, A.L., and Heinrich, M. (2018). 1662TiPVOYAGER: An open-label, randomised, phase III study of avapritinib vs regorafenib in patients (pts) with locally advanced (adv) metastatic or unresectable gastrointestinal stromal tumour (GIST). Ann. Oncol. *29*.

Bernstein, E., Caudy, A.A., Hammond, S.M., and Hannon, G.J. (2001). Role for a bidentate ribonuclease in the initiation step of RNA interference. Nature *409*, 363–366.

Bohnsack, M.T. (2004). Exportin 5 is a RanGTP-dependent dsRNA-binding protein that mediates nuclear export of pre-miRNAs. RNA *10*, 185–191.

Brenca, M., Rossi, S., Polano, M., Gasparotto, D., Zanatta, L., Racanelli, D., Valori, L., Lamon, S., Dei Tos, A.P., and Maestro, R. (2016). Transcriptome sequencing identifies ETV6-NTRK3 as a gene fusion involved in GIST. J. Pathol. *238*, 543–549.

Cajal, S.R. (1911). Histologie du système nerveux de l'homme et des vertébrés. Histol. Système Nerv. L'homme Vertébrés *Paris: Maloine*, 891–942.

Calin, G.A., Dumitru, C.D., Shimizu, M., Bichi, R., Zupo, S., Noch, E., Aldler, H., Rattan, S., Keating, M., Rai, K., et al. (2002). Nonlinear partial differential equations and applications: Frequent deletions and down-regulation of micro- RNA genes miR15 and miR16 at 13q14 in chronic lymphocytic leukemia. Proc. Natl. Acad. Sci. *99*, 15524–15529.

Calin, G.A., Sevignani, C., Dumitru, C.D., Hyslop, T., Noch, E., Yendamuri, S., Shimizu, M., Rattan, S., Bullrich, F., Negrini, M., et al. (2004). Human microRNA genes are frequently located at fragile sites and genomic regions involved in cancers. Proc. Natl. Acad. Sci. *101*, 2999–3004.

Carthew, R.W., and Sontheimer, E.J. (2009). Origins and Mechanisms of miRNAs and siRNAs. Cell *136*, 642–655.

Casali, P.G., Abecassis, N., Bauer, S., Biagini, R., Bielack, S., Bonvalot, S., Boukovinas, I., Bovee, J.V.M.G., Brodowicz, T., Broto, J.M., et al. (2018). Gastrointestinal stromal tumours: ESMO–EURACAN Clinical Practice Guidelines for diagnosis, treatment and follow-up†. Ann. Oncol. *29*, iv68–iv78.

Casella, C., Villanacci, V., D'adda, F., Codazzi, M., and Salerni, B. (2012). Primary Extra-gastrointestinal Stromal Tumor of Retroperitoneum. Clin. Med. Insights Oncol. *6*, CMO.S9180.

Catalanotto, C., Cogoni, C., and Zardo, G. (2016). MicroRNA in Control of Gene Expression: An Overview of Nuclear Functions. Int. J. Mol. Sci. *17*, 1712.

Charo, L.M., Burgoyne, A.M., Fanta, P.T., Patel, H., Chmielecki, J., Sicklick, J.K., and McHale, M.T. (2018). A Novel *PRKAR1B-BRAF* Fusion in Gastrointestinal Stromal Tumor Guides Adjuvant Treatment Decision-Making During Pregnancy. J. Natl. Compr. Canc. Netw. *16*, 238–242.

Chatterjee, S., and Sil, P.C. (2019). Targeting the crosstalks of Wnt pathway with Hedgehog and Notch for cancer therapy. Pharmacol. Res. *142*, 251–261.

Chen, H., Hirota, S., Isozaki, K., Sun, H., Ohashi, A., Kinoshita, K., O'Brien, P., Kapusta, L., Dardick, I., Obayashi, T., et al. (2002). Polyclonal nature of diffuse proliferation of interstitial cells of Cajal in patients with familial and multiple gastrointestinal stromal tumours. Gut *51*, 793–796.

Chen, H., Ördög, T., Chen, J., Young, D.L., Bardsley, M.R., Redelman, D., Ward, S.M., and Sanders, K.M. (2007). Differential gene expression in functional classes of interstitial cells of Cajal in murine small intestine. Physiol. Genomics *31*, 492–509.

Chen, W.-B., Cheng, X.-B., Ding, W., Wang, Y.-J., Chen, D., Wang, J.-H., and Fei, R.-S. (2011). Centromere protein F and survivin are associated with high risk and a poor prognosis in colorectal gastrointestinal stromal tumours. J. Clin. Pathol. *64*, 751–755.

Chen, Y., Tzeng, C.-C., Liou, C.-P., Chang, M.-Y., Li, C.-F., and Lin, C.-N. (2004). Biological Significance of Chromosomal Imbalance Aberrations in Gastrointestinal Stromal Tumors. J. Biomed. Sci. *11*, 65–71.

Chen, Z., Li, Q., Wang, S., and Zhang, J. (2015). miR-485-5p inhibits bladder cancer metastasis by targeting HMGA2. Int. J. Mol. Med. *36*, 1136–1142.

Chetty, R., and Serra, S. (2016). Molecular and morphological correlation in gastrointestinal stromal tumours (GISTs): an update and primer. J. Clin. Pathol. *69*, 754–760.

Chibon, F., Lagarde, P., Salas, S., Pérot, G., Brouste, V., Tirode, F., Lucchesi, C., de Reynies, A., Kauffmann, A., Bui, B., et al. (2010). Validated prediction of clinical outcome in sarcomas and multiple types of cancer on the basis of a gene expression signature related to genome complexity. Nat. Med. *16*, 781–787.

Choi, H.-J., Lee, H., Kim, H., Kwon, J.E., Kang, H.J., You, K.T., Rhee, H., Noh, S.H., Paik, Y.-K., Hyung, W.J., et al. (2010). MicroRNA expression profile of gastrointestinal stromal tumors is distinguished by 14q loss and anatomic site. Int. J. Cancer *126*, 1640–1650.

Conti, B., K. Slemmons, K., Rota, R., and M. Linardic, C. (2016). Recent Insights into Notch Signaling in Embryonal Rhabdomyosarcoma. Curr. Drug Targets *17*, 1235–1244.

Cooper, P.N., Quirke, P., Hardy, G.J., and Dixon, M.F. (1992). A flow cytometric, clinical, and histological study of stromal neoplasms of the gastrointestinal tract. Am. J. Surg. Pathol. *16*, 163–170.

Corless, C.L., Barnett, C.M., and Heinrich, M.C. (2011). Gastrointestinal stromal tumours: origin and molecular oncology. Nat. Rev. Cancer *11*, 865–878.

Costinean, S., Zanesi, N., Pekarsky, Y., Tili, E., Volinia, S., Heerema, N., and Croce, C.M. (2006). Pre-B cell proliferation and lymphoblastic leukemia/high-grade lymphoma in E -miR155 transgenic mice. Proc. Natl. Acad. Sci. *103*, 7024–7029.

Debiec-Rychter, M., Lasota, J., Sarlomo-Rikala, M., Kordek, R., and Miettinen, M. (2001). Chromosomal aberrations in malignant gastrointestinal stromal tumors: correlation with c-KIT gene mutation. Cancer Genet. Cytogenet. *128*, 24–30.

Debiec-Rychter, M., Cools, J., Dumez, H., Sciot, R., Stul, M., Mentens, N., Vranckx, H., Wasag, B., Prenen, H., Roesel, J., et al. (2005). Mechanisms of resistance to imatinib mesylate in gastrointestinal stromal tumors and activity of the PKC412 inhibitor against imatinib-resistant mutants. Gastroenterology *128*, 270–279.

Dedes, K.J., Natrajan, R., Lambros, M.B., Geyer, F.C., Lopez-Garcia, M.A., Savage, K., Jones, R.L., and Reis-Filho, J.S. (2011). Down-regulation of the miRNA master regulators Drosha and Dicer is associated with specific subgroups of breast cancer. Eur. J. Cancer *47*, 138–150.

Demetri, G.D., von Mehren, M., Blanke, C.D., Van den Abbeele, A.D., Eisenberg, B., Roberts, P.J., Heinrich, M.C., Tuveson, D.A., Singer, S., Janicek, M., et al. (2002). Efficacy and Safety of Imatinib Mesylate in Advanced Gastrointestinal Stromal Tumors. N. Engl. J. Med. *347*, 472–480.

Dobin, A., Davis, C.A., Schlesinger, F., Drenkow, J., Zaleski, C., Jha, S., Batut, P., Chaisson, M., and Gingeras, T.R. (2013). STAR: ultrafast universal RNA-seq aligner. Bioinformatics *29*, 15–21.

Drilon, A., Laetsch, T.W., Kummar, S., DuBois, S.G., Lassen, U.N., Demetri, G.D., Nathenson, M., Doebele, R.C., Farago, A.F., Pappo, A.S., et al. (2018). Efficacy of Larotrectinib in *TRK* Fusion–Positive Cancers in Adults and Children. N. Engl. J. Med. *378*, 731–739.

Druker, B.J., Tamura, S., Buchdunger, E., Ohno, S., Segal, G.M., Fanning, S., Zimmermann, J., and Lydon, N.B. (1996). Effects of a selective inhibitor of the Abl tyrosine kinase on the growth of Bcr–Abl positive cells. Nat. Med. *2*, 561–566.

El-Rifai, W., Sarlomo-Rikala, M., Andersson, L.C., Knuutila, S., and Miettinen, M. (2000). DNA sequence copy number changes in gastrointestinal stromal tumors: tumor progression and prognostic significance. Cancer Res. *60*, 3899–3903.

Fabbri, M., Garzon, R., Cimmino, A., Liu, Z., Zanesi, N., Callegari, E., Liu, S., Alder, H., Costinean, S., Fernandez-Cymering, C., et al. (2007). MicroRNA-29 family reverts aberrant methylation in lung cancer by targeting DNA methyltransferases 3A and 3B. Proc. Natl. Acad. Sci. *104*, 15805–15810.

Falkenhorst, J., Grunewald, S., Mühlenberg, T., Marino-Enriquez, A., Reis, A.-C., Corless, C., Heinrich, M., Treckmann, J., Podleska, L.E., Schuler, M., et al. (2016). Inhibitor of Apoptosis Proteins (IAPs) are commonly dysregulated in GIST and can be pharmacologically targeted to enhance the pro-apoptotic activity of imatinib. Oncotarget *7*.

Fire, A., Xu, S., Montgomery, M.K., Kostas, S.A., Driver, S.E., and Mello, C.C. (1998). Potent and specific genetic interference by double-stranded RNA in Caenorhabditis elegans. Nature *391*, 806–811.

Fletcher, C.D.M., Bridge, J.A., Hogendoorn, P.C.W., and Mertens, F. (2013). WHO classification of tumours of soft tissue and bone.

Gasparotto, D., Rossi, S., Polano, M., Tamborini, E., Lorenzetto, E., Sbaraglia, M., Mondello, A., Massani, M., Lamon, S., Bracci, R., et al. (2017). Quadruple-Negative GIST Is a Sentinel for Unrecognized Neurofibromatosis Type 1 Syndrome. Clin. Cancer Res. *23*, 273–282.

Gastrointestinal Stromal Tumor Meta-Analysis Group (MetaGIST) (2010). Comparison of Two Doses of Imatinib for the Treatment of Unresectable or Metastatic Gastrointestinal Stromal Tumors: A Meta-Analysis of 1,640 Patients. J. Clin. Oncol. *28*, 1247–1253.

Gebeshuber, C.A., Zatloukal, K., and Martinez, J. (2009). miR-29a suppresses tristetraprolin, which is a regulator of epithelial polarity and metastasis. EMBO Rep. *10*, 400–405.

Giachino, C., Boulay, J.-L., Ivanek, R., Alvarado, A., Tostado, C., Lugert, S., Tchorz, J., Coban, M., Mariani, L., Bettler, B., et al. (2015). A Tumor Suppressor Function for Notch Signaling in Forebrain Tumor Subtypes. Cancer Cell *28*, 730–742.

González-Cámpora, R., Delgado, M.D., Amate, A.H., Gallardo, S.P., León, M.S., and Beltrán, A.L. (2011). Old and new immunohistochemical markers for the diagnosis of gastrointestinal stromal tumors. Anal. Quant. Cytol. Histol. *33*, 1–11.

Gunawan, B., Schulten, H.-J., von Heydebreck, A., Schmidt, B., Enders, C., Höer, J., Langer, C., Schüler, P., Schindler, C.G., Kuhlgatz, J., et al. (2004). Site-independent prognostic value of chromosome 9q loss in primary gastrointestinal stromal tumours. J. Pathol. *202*, 421–429.

Guo, Z., Maki, M., Ding, R., Yang, Y., zhang, B., and Xiong, L. (2015). Genome-wide survey of tissue-specific microRNA and transcription factor regulatory networks in 12 tissues. Sci. Rep. *4*, 5150.

Gyvyte, U., Juzenas, S., Salteniene, V., Kupcinskas, J., Poskiene, L., Kucinskas, L., Jarmalaite, S., Stuopelyte, K., Steponaitiene, R., Hemmrich-Stanisak, G., et al. (2017). MiRNA profiling of gastrointestinal stromal tumors by next-generation sequencing. Oncotarget *8*, 37225–37238.

Ha, M., and Kim, V.N. (2014). Regulation of microRNA biogenesis. Nat. Rev. Mol. Cell Biol. *15*, 509–524.

Haller, F., Happel, N., Schulten, H.-J., von Heydebreck, A., Schwager, S., Armbrust, T., Langer, C., Gunawan, B., Doenecke, D., and Füzesi, L. (2007). Site-dependent differential KIT and PDGFRA expression in gastric and intestinal gastrointestinal stromal tumors. Mod. Pathol. *20*, 1103–1111.

Haller, F., von Heydebreck, A., Zhang, J.D., Gunawan, B., Langer, C., Ramadori, G., Wiemann, S., and Sahin, Ã. (2010). Localization- and mutation-dependent microRNA (miRNA) expression signatures in gastrointestinal stromal tumours (GISTs), with a cluster of co-expressed miRNAs located at 14q32.31. J. Pathol. *220*, 71–86.

Hanna, A., Metge, B.J., Bailey, S.K., Chen, D., Chandrashekar, D.S., Varambally, S., Samant, R.S., and Shevde, L.A. (2019). Inhibition of Hedgehog signaling reprograms the dysfunctional immune microenvironment in breast cancer. OncoImmunology *8*, 1548241.

Heinrich, M., von Mehren, M., Jones, R.L., and Bauer, S. (2018). Avapritinib is highly active and well tolerated in patients with advanced GIST driven by diverse variety of oncogenic mutations in KIT and PDGFRA. *CTOS Annual Meeting 2018; Rome, Itlay*.

Heinrich, M.C., Griffith, D.J., Druker, B.J., Wait, C.L., Ott, K.A., and Zigler, A.J. (2000). Inhibition of c-kit receptor tyrosine kinase activity by STI 571, a selective tyrosine kinase inhibitor. Blood *96*, 925–932.

Heinrich, M.C., Corless, C.L., Duensing, A., McGreevey, L., Chen, C.-J., Joseph, N., Singer, S., Griffith, D.J., Haley, A., Town, A., et al. (2003a). PDGFRA activating mutations in gastrointestinal stromal tumors. Science *299*, 708–710.

Heinrich, M.C., Corless, C.L., Demetri, G.D., Blanke, C.D., von Mehren, M., Joensuu, H., McGreevey, L.S., Chen, C.-J., Van den Abbeele, A.D., Druker, B.J., et al. (2003b). Kinase Mutations and Imatinib Response in Patients With Metastatic Gastrointestinal Stromal Tumor. J. Clin. Oncol. *21*, 4342–4349.

Hingorani, P., Dickman, P., Garcia-Filion, P., White-Collins, A., Kolb, E.A., and Azorsa, D.O. (2013). BIRC5 expression is a poor prognostic marker in Ewing sarcoma. Pediatr. Blood Cancer *60*, 35–40.

Hirano, H., Maeda, H., Yamaguchi, T., Yokota, S., Mori, M., and Sakoda, S. (2015). Survivin expression in lung cancer: Association with smoking, histological types and pathological stages. Oncol. Lett. *10*, 1456–1462.

Hirota, S. (1998). Gain-of-Function Mutations of c-kit in Human Gastrointestinal Stromal Tumors. Science *279*, 577–580.

Hirota, S. (2018). Differential diagnosis of gastrointestinal stromal tumor by histopathology and immunohistochemistry. Transl. Gastroenterol. Hepatol. *3*, 27–27.

Huang, F.W., and Feng, F.Y. (2019). A Tumor-Agnostic NTRK (TRK) Inhibitor. Cell *177*, 8.

Hulzinga, J.D., Thuneberg, L., Klüppel, M., Malysz, J., Mikkelsen, H.B., and Bernstein, A. (1995). W/kit gene required for interstitial cells of Cajal and for intestinal pacemaker activity. Nature *373*, 347–349.

Iorio, M.V., and Croce, C.M. (2012). microRNA involvement in human cancer. Carcinogenesis *33*, 1126–1133.

Ito, T., Yamamura, M., Hirai, T., Ishikawa, T., Kanda, T., Nakai, T., Ohkouchi, M., Hashikura, Y., Isozaki, K., and Hirota, S. (2014). Gastrointestinal stromal tumors with exon 8 c-kit gene mutation might occur at extragastric sites and have metastasis-prone nature. Int. J. Clin. Exp. Pathol. *7*, 8024–8031.

Jansson, M.D., and Lund, A.H. (2012). MicroRNA and cancer. Mol. Oncol. *6*, 590–610.

Jessen, W.J., Miller, S.J., Jousma, E., Wu, J., Rizvi, T.A., Brundage, M.E., Eaves, D., Widemann, B., Kim, M.-O., Dombi, E., et al. (2013). MEK inhibition exhibits efficacy in human and mouse neurofibromatosis tumors. J. Clin. Invest. *123*, 340–347.

Jett, K., and Friedman, J.M. (2010). Clinical and genetic aspects of neurofibromatosis 1. Genet. Med. *12*, 1–11.

Joensuu, H., Roberts, P.J., Sarlomo-Rikala, M., Andersson, L.C., Tervahartiala, P., Tuveson, D., Silberman, S., Capdeville, R., Dimitrijevic, S., Druker, B., et al. (2001). Effect of the tyrosine kinase inhibitor STI571 in a patient with a metastatic gastrointestinal stromal tumor. N. Engl. J. Med. *344*, 1052–1056.

Kang, M., Ren, M.-P., Zhao, L., Li, C.-P., and Deng, M.-M. (2015). miR-485-5p acts as a negative regulator in gastric cancer progression by targeting flotillin-1. Am. J. Transl. Res. *7*, 2212–2222.

Kelly, L., Bryan, K., Kim, S.Y., Janeway, K.A., Killian, J.K., Schildhaus, H.-U., Miettinen, M., Helman, L., Meltzer, P.S., van de Rijn, M., et al. (2013). Post-transcriptional dysregulation by miRNAs is implicated in the pathogenesis of gastrointestinal stromal tumor [GIST]. PloS One *8*, e64102.

Killian, J.K., Kim, S.Y., Miettinen, M., Smith, C., Merino, M., Tsokos, M., Quezado, M., Smith, W.I., Jahromi, M.S., Xekouki, P., et al. (2013). Succinate Dehydrogenase Mutation Underlies Global Epigenomic Divergence in Gastrointestinal Stromal Tumor. Cancer Discov. *3*, 648–657.

Killian, J.K., Miettinen, M., Walker, R.L., Wang, Y., Zhu, Y.J., Waterfall, J.J., Noyes, N., Retnakumar, P., Yang, Z., Smith, W.I., et al. (2014). Recurrent epimutation of SDHC in gastrointestinal stromal tumors. Sci. Transl. Med. *6*, 268ra177-268ra177.

Kindblom, L.-G., Remotti, H.E., and Aldenborg, Frank (1998). Gastrointestinal Pacemaker Cell Tumor (GIPACT). Gastrointestinal Stromal Tumors Show Phenotypic Characteristics of the Interstitial Cells of Cajal. Am. J. OfPathology.

Knutsen, E., Fiskaa, T., Ursvik, A., Jørgensen, T.E., Perander, M., Lund, E., Seternes, O.M., Johansen, S.D., and Andreassen, M. (2013). Performance Comparison of Digital microRNA Profiling Technologies Applied on Human Breast Cancer Cell Lines. PLoS ONE *8*, e75813.

Komuro, T. (2006). Structure and organization of interstitial cells of Cajal in the gastrointestinal tract: ICC in the gastrointestinal tract. J. Physiol. *576*, 653–658.

Kozomara, A., Birgaoanu, M., and Griffiths-Jones, S. (2019). miRBase: from microRNA sequences to function. Nucleic Acids Res. *47*, D155–D162.

Kumar, M.S., Pester, R.E., Chen, C.Y., Lane, K., Chin, C., Lu, J., Kirsch, D.G., Golub, T.R., and Jacks, T. (2009). Dicer1 functions as a haploinsufficient tumor suppressor. Genes Dev. *23*, 2700–2704.

Kwon, J.G., Hwang, S.J., Hennig, G.W., Bayguinov, Y., McCann, C., Chen, H., Rossi, F., Besmer, P., Sanders, K.M., and Ward, S.M. (2009). Changes in the Structure and Function of ICC Networks in ICC Hyperplasia and Gastrointestinal Stromal Tumors. Gastroenterology *136*, 630–639.

Lagarde, P., Perot, G., Kauffmann, A., Brulard, C., Dapremont, V., Hostein, I., Neuville, A., Wozniak, A., Sciot, R., Schoffski, P., et al. (2012). Mitotic Checkpoints and Chromosome Instability Are Strong Predictors of Clinical Outcome in Gastrointestinal Stromal Tumors. Clin. Cancer Res. *18*, 826–838.

Lartigue, L., Neuville, A., Lagarde, P., Brulard, C., Rutkowski, P., Tos, P.D., Wardelmann, E., Debiec-Rychter, M., Italiano, A., Coindre, J.-M., et al. (2015). Genomic index predicts clinical outcome of intermediate-risk gastrointestinal stromal tumours, providing a new inclusion criterion for imatinib adjuvant therapy. Eur. J. Cancer *51*, 75–83.

Lasota, J., Jasinski, M., Sarlomo-Rikala, M., and Miettinen, M. (1999). Mutations in Exon 11 of c-Kit Occur Preferentially in Malignant versus Benign Gastrointestinal Stromal Tumors and Do Not Occur in Leiomyomas or Leiomyosarcomas. Am. J. Pathol. *154*, 53–60.

Lasota, J., Corless, C.L., Heinrich, M.C., Debiec-Rychter, M., Sciot, R., Wardelmann, E., Merkelbach-Bruse, S., Schildhaus, H.-U., Steigen, S.E., Stachura, J., et al. (2008). Clinicopathologic profile of gastrointestinal stromal tumors (GISTs) with primary KIT exon 13 or exon 17 mutations: a multicenter study on 54 cases. Mod. Pathol. Off. J. U. S. Can. Acad. Pathol. Inc *21*, 476–484.

Lecoin, L., Gabella, G., and Le Douarin, N. (1996). Origin of the c-kit-positive interstitial cells in the avian bowel. Development 725–733.

Lee, R.C., Feinbaum, R.L., and Ambros, V. (1993). The C. elegans heterochronic gene lin-4 encodes small RNAs with antisense complementarity to lin-14. Cell *75*, 843–854.

Li K., K., Cheng, H., Li, Z., Pang, Y., Jia, X., Xie, F., Hu, G., Cai, Q., and Wang, Y. (2017). Genetic progression in gastrointestinal stromal tumors: mechanisms and molecular interventions. Oncotarget *8*.

Li S., S., Wang, L., Meng, Y., Chang, Y., Xu, J., and Zhang, Q. (2017). Increased levels of LAPTM4B, VEGF and survivin are correlated with tumor progression and poor prognosis in breast cancer patients. Oncotarget *8*.

Love, M.I., Huber, W., and Anders, S. (2014). Moderated estimation of fold change and dispersion for RNA-seq data with DESeq2. Genome Biol. *15*, 550.

Lujambio, A., Ropero, S., Ballestar, E., Fraga, M.F., Cerrato, C., Setien, F., Casado, S., Suarez-Gauthier, A., Sanchez-Cespedes, M., Gitt, A., et al. (2007). Genetic Unmasking of an Epigenetically Silenced microRNA in Human Cancer Cells. Cancer Res. *67*, 1424–1429.

Mariño-Enríquez, A., and Bovée, J.V.M.G. (2016). Molecular Pathogenesis and Diagnostic, Prognostic and Predictive Molecular Markers in Sarcoma. Surg. Pathol. Clin. *9*, 457–473.

Mayr, C., and Bartel, D.P. (2009). Widespread Shortening of 3'UTRs by Alternative Cleavage and Polyadenylation Activates Oncogenes in Cancer Cells. Cell *138*, 673–684.

Mayr, C., Hemann, M.T., and Bartel, D.P. (2007). Disrupting the Pairing Between let-7 and Hmga2 Enhances Oncogenic Transformation. Science *315*, 1576–1579.

Meijer, H.A., Smith, E.M., and Bushell, M. (2014). Regulation of miRNA strand selection: follow the leader? Biochem. Soc. Trans. *42*, 1135–1140.

Mello, C.C., and Conte, D. (2004). Revealing the world of RNA interference. Nature *431*, 338–342.

Merritt, W.M., Lin, Y.G., Han, L.Y., Kamat, A.A., Spannuth, W.A., Schmandt, R., Urbauer, D., Pennacchio, L.A., Cheng, J.-F., Nick, A.M., et al. (2008). Dicer, Drosha, and Outcomes in Patients with Ovarian Cancer. N. Engl. J. Med. *359*, 2641–2650.

Miettinen, M., and Lasota, J. (2006). Gastrointestinal stromal tumors: pathology and prognosis at different sites. Semin. Diagn. Pathol. *23*, 70–83.

Miettinen, M., Virolainen, M., and Maarit-Sarlomo-Rikala (1995). Gastrointestinal stromal tumors-value of CD34 antigen in their identification and separation from true leiomyomas and schwannomas. *Am J Surg Pathol.*

Miettinen, M., Majidi, M., and Lasota, J. (2002). Pathology and diagnostic criteria of gastrointestinal stromal tumors (GISTs): a review. Eur. J. Cancer *38*, S39–S51.

Miettinen, M., Lasota, J., and Sobin, L.H. (2005). Gastrointestinal stromal tumors of the stomach in children and young adults: a clinicopathologic, immunohistochemical, and molecular genetic study of 44 cases with long-term follow-up and review of the literature. Am. J. Surg. Pathol. *29*, 1373–1381.

Mishra, P.J., Mishra, P.J., Banerjee, D., and Bertino, J.R. (2008). MiRSNPs or MiR-polymorphisms, new players in microRNA mediated regulation of the cell: Introducing microRNA pharmacogenomics. Cell Cycle *7*, 853–858.

Mitelman, F., Johansson, B., and Mertens, F. (2007). The impact of translocations and gene fusions on cancer causation. Nat. Rev. Cancer *7*, 233–245.

Mootha, V.K., Lindgren, C.M., Eriksson, K.-F., Subramanian, A., Sihag, S., Lehar, J., Puigserver, P., Carlsson, E., Ridderstråle, M., Laurila, E., et al. (2003). PGC-1α-responsive genes involved in oxidative phosphorylation are coordinately downregulated in human diabetes. Nat. Genet. *34*, 267.

Niinuma, T., Suzuki, H., and Sugai, T. (2018). Molecular characterization and pathogenesis of gastrointestinal stromal tumor. Transl. Gastroenterol. Hepatol. *3*, 2–2.

Okamura, K., Liu, N., and Lai, E.C. (2009). Distinct Mechanisms for MicroRNA Strand Selection by Drosophila Argonautes. Mol. Cell *36*, 431–444.

Palazzo, A.F., and Lee, E.S. (2015). Non-coding RNA: what is functional and what is junk? Front. Genet. *6*.

Pantaleo, M.A., Ravegnini, G., Astolfi, A., Simeon, V., Nannini, M., Saponara, M., Urbini, M., Gatto, L., Indio, V., Sammarini, G., et al. (2016). Integrating miRNA and gene expression profiling analysis revealed regulatory networks in gastrointestinal stromal tumors. Epigenomics *8*, 1347–1366.

Pasternak, A., Szura, M., Gil, K., and Matyja, A. (2016). Interstitial cells of Cajal — systematic review. Folia Morphol. *75*, 281–286.

Patro, R., Duggal, G., Love, M.I., Irizarry, R.A., and Kingsford, C. (2017). Salmon provides fast and bias-aware quantification of transcript expression. Nat. Methods *14*, 417–419.

Pelczar, P., Zibat, A., van Dop, W.A., Heijmans, J., Bleckmann, A., Gruber, W., Nitzki, F., Uhmann, A., Guijarro, M.V., Hernando, E., et al. (2013). Inactivation of Patched1 in mice leads to development of gastrointestinal stromal-like tumors that express Pdgfrα but not kit. Gastroenterology *144*, 134-144.e6.

Poliseno, L., Salmena, L., Zhang, J., Carver, B., Haveman, W.J., and Pandolfi, P.P. (2010). A coding-independent function of gene and pseudogene mRNAs regulates tumour biology. Nature *465*, 1033–1038.

Postow, M.A., and Robson, M.E. (2012). Inherited gastrointestinal stromal tumor syndromes: mutations, clinical features, and therapeutic implications. Clin. Sarcoma Res. *2*, 16.

Pritchard, C.C., Cheng, H.H., and Tewari, M. (2012). MicroRNA profiling: approaches and considerations. Nat. Rev. Genet. *13*, 358–369.

Rahmati, S., Abovsky, M., Pastrello, C., and Jurisica, I. (2017). pathDIP: an annotated resource for known and predicted human gene-pathway associations and pathway enrichment analysis. Nucleic Acids Res. *45*, D419–D426.

Robinson, T.L., Sircar, K., Hewlett, B.R., Chorneyko, K., Riddell, R.H., and Huizinga, J.D. (2000). Gastrointestinal Stromal Tumors May Originate from a Subset of CD34-Positive Interstitial Cells of Cajal. Am. J. Pathol. *156*, 1157–1163.

Romano, G., Veneziano, D., Acunzo, M., and Croce, C.M. (2017). Small non-coding RNA and cancer. Carcinogenesis *38*, 485–491.

Rossi, S., Gasparotto, D., Toffolatti, L., Pastrello, C., Gallina, G., Marzotto, A., Sartor, C., Barbareschi, M., Cantaloni, C., Messerini, L., et al. (2010). Molecular and clinicopathologic characterization of gastrointestinal stromal tumors (GISTs) of small size. Am. J. Surg. Pathol. *34*, 1480–1491.

Rossi, S., Gasparotto, D., Miceli, R., Toffolatti, L., Gallina, G., Scaramel, E., Marzotto, A., Boscato, E., Messerini, L., Bearzi, I., et al. (2015). KIT, PDGFRA, and BRAF Mutational Spectrum Impacts on the Natural History of Imatinib-naive Localized GIST: A Population-based Study. Am. J. Surg. Pathol. *39*, 922–930.

Rossi, S., Gasparotto, D., Cacciatore, M., Sbaraglia, M., Mondello, A., Polano, M., Mandolesi, A., Gronchi, A., Reuss, D.E., von Deimling, A., et al. (2017). Neurofibromin C terminus-specific antibody (clone NFC) is a valuable tool for the identification of NF1-inactivated GISTs. Mod. Pathol.

Ruby, J.G., Jan, C.H., and Bartel, D.P. (2007). Intronic microRNA precursors that bypass Drosha processing. Nature *448*, 83–86.

Rudolph, P., Gloeckner, K., Parwaresch, R., Harms, D., and Schmidt, D. (1998). Immunophenotype, proliferation, DNA ploidy, and biological behavior of gastrointestinal stromal tumors: A multivariate clinicopathologic study. Hum. Pathol. *29*, 791–800.

Sabarimurugan, S., Kumarasamy, C., Baxi, S., Devi, A., and Jayaraj, R. (2019). Systematic review and meta-analysis of prognostic microRNA biomarkers for survival outcome in nasopharyngeal carcinoma. PloS One *14*, e0209760.

Saini, H.K., Griffiths-Jones, S., and Enright, A.J. (2007). Genomic analysis of human microRNA transcripts. Proc. Natl. Acad. Sci. *104*, 17719–17724.

Sanders, K. (1996). A case for interstitial cells of Cajal as pacemakers and mediators of neurotransmission in the gastrointestinal tract. Gastroenterology *111*, 492–515.

Sanders, K.M., Ordög, T., Koh, S.D., Torihashi, S., and Ward, S.M. (1999). Development and plasticity of interstitial cells of Cajal. Neurogastroenterol. Motil. Off. J. Eur. Gastrointest. Motil. Soc. *11*, 311–338.

Sanders, K.M., Ward, S.M., and Koh, S.D. (2014). Interstitial Cells: Regulators of Smooth Muscle Function. Physiol. Rev. *94*, 859–907.

Sankhala, K.K. (2017). Clinical development landscape in GIST: from novel agents that target accessory pathways to revisiting non-targeted therapies. Expert Opin. Investig. Drugs *26*, 427–443.

Schaefer, I.-M., Mariño-Enríquez, A., and Fletcher, J.A. (2017). What is New in Gastrointestinal Stromal Tumor?: Adv. Anat. Pathol. *24*, 259–267.

Scott, A.M., Wolchok, J.D., and Old, L.J. (2012). Antibody therapy of cancer. Nat. Rev. Cancer *12*, 278–287.

Shi, E., Chmielecki, J., Tang, C.-M., Wang, K., Heinrich, M.C., Kang, G., Corless, C.L., Hong, D., Fero, K.E., Murphy, J.D., et al. (2016). FGFR1 and NTRK3 actionable alterations in “Wild-Type” gastrointestinal stromal tumors. J. Transl. Med. *14*, 339.

Simonson, B., and Das, S. (2015). MicroRNA Therapeutics: the Next Magic Bullet? Mini Rev. Med. Chem. *15*, 467–474.

Sommer, G., Agosti, V., Ehlers, I., Rossi, F., Corbacioglu, S., Farkas, J., Moore, M., Manova, K., Antonescu, C.R., and Besmer, P. (2003). Gastrointestinal stromal tumors in a mouse model by targeted mutation of the Kit receptor tyrosine kinase. Proc. Natl. Acad. Sci. *100*, 6706–6711.

Subramanian, A., Tamayo, P., Mootha, V.K., Mukherjee, S., Ebert, B.L., Gillette, M.A., Paulovich, A., Pomeroy, S.L., Golub, T.R., Lander, E.S., et al. (2005). Gene set enrichment analysis: A knowledge-based approach for interpreting genome-wide expression profiles. Proc. Natl. Acad. Sci. *102*, 15545–15550.

Subramanian, S., Lui, W.O., Lee, C.H., Espinosa, I., Nielsen, T.O., Heinrich, M.C., Corless, C.L., Fire, A.Z., and van de Rijn, M. (2008). MicroRNA expression signature of human sarcomas. Oncogene *27*, 2015–2026.

Sun, X., Liu, Y., Li, M., Wang, M., and Wang, Y. (2015). Involvement of miR-485-5p in hepatocellular carcinoma progression targeting EMMPRIN. Biomed. Pharmacother. Biomedecine Pharmacother. *72*, 58–65.

Taylor, B.S., Barretina, J., Maki, R.G., Antonescu, C.R., Singer, S., and Ladanyi, M. (2011). Advances in sarcoma genomics and new therapeutic targets. Nat. Rev. Cancer *11*, 541–557.

Tokar, T., Pastrello, C., Rossos, A.E.M., Abovsky, M., Hauschild, A.-C., Tsay, M., Lu, R., and Jurisica, I. (2018). mirDIP 4.1-integrative database of human microRNA target predictions. Nucleic Acids Res. *46*, D360–D370.

Torihashi, S., Nishi, K., Tokutomi, Y., Nishi, T., Ward, S., and Sanders, K.M. (1999). Blockade of kit signaling induces transdifferentiation of interstitial cells of Cajal to a smooth muscle phenotype. Gastroenterology *117*, 140–148.

Torres, A., Torres, K., Paszkowski, T., Jodłowska-Jędrych, B., Radomański, T., Książek, A., and Maciejewski, R. (2011). Major regulators of microRNAs biogenesis Dicer and Drosha are down-regulated in endometrial cancer. Tumor Biol. *32*, 769–776.

Tzen, C.-Y. (2005). Analysis of CD117-negative gastrointestinal stromal tumors. World J. Gastroenterol. *11*, 1052.

Valinezhad Orang, A., Safaralizadeh, R., and Kazemzadeh-Bavili, M. (2014). Mechanisms of miRNA-Mediated Gene Regulation from Common Downregulation to mRNA-Specific Upregulation. Int. J. Genomics *2014*, 1–15.

Vannucchi, M.-G. (1999). Receptors in interstitial cells of Cajal: Identification and possible physiological roles. Microsc. Res. Tech. *47*, 325–335.

Vlachos, I.S., Zagganas, K., Paraskevopoulou, M.D., Georgakilas, G., Karagkouni, D., Vergoulis, T., Dalamagas, T., and Hatzigeorgiou, A.G. (2015). DIANA-miRPath v3.0: deciphering microRNA function with experimental support. Nucleic Acids Res. *43*, W460–W466.

Von Mehren, M., and Joensuu, H. (2018). Gastrointestinal Stromal Tumors. J. Clin. Oncol. *36*, 136–143.

Wagner, A.J., Kindler, H., Gelderblom, H., Schöffski, P., Bauer, S., Hohenberger, P., Kopp, H.-G., Lopez-Martin, J.A., Peeters, M., Reichardt, P., et al. (2017). A phase II study of a human anti-PDGFRα monoclonal antibody (olaratumab, IMC-3G3) in previously treated patients with metastatic gastrointestinal stromal tumors. Ann. Oncol. *28*, 541–546.

Wang, G., Zhou, H., Gu, Z., Gao, Q., and Shen, G. (2018). Oct4 promotes cancer cell proliferation and migration and leads to poor prognosis associated with the survivin/STAT3 pathway in hepatocellular carcinoma. Oncol. Rep.

Wang, H., Horbinski, C., Wu, H., Liu, Y., Sheng, S., Liu, J., Weiss, H., Stromberg, A.J., and Wang, C. (2016). NanoStringDiff: a novel statistical method for differential expression analysis based on NanoString nCounter data. Nucleic Acids Res. *44*, e151.

Wang, Y., Marino-Enriquez, A., Bennett, R.R., Zhu, M., Shen, Y., Eilers, G., Lee, J.-C., Henze, J., Fletcher, B.S., Gu, Z., et al. (2014). Dystrophin is a tumor suppressor in human cancers with myogenic programs. Nat. Genet. *46*, 601–606.

Ward, S.M., Burns, A.J., Torihashi, S., and Sanders, K.M. (1994). Mutation of the proto-oncogene c-kit blocks development of interstitial cells and electrical rhythmicity in murine intestine. J. Physiol. *480 (Pt 1)*, 91–97.

Ward, S.M., Morris, G., Reese, L., Wang, X.-Y., and Sanders, K.M. (1998). Interstitial cells of Cajal mediate enteric inhibitory neurotransmission in the lower esophageal and pyloric sphincters. Gastroenterology *115*, 314–329.

Weber, B., Stresemann, C., Brueckner, B., and Lyko, F. (2007). Methylation of Human MicroRNA Genes in Normal and Neoplastic Cells. Cell Cycle *6*, 1001–1005.

Wheatley, S.P., and Altieri, D.C. (2019). Survivin at a glance. J. Cell Sci. *132*, jcs223826.

Wozniak, A., Sciot, R., Guillou, L., Pauwels, P., Wasag, B., Stul, M., Vermeesch, J.R., Vandenberghe, P., Limon, J., and Debiec-Rychter, M. (2007). Array CGH analysis in primary gastrointestinal stromal tumors: Cytogenetic profile correlates with anatomic site and tumor aggressiveness, irrespective of mutational status. Genes. Chromosomes Cancer *46*, 261–276.

Yang, J., Du, X., Lazar, A.J.F., Pollock, R., Hunt, K., Chen, K., Hao, X., Trent, J., and Zhang, W. (2008). Genetic aberrations of gastrointestinal stromal tumors. Cancer *113*, 1532–1543.

Yun, S., Kim, W.K., Kwon, Y., Jang, M., Bauer, S., and Kim, H. (2018). Survivin is a novel transcription regulator of KIT and is downregulated by miRNA-494 in gastrointestinal stromal tumors: MiR-494 targets survivin and KIT in GISTs. Int. J. Cancer *142*, 2080–2093.

Zhou, G., Soufan, O., Ewald, J., Hancock, R.E.W., Basu, N., and Xia, J. (2019). NetworkAnalyst 3.0: a visual analytics platform for comprehensive gene expression profiling and meta-analysis. Nucleic Acids Res. *47*, W234–W241.

Zhou, L., Lu, J., Liang, Z.-Y., Zhou, W.-X., Yuan, D., Li, B.-Q., You, L., Guo, J.-C., and Zhao, Y.-P. (2018). High nuclear Survivin expression as a poor prognostic marker in pancreatic ductal adenocarcinoma: ZHOU ET AL. J. Surg. Oncol. *118*, 1115–1121.

7. Published articles

Published OnlineFirst July 7, 2016; DOI: 10.1158/1078-0432.CCR-16-0152

Biology of Human Tumors

Clinical Cancer Research

Quadruple-Negative GIST Is a Sentinel for Unrecognized Neurofibromatosis Type 1 Syndrome

Daniela Gasparotto[1], Sabrina Rossi[2], Maurizio Polano[1], Elena Tamborini[3], Erica Lorenzetto[1], Marta Sbaraglia[2], Alessia Mondello[1], Marco Massani[4], Stefano Lamon[5], Raffaella Bracci[6], Alessandra Mandolesi[6], Elisabetta Frate[7], Franco Stanzial[8], Jerin Agaj[9], Guido Mazzoleni[10], Silvana Pilotti[3], Alessandro Gronchi[11], Angelo Paolo Dei Tos[2], and Roberta Maestro[1]

Abstract

Purpose: The majority of gastrointestinal stromal tumors (GIST) are driven by *KIT*, *PDGFRA*, or, less commonly, *BRAF* mutations, and *SDH* gene inactivation is involved in a limited fraction of gastric lesions. However, about 10% of GISTs are devoid of any of such alterations and are poorly responsive to standard treatments. This study aims to shed light on the molecular drivers of quadruple-negative GISTs.

Experimental Design: Twenty-two sporadic quadruple-negative GISTs with no prior association with Neurofibromatosis Type 1 syndrome were molecularly profiled for a panel of genes belonging to tyrosine kinase pathways or previously implicated in GISTs. For comparison purposes, 24 GISTs carrying *KIT*, *PDGFRA*, or *SDH* gene mutations were also analyzed. Molecular findings were correlated to clinicopathologic features.

Results: Most quadruple-negative GISTs featured intestinal localization, with a female predilection. About 60% (13/22) of quadruple-negative tumors carried *NF1* pathogenic mutations, often associated with biallelic inactivation. The analysis of normal tissues, available in 11 cases, indicated the constitutional nature of the *NF1* mutation in 7 of 11 cases, unveiling an unrecognized Neurofibromatosis Type 1 syndromic condition. Multifocality and a multinodular pattern of growth were common findings in *NF1*-mutated quadruple-negative GISTs.

Conclusions: *NF1* gene mutations are frequent in quadruple-negative GISTs and are often constitutional, indicating that a significant fraction of patients with apparently sporadic quadruple-negative GISTs are affected by unrecognized Neurofibromatosis Type 1 syndrome. Hence, a diagnosis of quadruple-negative GIST, especially if multifocal or with a multinodular growth pattern and a nongastric location, should alert the clinician to a possible Neurofibromatosis Type 1 syndromic condition. *Clin Cancer Res; 23(1); 273–82. ©2016 AACR.*

Introduction

Gastrointestinal stromal tumors (GISTs) are the most frequent mesenchymal neoplasm of the digestive tract, with an incidence of around 1.5 per 100,000/year. GISTs are thought to arise from the interstitial Cajal cells and are typically considered to be KIT/PDGFRA-driven tumors (1). In fact, about 85% of sporadic GISTs are characterized by activating mutations of either *KIT* or *PDGFRA* tyrosine kinase receptor genes, which account for their sensitivity to the kinase inhibitor imatinib. *KIT* and *PDGFRA* mutations result in constitutive activation of the RAS–RAF–MAPK pathway. In about 1% of *KIT*/*PDGFRA* wild-type cases, the same pathway is activated as a result of *BRAF* mutations (1, 2), and we have recently reported the involvement of the *ETV6-NTRK3* gene fusion (3). About 15% of sporadic GISTs are devoid of *KIT*/*PDGFRA*/*BRAF* mutations and are sometimes referred to as triple-negative GISTs. Triple-negative GISTs can be observed in the context of rare hereditary syndromes, including succinate dehydrogenase (SDH) protein complex-related syndromes (4), and, although not comprised in the diagnostic criteria, also in the context of Neurofibromatosis Type 1 (NF-Type 1; refs. 5, 6). Recent studies indicate that SDH-deficient GISTs represent about one third of triple-negative GISTs (7). SDH-associated GISTs are typically gastric, often multifocal, and affect young people, especially females (1, 7–9). They frequently arise in the context of the Carney–Stratakis Syndrome (GIST and paraganglioma dyad), characterized by germline inactivating mutations in any of the four genes encoding the SDH complex (*SDHA-D*; refs. 10, 11), or in the Carney Triad (GIST, paraganglioma, chondroma), associated with *SDHC* promoter hypermethylation (12, 13).

[1]Experimental Oncology 1, CRO Aviano National Cancer Institute, Aviano, Italy. [2]Department of Pathology and Molecular Genetics, Treviso General Hospital, Treviso, Italy. [3]Department of Pathology and Molecular Biology, Fondazione IRCCS Istituto Nazionale dei Tumori di Milano, Milano, Italy. [4]Department of Surgery, Treviso General Hospital, Treviso, Italy. [5]Department of Oncology, Treviso General Hospital, Treviso, Italy. [6]Department of Internal Medicine, Ospedali Riuniti di Ancona, Ancona, Italy. [7]Medical Genetics Unit, Treviso General Hospital, Treviso, Italy. [8]Clinical Genetics Service, Bolzano General Hospital, Bolzano/Bozen, Italy. [9]Department of Surgery, Vipiteno General Hospital, Vipiteno/Sterzing, Italy. [10]Department of Pathology, Bolzano General Hospital, Bolzano/Bozen, Italy. [11]Department of Surgery, Fondazione IRCCS Istituto Nazionale dei Tumori di Milano, Milano, Italy.

Note: Supplementary data for this article are available at Clinical Cancer Research Online (http://clincancerres.aacrjournals.org/).

D. Gasparotto and S. Rossi share first authorship.

A.P. Dei Tos and R. Maestro share last authorship.

Corresponding Author: Roberta Maestro, CRO Aviano National Cancer Institute, Via Franco Gallini 2, 33081 Aviano (PN), Italy. Phone: 39-0434659670; Fax: 39-0434659659; E-mail: maestro@cro.it

doi: 10.1158/1078-0432.CCR-16-0152

Published OnlineFirst July 7, 2016; DOI: 10.1158/1078-0432.CCR-16-0152

Translational Relevance

About 10% of gastrointestinal stromal tumors (GIST) are devoid of canonical *KIT*, *PDGFRA*, *BRAF*, or *SDH* mutations. These quadruple-negative GISTs, currently orphans of driver alterations, are poorly responsive to standard treatments. The lack of knowledge on their genetics prevents the implementation of targeted treatments. This work demonstrates that a significant fraction of apparently sporadic quadruple-negative GISTs arise in the context of unrecognized Neurofibromatosis Type 1 (NF-Type 1) syndrome. About 60% of the quadruple-negative GISTs analyzed bore pathogenic mutations of the *NF1* gene. A relevant proportion of these mutations were constitutional. *NF1*-mutated GISTs featured distinctive clinicopathologic characteristics. Thus, a diagnosis of a quadruple-negative GIST, especially if multifocal or with a multinodular growth pattern and a nongastric location, should alert the clinician to a possible NF-Type 1 syndromic condition. These patients should be referred to specialists for definitive individual and familial risk assessment.

In the remaining two third of triple-negative sporadic GISTs, hereafter referred to as "quadruple-negative" GISTs (KIT/PDGFRA/BRAF mutation-negative/SDH-proficient), no oncogenic driver alteration has been yet identified. Quadruple-negative GISTs represent an ill-defined and likely heterogeneous category of tumors which overall respond poorly to standard treatments (1). Hence, a better molecular characterization of these neoplasms, which account for about 10% of all GISTs, could pave the way to novel therapeutic avenues.

To shed light on this issue, we sought to investigate a series of 22 quadruple-negative sporadic GISTs arisen in patients with no prior association to NF-Type 1 (no diagnosis or recorded clinical manifestations of NF-Type 1 nor familial history for the disease).

The mutational status of a panel of genes either belonging to the receptor tyrosine kinase pathway or previously associated with GIST or GIST-including syndromic conditions was analyzed. For comparison purposes, 24 consecutive GISTs carrying mutations in either *KIT*, *PDGFRA*, or *SDH* (*KIT*/*PDGFRA*/*SDH*^{m}) were also profiled.

Intriguingly, 13 of 22 (59%) quadruple-negative GISTs analyzed turned out to carry pathogenic *NF1* gene mutations; in 7 of the 11 cases for which normal matched DNA was available, we were able to ascertain the constitutional nature of the alteration. These results indicate that NF1 plays a relevant role in the pathogenesis of quadruple-negative GISTs, and, more importantly, a significant fraction of apparently "sporadic" quadruple-negative GISTs actually arise in undiagnosed NF-Type 1 patients.

Materials and Methods

Patients population and result communication

The series consisted of 22 GIST negative for *KIT*/*PDGFRA*/*BRAF*/*SDH* mutations (quadruple-negative GIST) submitted as sporadic cases by the referral clinicians. Fifteen of these tumors were consultation cases of one of the authors (A.P. Dei Tos), who is the reference pathologist for the Italian Sarcoma Group and for the Italian Rare Cancer Network. For comparison purposes, 24 consecutive sporadic GISTs carrying mutations in KIT, PDGFRA, or SDH were also analyzed (*KIT*/*PDGFRA*/*SDH*^{m} group). The study was approved by the Institutional Review Boards, and informed consent was provided by all living patients.

GIST diagnosis was based on morphology and CD117 expression as assessed by immunohistochemistry (IHC). Site, size, and mitotic count per 5 mm^2 were recorded in most cases. Multifocality, tumor growth pattern (multinodular with fibromuscular septa vs. a single expansive nodule), cell type, degree of cellularity, and presence of skenoid fibers were recorded in all quadruple-negative GISTs.

KIT, *PDGFRA*, *BRAF* mutational status was originally determined by Sanger sequencing. In *KIT*/*PDGFRA*/*BRAF*-negative cases, SDH deficiency was assessed by IHC for SDHB, followed by sequencing. Of the 24 GISTs of the *KIT*/*PDGFRA*/*SDH*^{m} group, 16 cases harbored mutations in KIT, 3 in PDGFRA, 2 in SDHA, and 2 in SDHB; one case (# 46) had a concomitant KIT and SDHA mutation. No tumor included in the study carried BRAF mutations.

Demographic and pathologic features of the series are summarized in Supplementary Table S1. Clinical data, including indications of syndromic conditions, concurrence of other diseases, familial history, and follow-up information, were obtained from review of medical records and interview of referring physicians. No patient with familial history or genetic diagnosis of NF-Type1, or recorded clinical manifestations diagnostic of NF-Type 1 (6, 14), was included in the study. Pediatric GISTs were also excluded from the study.

The results of the mutation screening were returned to the referring clinician. In the presence of ascertained constitutional mutations, namely *NF1* constitutional mutations, living patients were referred to a NF-Type 1 expert. The specialist, according to international guidelines (14–16), integrated molecular data with patient's clinical findings and family history, and informed the patient about the characteristics of the disease and the probability of transmission to the offspring. Further tests and checkups were eventually prescribed, as appropriate.

Massive parallel sequencing and mutation validation

DNA from frozen or formalin-fixed paraffin-embedded (FFPE) tumors and matched normal samples was extracted using the EZ1 biorobot (QIAGEN) or the QIAamp DNA FFPE Tissue Kit (QIAGEN). Massive parallel sequencing (MPS) libraries were prepared with a TruSeq Custom Amplicon v1.5 panel (Illumina) targeting the coding sequence and a 5-nt flanking intronic region of the following genes: *KIT*, *PDGFRA*, *BRAF*, *SDHA*, *SDHB*, *SDHC*, *SDHD*, *HRAS*, *KRAS*, *NRAS*, *NF1*, *NF2*, *HIF1A*, *PTEN*, *RAF1*, *RUNX1*, *SMARCB1*, *VHL*, *CDKN2A*, *PIK3CA*, *RB1*, *SPRED1*, and *TP53*.

MPS libraries were sequenced on the MiSeq platform (Illumina) using a v3 kit 2 × 150 cycles. Data were analyzed with the Miseq Reporter software v2.5, using the custom amplicon workflow and somatic variant caller. Mean amplicon coverage was 4367. Variants were analyzed with VariantStudio software (Illumina) and filtered with 100x coverage threshold, and allelic fraction was $\geq$20%. Neutral population polymorphisms, as well as pseudogene sequences, were filtered out.

In the case of the *NF1* gene, regions with low coverage were also PCR-amplified and sequenced on an ABI PRISM 3100 Genetic Analyzer (Applied Biosystems). Mutations detected by MPS in

Published OnlineFirst July 7, 2016; DOI: 10.1158/1078-0432.CCR-16-0152

tumor DNA were validated by PCR-sequencing; where available, matched normal DNA was also analyzed. PCRs were optimized to avoid amplification of pseudogenes.

To assess *NF1* copy-number variations, the MPS depth obtained for a given amplicon was compared with the mean sequencing depth obtained in the other samples of the run for the same amplicon, normalized against the sequencing efficiency of the test sample. Multiplex ligation-dependent probe amplification (MLPA NF1 probemix P081 and P082; MRC Holland) was used to validate the deletions detected in cases # 5 and 19. In case # 5, carrying a large *NF1* deletion, the copy-number loss was also validated by qPCR. To this end, DNAs extracted from FFPE normal specimens from 5 healthy individuals were used as reference. Amplicons were centered on *NF1* exon 14, comprised in the deletion, and exon 53, external to the deletion. *ADA*, *KIT*, *RET*, and *IGF1R* were used as internal normalization controls. Primers and PCR conditions are provided in Supplementary Table S2. Reactions were performed in triplicate with SsoFast EvaGreen Supermix (BioRad) on a CFX96 Real-Time System (Bio-Rad). Relative levels were normalized to the geometric average of the four control genes by the comparative Ct (ΔΔCt) method using the Bio-Rad CFX manager software. Reduction of the signal greater than 80% was considered indicative of homozygous deletion; reduction of the signal to about 50% was considered as suggestive of loss of one allele.

The expression of *NF1*-mutated alleles was investigated on the cDNA of 5 GISTs for which RNA was available (cases # 8, 9, 13, 28, and 38). RNA extraction and cDNA synthesis were as previously described (3).

The Human Gene Mutation Database (HGMD; http://www.hgmd.cf.ac.uk) was interrogated to assess for previous association with NF-Type 1 syndrome of the identified mutations. Moreover, five different prediction algorithms, Provean (http://provean.jcvi.org; ref. 17), SIFT (http://sift.bii.a-star.edu.sg; ref. 18), Polyphen2 (genetics.bwh.harvard.edu/pph2; ref. 19), MutationAssessor (http://mutationassessor.org/; ref. 20), and PaPI (http://papi.unipv.it; ref. 21), were used to predict the effect of coding nonsynonymous variants. The Human Splicing Finder software (http://www.umd.be/HSF3/) was used to evaluate splice site mutations (22).

Statistical analyses

Categorical variables were compared by the Fisher two-tailed exact test. Continuous data were compared between groups by the unpaired Student *t* test.

Results

Molecular findings

The series of 46 sporadic GISTs analyzed in this study included 22 quadruple-negative GISTs and 24 tumors belonging to the *KIT/PDGFRA/SDH*^{m} group. MPS analysis confirmed the mutations in *KIT*, *PDGFRA*, or *SDH* genes previously identified by Sanger sequencing (Supplementary Table S1). No mutation in *BRAF*, *SDHC*, *SDHD*, *RB1*, *HRAS*, *KRAS*, *NRAS*, *NF2*, *HIF1A*, *PTEN*, *RAF1*, *RUNX1*, *SMARCB1*, *SPRED1*, and *VHL* was detected in any of the cases analyzed. Three tumors carried missense nucleotide changes in the coding sequence of *CDKN2A*, *TP53*, or *PIK3CA*, respectively (Supplementary Table S3).

Intriguingly, 15 tumors turned out to carry *NF1* mutations (Table 1). These included 13 quadruple-negative GISTs (13/22; 59%) and 2 tumors of the *KIT/PDGFRA/SDH*^{m} group (2/24; 8.3%).

NF1 mutations detected in the quadruple-negative group consisted of small changes (missense mutations, nonsense, frameshift-induced protein truncation, mutations in proximity to splicing sites) as well as large deletions. Most of these mutations had previously been associated with NF-Type 1 (HGMD database) and were predicted to be deleterious (Table 1). The mutation detected in case #17 (His1374Tyr) has been previously reported as a germline mutation of uncertain significance in a subject affected by a not otherwise specified cancer-predisposing syndrome (SCV000215178.1 in ClinVar database; http://www.ncbi.nlm.nih.gov/clinvar). Three of the five prediction algorithms used in this study classified it as damaging or possibly damaging. The *NF1* missense variants detected in the two KIT-mutated GISTs (case # 28, Ala456Val; # 38, Ala1676Thr) were classified as nonpathogenic by at least four of five prediction tools.

Differently from the two *NF1*-mutated GISTs of the *KIT/PDGFRA/SDH*^{m} group, most quadruple-negative/*NF1*-mutated tumors bore a second *NF1* mutation (4 cases) or the mutation was homo/hemizygous (6 cases), suggestive of biallelic *NF1* inactivation (Table 1).

The actual expression of *NF1*-mutated alleles was confirmed in five GISTs for which RNA was available (cases # 8, 9, 13, 28, and 38).

Matched normal DNA was available for 12 of 15 *NF1*-mutated cases (11 quadruple-negative and 1 KIT-mutated GIST). The *NF1* alteration detected in the tumor was also detected in the matched normal tissue, indicative of its constitutional nature, in 7 of 11 (64%) quadruple-negative and in the KIT-mutated case analyzed (Table 1). In case # 19, the *NF1* alteration (a constitutional intragenic deletion encompassing exon 3) was detected in histologically tumor-free normal tissue adjacent to the tumor but was absent in peripheral blood cells, suggesting a postzygotic mosaicism.

Clinicopathologic correlations

Quadruple-negative versus KIT/PDGFRA/SDH*^{m} *GISTs. Comparison of the clinical characteristics of quadruple-negative versus *KIT/PDGFRA/SDH*^{m} groups revealed a trend toward female predominance in the quadruple-negative group (male-to-female ratio, 8:14 vs. 14:10; $P = 0.15$; Fisher exact test). The two groups did not significantly differ in terms of age (median, 60 vs. 64.5 years), history of other malignancies (3/22 vs. 3/24), mitotic index (median 8 in both groups), and size (6.0 vs. 5.4 cm), but were instead heterogeneous in terms of anatomical location. The stomach was the prevalent site in the *KIT/PDGFRA/SDH*^{m} group (75%), in line with literature data (1, 8, 23), whereas was uncommon in the quadruple-negative group (19%; $P < 0.001$, Fisher exact test). In this latter group, the majority of the tumors developed in the intestine (71%; 12 small intestine; 2 duodenum; 1 in the sigmoid colon) or other sites (1 peritoneum and 1 retroperitoneum).

In the quadruple-negative group, 8 patients were either metastatic at diagnosis (4 cases) or developed subsequent metastases (4 cases); 5 patients were dead of disease at the last follow-up. In the *KIT/PDGFRA/SDH*^{m} group, 3 of 20 assessable cases developed distant metastases (liver, peritoneum, bone) and 1 patient (*SDH*-mutated) presented at diagnosis with lymph node invasion; only

Published OnlineFirst July 7, 2016; DOI: 10.1158/1078-0432.CCR-16-0152

Table 1. *NF1* gene mutations

Case #	Group (mutated gene)	*NF1* gene mutation	Mutant variant frequency (%)	Biallelic inactivation	Nature of *NF1* mutation	*NF1* mutation consequence	NF1 protein change	HGMD report of NF-Type 1	Prediction of pathogenicity					
									Provean	*SIFT*	*PolyPhen2*	*Mutation assessor*	*PaPI*	*Human splicing finder*
2	Quadruple-negative	c.6855C>A	96	Yes	U	Stop gained	p.Tyr2285Ter	CM981382; CM972796	Deleterious	–	–	–	–	–
3	Quadruple-negative	c.4725-2A>G	32	No	U	Splice acceptor variant	?	CS086424	–	–	–	–	–	Alteration of the wt acceptor site, most probably affecting splicing
5	Quadruple-negative	exon 2-28 del	>80	Yes	C	Deletion	?	CG060178	–	–	–	–	–	–
7	Quadruple-negative	c.1105C>T	51	Yes	C	Stop gained	p.Gln369Ter	–	Deleterious	–	–	–	–	–
		c.6380delT	35		S	Frameshift variant, truncation	p.Asn2128Ile fsTer22	–	Deleterious	–	–	–	–	–
8	Quadruple-negative	c.4600C>T	89	Yes	C	Stop gained	p.Arg1534Ter	CM941093	Deleterious	–	–	–	–	–
9	Quadruple-negative	c.1658A>G	95	Yes	C	Missense variant	p.His553Arg	HM0703	Deleterious	Damaging	Probably damaging	Medium	Damaging	–
11	Quadruple-negative	c.2514delC	34	Yes	S	Frameshift variant, truncation	p.Asn839Thr fsTer2	–	Deleterious	–	–	–	–	–
		c.1641+1G>T	36		S	Splice donor variant	?	CS000896	–	–	–	–	–	Alteration of the wt donor site, most probably affecting splicing
12	Quadruple-negative	c.6148-1G>A	48	Yes	S	Splice acceptor variant	?	CS086428	–	–	–	–	–	Broken wt donor site, activation of an intronic cryptic acceptor site, potential alteration of splicing
		c.7869+1G>T	48		S	Splice donor variant	?	CS031796; CS086439	–	–	–	–	–	Alteration of the wt donor site, most probably affecting splicing
13	Quadruple-negative	c.2511G>A	50	No	S	Stop gained	p.Trp837Ter	CM076345	Deleterious	–	–	–	–	–
17	Quadruple-negative	c.4120C>T	50	No	C	Missense variant	p.His1374Tyr	–	Neutral	Damaging	Possibly damaging	Low	Damaging	–
18	Quadruple-negative	c.2272_2273delAG	89	Yes	C	Frameshift variant, truncation	p.Arg758Ser fsTer9	CD000965	Deleterious	–	–	–	–	–
19	Quadruple-negative	exon 3 del	42	Yes	C	Deletion	?	–	–	–	–	–	–	–
		c.1398_1399insA	34		S	Frameshift variant, truncation	p.Thr467Asn fsTer3	CI031910	Deleterious	–	–	–	–	
21	Quadruple-negative	c.5430_5431insA	72	Yes	S	Frameshift variant, truncation	p.Thr1811AsnfsTer8	–	Deleterious	–	–	–	–	
28	*KIT* p.Val559_Glu561del	c.1367C>T	48	No	U	Missense variant	p.Ala456Val	–	Neutral	Tolerated	Benign	Low	Tolerated	–
38	*KIT* p.Val560Asp	c.5026G>A	51	No	C	Missense variant	p.Ala1676Thr	–	Deleterious	Tolerated	Benign	Low	Tolerated	–

NOTE: *NF1* mutation. Reference gene sequence: NM_001042492.2; Reference protein sequence: NP_001035957.1.

Nature of *NF1* mutation: U, undetermined; C, constitutional; S, somatic, detected in tumor only.

HGMD report of NF-Type 1 association: http://www.hgmd.cf.ac.uk/ac/gene.php?gene=NF1.

Published OnlineFirst July 7, 2016; DOI: 10.1158/1078-0432.CCR-16-0152

Table 2. Clinical characteristics of quadruple-negative GIST patients

Case #	Group	Nature of *NF1* mutation	Sex	Age	Disease status at diagnosis	Other malignancies	Relapse	Time to relapse (months)	GIST Medical therapy	Status at last follow-up (months)
1	*NF1* wild-type	—	F	58	NA	NA	NA		NA	NA
4		—	F	69	Localized	No	Yes (liver)	67	Imatinib (at relapse)	AWD (67)
6		—	M	53	Localized	NA	No		NA	NA
10		—	F	77	Localized	No	No		No	NED (15)
14		—	F	68	Localized	No	No		No	NED (72)
15		—	M	68	Localized	No	No		No	NED (72)
16		—	F	70	Localized	No	Yes (liver + peritoneum)	38	Imatinib (at relapse), sunitinib	DOD (89)
20		—	M	60	Localized	No	No		No	NED (26)
22		—	F	30	Localized	No	No		No	NED (13)
2	*NF1* mutated	U	M	35	NA	NA	NA	NA	NA	NA
3		U	F	76	Localized	No	NA	NA	NA	NA
5		C	F	73	Metastatic (peritoneum)	Breast carcinoma	Yes (liver)	25	No imatinib (chemotherapy for breast cancer)	DOD (39)
7		C	F	60	Localized	Breast carcinoma	Yes (peritoneum)	122	Imatinib (at relapse)	DOD (129)
8		C	F	31	Metastatic (peritoneum)	No	Yes (liver)	12	Imatinib (ab initio)	DOD (16)
9		C	F	73	Localized	No	Yes (peritoneum)	15	Imatinib (at relapse), sunitinib	DOD (39)
11		S	M	59	Localized	Chromophobe renal cell carcinoma; colon adenocarcinoma	No		No	NED (6)
12		S	M	50	Localized	No	No		No	NED (24)
13		S	F	86	Localized	No	No		No	NED (26)
17		C	F	42	Metastatic (peritoneum)	No	Yes (peritoneum)	7	Imatinib (ab initio), sunitinib, regorafenib	AWD (59)
18		C	M	56	Localized	No	No		No	NED (27)
19		C	F	67	Localized	No	No		No	NED (3)
21		S	M	36	Metastatic (peritoneum)	No	No		No	NED (12)

NOTE: Nature of *NF1* mutation: U, undetermined; C, constitutional; S, somatic, detected in tumor only.
Clinical information: NA, not available; AWD, alive with disease; DOD, dead of disease; NED, no evidence of disease.

1 patient (*KIT*-mutated gastric GIST) was dead of disease at the last follow-up.

NF1-mutated versus NF1-wild-type quadruple-negative GISTs. To understand whether the mutation of *NF1* was associated with distinctive biological features, *NF1*-mutated and *NF1*-wild-type quadruple-negative tumors were compared for a number of clinicopathologic characteristics (Tables 2 and 3).

Neither personal/familial history of NF-Type 1 nor dermatological signs or neoplasias referable to NF-Type 1 were documented in the clinical records of any patient prior inclusion in this study. Although we failed to retrieve complete clinical history of 1 patient (case # 2), this case was submitted for consultation as a sporadic GIST.

No statistical difference between *NF1*-mutated and *NF1*-wild-type quadruple-negative cases was observed in terms of sex (male-to-female ratio, 5:8 vs. 3:6), age (median, 59 vs. 68 years), mitotic index (median, 8 vs. 5), tumor size (median, 7 vs. 5.8 cm), and distribution of tumor locations.

Although no other malignancies were reported in the *NF1*-wild-type group, 3 *NF1*-mutated patients had a concurrent malignancy. Specifically, 2 patients with a *NF1* constitutional mutation (cases # 5 and 7) had a history of breast carcinoma; patient # 11, with a somatic *NF1* mutation in the GIST, presented with 2 other concomitant tumors (chromophobe renal cell carcinoma and colon cancer).

Multifocality at diagnosis was observed only in the *NF1*-mutated group. Two patients (# 3 and # 19) presented with synchronous small intestinal lesions. An unusual pattern of progression was noticed in two other cases: patient # 7 developed two subsequent GISTs within the small intestine wall seven years after first surgery for a low-risk small intestinal GIST; patient # 9, with a primary peritoneal GIST, relapsed twice with a predominant small intestinal GIST associated with smaller peritoneal nodules. All these cases carried a *NF1* constitutional defect.

A multinodular growth pattern with fibromuscular septa, similar to that described for SDH-deficient GISTs, was evident in four cases, all with constitutional *NF1* alterations (Fig. 1).

NF1-wild-type tumors exhibited spindle morphology in four cases, mixed in two, and epithelioid in three.

The morphology in the *NF1*-mutated group was spindle in seven cases, mixed in three, and epithelioid in two (Fig. 1). Interestingly, six of seven *NF1*-mutated GISTs with spindle cell morphology showed features typical of GISTs arising in the context of NF-Type 1: they were hypocellular throughout and featured abundant extracellular collagen with skenoid fibers. Areas with such features were also found in one of the three GISTs with mixed morphology. Unusual features were detected in

Published OnlineFirst July 7, 2016; DOI: 10.1158/1078-0432.CCR-16-0152

Table 3. Pathologic features of quadruple-negative GISTs

Case #	Group	Nature of *NF1* mutation	Tumor multifocality	Growth pattern	Site of primary GIST	Size	Mitotic index	Morphology	Degree of cellularity	Presence of skenoid fibers
1	*NF1* wild-type	—	No	Single nodule	Small intestine	6.0	2	Spindle	Moderate	No
4		—	No	NA	Small intestine	NA	21	Mixed	High	NA
6		—	No	Single nodule	Retroperitoneum	8.0	20	Epithelioid	High	No
10		—	No	Single nodule	Stomach	15.0	29	Spindle	High	No
14		—	No	Single nodule	Stomach	5.5	5	Epithelioid	NA	No
15		—	No	Single nodule	Duodenum	2.3	1	Spindle	NA	No
16		—	No	Single nodule	Small intestine	11.5	87	Epithelioid	High	No
20		—	No	Single nodule	Small intestine	4.5	3	Spindle	Low	Yes
22		—	No	Single nodule	Small intestine	3.2	3	Mixed	Moderate	No
2	*NF1* mutated	U	NA	NA	NA	NA	NA	NA	NA	NA
3		U	Yes	Single nodule	Small intestine (Ileum + Jejunum)	1.5+2.5	1	Spindle	Low	Yes
5		C	No	Multinodular	Duodenum	8.0	18	Mixed	Moderate (spindle cell areas of low cellularity)	Yes
7		C	Yes (metachronous[a])	Multinodular	Small intestine	6.0	2	Spindle	Low	Yes
8		C	No	Multinodular	Small intestine	9.0	83	Mixed	High	No
9		C	Yes (metachronous[b])	Single nodule	Peritoneum	16.0	30	Epithelioid/ Plasmacytoid	High	No
11		S	No	Single nodule	Small intestine	1.5	0	Spindle	Low	Yes
12		S	No	Single nodule	Small intestine	6.0	1	Spindle	Low	Yes
13		S	No	Single nodule	Small intestine	8.0	8	Spindle	Low	Yes
17		C	No	NA	Sigmoid colon	8.0	39	Epithelioid/ Small round cell	High	No
18		C	No	Single nodule	Stomach	3.2	8	Mixed	Moderate	No
19		C	Yes	Multinodular	Small intestine	3 + other[c]	2	Spindle	Low	Yes
21		S	No	Single nodule	Stomach	11	10	Spindle	High	No

NOTE: Nature of *NF1* mutation: U, undetermined; C, constitutional; S, somatic, detected in tumor only.
Abbreviation: NA, not available.
[a]This patient developed two subsequent GISTs of small size and low mitotic index in the small intestinal wall, seven years after first surgery.
[b]This patient relapsed twice, 15 and 30 months after first surgery, with a predominant small intestinal tumor and smaller peritoneal nodules.
[c]This patient presented with a predominant tumor (3 cm) and 6 additional smaller subserosal nodules (size range, 0.2–1.2 cm).

the two *NF1*-mutated GISTs with epithelioid morphology: one case displayed a striking plasmacytoid phenotype with eccentric vesicular nuclei, evident nucleoli, and abundant eosinophilic cytoplasm; the other was a small round cell tumor. Both these cases featured a very high mitotic index (Fig. 1).

Disease status at diagnosis was known for 12 *NF1*-mutated and 8 *NF1*-wild-type cases. All *NF1*-wild-type patients presented with localized disease; two of them developed metastasis 38 and 67 months after surgery. Among *NF1*-mutated patients, 4 had peritoneal metastases at diagnosis; progression was reported in 2 cases localized at the diagnosis, at 15 and 122 months, respectively.

Data on the clinical therapy were available for 7 *NF1*-wild-type and 11 *NF1*-mutated cases (Table 2). Imatinib was administered to 2 metastatic patients *ab initio*, both *NF-1* mutated, and upon relapse in 4 cases, 2 *NF1*-wild-type and 2 *NF1*-mutated. One *NF1*-wild-type and 2 *NF1*-mutated cases were shifted to second- and third-line therapy. For *NF1*-mutated cases, median time to progression under imatinib was 9.5 months (range, 7–18 months).

Regarding patients' outcome, follow-up information was available for 7 *NF1*-wild-type patients and 11 cases with *NF1* mutation. Within the *NF1*-wild-type group, patient # 16 died of disease (89 months); patient # 4 was alive with disease (67 months after surgery); 5 patients were disease-free at the last follow-up. Within the *NF1*-mutated group, 4 patients died of disease (median time to death 39 months), 1 patient was alive with disease 59 months after surgery, and 6 patients were disease-free at the last follow-up.

NF-Type 1 expert re-evaluation of patients with constitutional NF1 mutation. Of the 7 patients with ascertained constitutional *NF1* mutation, 4 were deceased and the 3 living patients agreed to be referred to a NF-Type 1 expert. According to the specialist, patient #17 failed to fulfill NIH diagnostic criteria for NF-Type 1 (6). A diagnosis of NF-Type 1 was instead eventually made for patients # 18 and #19 who had a negative family history for NF-Type 1. Patient # 18 presented with axillary/inguinal freckling, several neurofibromas, and 14 *café-au-lait* macules greater than 15 mm. The patient suffered also of severe vision impairment attributed to *Retinitis pigmentosa*. In patient # 19, the medical geneticist detected small cutaneous neurofibromas in the trunk, 2 *café-au-lait* spots and skin-fold freckles, consistent with mild

Published OnlineFirst July 7, 2016; DOI: 10.1158/1078-0432.CCR-16-0152

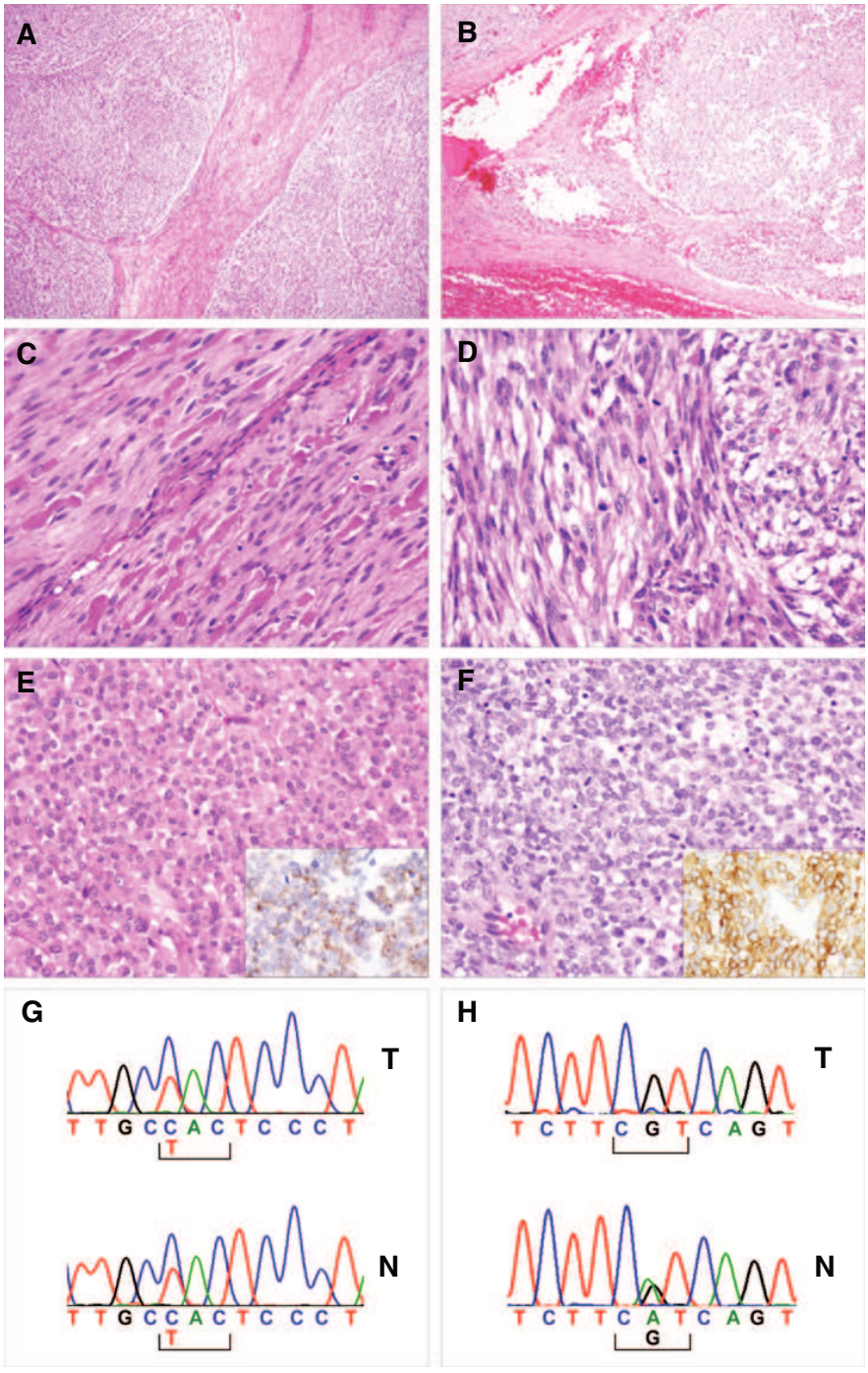

Figure 1.
Pathologic and molecular features of *NF1*-mutated GISTs. **A** and **B,** Multinodular growth pattern with thick fibrous septa in cases # 8 (**A**) and # 5 (**B**). **C,** Spindle cell morphology with abundant skenoid fibers, hypocellularity, and low mitotic activity in case # 3. **D,** Hypercellularity, nuclear atypia, and high mitotic index in case # 8. **E,** Plasmacytoid morphology and high mitotic index in case # 9. CD117 expression was diffused with a membranous and dot-like pattern of staining (inset). **F,** Small round cell morphology and high mitotic index in case # 17. CD117 expression was diffused with a membranous and cytoplasmic pattern of staining (inset). **G,** Case # 17 carried a constitutional C to T transition, resulting in a His to Tyr amino acid substitution at codon 1374. Both tumor (T) and normal tissue (N) were heterozygous for the mutation. **H,** Case # 9 carried a constitutional A to G transition, resulting in a His to Arg amino acid substitution at codon 553. The wild-type allele was lost in the tumor (T).

form of NF-Type 1. Intriguingly, the intragenic deletion encompassing *NF1* exon 3 detected in the proband's tumor and in adjacent, histologically tumor-free, normal tissue was absent in peripheral blood cells, supporting a postzygotic mosaicism. No hallmarks of NF-Type 1 were detected in the patient's daughter (44 years).

Discussion

This study aimed at gaining insight into the genetics of quadruple-negative GISTs, representing a fraction of tumors currently "orphan" of oncogenic driver alterations. To this end, we collected 22 quadruple-negative sporadic GISTs arisen in patients with no

Published OnlineFirst July 7, 2016; DOI: 10.1158/1078-0432.CCR-16-0152

prior association with NF-Type 1. For comparison purposes, 24 consecutive GISTs with *KIT*, *PDGFRA*, or *SDH* alterations were also analyzed. The majority of the quadruple-negative GISTs turned out to be nongastric tumors. This finding may be explained by the fact that a large fraction of wild-type gastric GISTs rely on SDH inactivation as an alternative to *KIT/PDGFRA* oncogenic mutation (8), thus leaving the driver alteration of nongastric GISTs undetermined. This supports the notion that GISTs arising in different sites feature different genetic backgrounds.

The molecular profiling of our GIST series revealed an unexpected high frequency of *NF1* mutations, particularly in the quadruple-negative group (13/22; 59%). *NF1* encodes neurofibromin, a GTPase-activating protein that binds to active GTP-bound RAS, and works as an off signal for all members of the RAS GTPase family. Similarly to *KIT*-, *PDGFRA*-, or *BRAF*-activating mutations, loss of NF1 leads to the unleashing of the MAPK cascade (5). The detection of a high frequency of pathogenic *NF1* mutations in "sporadic" quadruple-negative GISTs indicates that the triggering of the RAS/RAF/MAPK pathway by means of NF1 inactivation plays a relevant role in the pathogenesis of GIST devoid of canonical tyrosine kinase receptor mutations.

Another and perhaps the most intriguing finding of our study is that *NF1* mutations in quadruple-negative GISTs were constitutional in 7 of 11 cases tested, and often associated with biallelic inactivation. We would like to emphasize that the design of our study excluded *a priori* all patients with documented familial history, genetic diagnosis, or recorded diagnostic stigmata of NF-Type 1. Thus, our results demonstrate that a significant fraction of patients presenting to surgical and medical oncology clinics with quadruple-negative "sporadic" GIST are *de facto* affected by unrecognized forms of the NF-Type 1 syndrome.

This is reminiscent of the SDH "saga," where *SDH* germline mutations were originally described in the Carney–Stratakis syndrome (familial paraganglioma and GIST; refs. 10, 11, 24, 25) and only subsequently acknowledged to contribute to a significant fraction of apparently "sporadic" GISTs (8, 24–28). It is also in line with recent reports that susceptibility to cancer due to unsuspected syndromic conditions is more frequent than commonly believed (29).

The association between NF-Type 1 syndrome and cancer is well known, but *NF1* mutation analysis has long been challenging because of the large gene size (58 exons), multiple alternatively spliced isoforms, and existence of multiple pseudogenes (5). The recent advent of MPS technologies is not only facilitating the molecular diagnosis of NF-Type 1 probands, but is also revealing that somatic *NF1* mutations are involved in up to 12% of sporadic tumors, including glioblastomas, lung, breast, ovarian, Merkel cell carcinomas, melanomas, and sarcomas (5, 30–32). Our report highlights that quadruple-negative "sporadic" GISTs often arise in the context of unrecognized NF-Type 1 syndrome.

NF-Type 1 is the most common autosomally dominant inherited disorder in humans, with an incidence of about 1:3,000 live births in Western Countries (14, 15, 33). *NF1* is one of the genes with the highest mutation rates, and approximately 50% of clinically diagnosed NF-Type 1 patients carry *de-novo NF1* mutations. These mutations can also occur late in embryo development and may therefore be present in a mosaic state, accounting for the segmental forms of the disease (33, 34). NF-Type 1 features a poor genotype–phenotype correlation and an extremely variable expression pattern, with the spectrum and extent of manifestations varying greatly among affected individuals within a single family and even within a single person at different times of life (16). NIH clinical diagnostic criteria comprise *café-au-lait* macules, multiple neurofibromas, axillary/groin freckling, iris hamartomas (Lisch nodules), optic pathway glioma, and distinctive osseous lesions (6). It should be kept in mind that these criteria, established in 1988, were originally aimed at selecting those individuals whose genetic profiling would have eventually lead to the identification of the *NF1* gene. They were therefore purposely stringent, essentially based on visual inspection of the subject and did not include malignant tumors. As a matter of fact, NF-Type 1 patients do have an increased risk of developing tumors of different types, primarily in nervous system (i.e., malignant peripheral nerve sheat tumors, gliomas, plexiform neurofibromas, ganglioneuromas) but also in other sites (33, 35–37). The risk of GIST is also augmented in NF-Type 1 patients (36, 37), although Miettinen and colleagues reported that only a minute fraction (1.5%) of GISTs included in the AFIP files were arisen in patients with a diagnosis of NF-Type 1 (38).

The remarkable frequency of *NF1* constitutional mutation detected in our series of quadruple-negative GISTs prompted a clinical reassessment of the carriers. NF-Type 1 expert re-evaluation of the 3 living patients carrying a constitutional mutation (#17, 18, and 19) confirmed a negative familial history for the disease. No clinical manifestations complying with the NIH diagnostic criteria were identified by the specialist in patient #17. The *NF1* mutation detected in this individual, His1374Tyr, has been previously identified in a subject affected by a not otherwise specified cancer-predisposing condition (ClinVar). Although originally classified as of uncertain significance, three of the five prediction algorithms used in our study indicated a damaging/possibly damaging effect. Overall, these findings are compatible with either a segmental disease or with a low-expressivity form. Interestingly, a 3-bp inframe deletion has been recently reported to be associated with a *forme fruste* of NF-Type 1 that is portrayed, in some individuals, by no other sign but few *café-au-lait* macules (39). It is tempting to speculate that the mutation detected in patient #17 may also convey a very attenuated phenotype. Intriguingly, this patient was diagnosed with a GIST located in the colon, an exceedingly rare site, since the so-called colorectal GISTs predominantly develop in the lower rectum (23, 40). The link between His1374Tyr mutation and GIST location in the colon is worth further investigation.

The clinical geneticist was instead able to identify pathognomonic signs consistent with NF-Type 1 in case #18 and, in a milder form, in case #19, who is a carrier of a post-zygotic mosaic *NF1* mutation. It is noteworthy that the syndromic condition of these patients was essentially overlooked by all the doctors (general practitioner, ophthalmologist, surgeon, oncologist, etc.), the patients have dealt with during their life (67 and 56 years, respectively), and that only the occurrence of a GIST with peculiar characteristics (quadruple negative) brought these cases to the attention of the genetic counselor, who eventually made the diagnosis of NF-Type 1.

The extreme variability of NF-Type 1 clinical presentations and expressivity, the fact that GIST are not considered a common finding in these patients, together with the complexity of the molecular diagnosis of NF-Type 1, likely explain the underestimation of the role of *NF1* in the pathogenesis of "sporadic" GISTs. Currently, in the absence of family history or obvious clinical stigmata, the presence of a quadruple-negative GIST is not considered suggestive of an NF-Type 1 syndromic condition. Nevertheless, besides being commonly devoid of *KIT/PDGFRA/BRAF/*

Published OnlineFirst July 7, 2016; DOI: 10.1158/1078-0432.CCR-16-0152

SDH mutations, *NF1*-associated GISTs are reported to have distinctive clinicopathologic features, including multifocality and hypocellularity, spindle cell morphology with skenoid fibers, preferential location in the small bowel, and onset in the late fifth decade (38, 41–44). These characteristics were also exhibited by most *NF1*-mutated GISTs in our series. Moreover, a multinodular growth pattern was observed in four cases. This pattern has previously been deemed as typical of SDH-deficient GISTs (8, 25, 27), but our findings suggest that it likely reflects a more general trait of GISTs arising in syndromic contexts. Finally, although only four *NF1*-mutated GISTs received imatinib, overall the clinical benefit was unsatisfactory (median time to progression 9.5 months), adding support to the concept that *NF1*-associated GISTs are poorly responsive to this drug (44).

In conclusion, this study unveiled the genetic bases of a significant fraction of quadruple-negative GISTs, identifying the inactivation of *NF1 as* a key driver alteration. Moreover, the finding that the *NF1* mutation was constitutional in an important fraction of these patients suggests a role for GIST as a sentinel tumor for NF-Type 1. Hence, a diagnosis of quadruple-negative GIST, especially if multifocal or with a multinodular growth pattern and a nongastric location, should alert the clinician to a possible NF-Type 1 syndromic condition. These patients should be referred to NF-Type 1 specialists for a thorough search for subtle disease manifestations and to genetic counseling for definitive individual and familial risk assessment.

Disclosure of Potential Conflicts of Interest

A. Gronchi holds ownership interest (including patents) in Novartis and is a consultant/advisory board member for Bayer, Novartis, and Pfizer. No potential conflicts of interest were disclosed by the other authors.

Authors' Contributions

Conception and design: A.P. Dei Tos, R. Maestro
Development of methodology: D. Gasparotto, S Rossi, E. Lorenzetto, A. Mondello, A.P. Dei Tos
Acquisition of data (provided animals, acquired and managed patients, provided facilities, etc.): E. Tamborini, M. Massani, S. Lamon, R. Bracci, A. Mandolesi, E. Frate, F. Stanzial, J. Agaj, G. Mazzoleni, S. Pilotti, A. Gronchi
Analysis and interpretation of data (e.g., statistical analysis, biostatistics, computational analysis): M. Polano, J. Agaj, A. Gronchi, A.P. Dei Tos, R. Maestro
Writing, review, and/or revision of the manuscript: D. Gasparotto, S Rossi, F. Stanzial, A. Gronchi, A.P. Dei Tos, R. Maestro
Administrative, technical, or material support (i.e., reporting or organizing data, constructing databases): M. Sbaraglia, A. Gronchi
Study supervision: A.P. Dei Tos, R. Maestro

Acknowledgments

The authors are grateful to Fabio Canal, Matilde Cacciatore, Laura Papi, Francesco Benedicenti, and Joanne Fleming for their suggestions.

Grant Support

This work was supported by the Italian Association for Cancer Research (AIRC), the Italian Ministry of Health (Ricerca Finalizzata), and by a CRO Aviano National Cancer Institute Intramural Grant.

The costs of publication of this article were defrayed in part by the payment of page charges. This article must therefore be hereby marked *advertisement* in accordance with 18 U.S.C. Section 1734 solely to indicate this fact.

Received January 19, 2016; revised May 26, 2016; accepted June 14, 2016; published OnlineFirst July 7, 2016.

References

1. Corless CL. Gastrointestinal stromal tumors: What do we know now? Mod Pathol 2014;27Suppl 1:S1–16.
2. Rossi S, Sbaraglia M, Dell'orto MC, Gasparotto D, Cacciatore M, Boscato E, et al. Concomitant KIT/BRAF and PDGFRA/BRAF mutations are rare events in gastrointestinal stromal tumors. Oncotarget 2016;7:30109–18.
3. Brenca M, Rossi S, Polano M, Gasparotto D, Zanatta L, Racanelli D, et al. Transcriptome sequencing identifies ETV6-NTRK3 as a gene fusion involved in GIST. J Pathol 2016;238:543–9.
4. Doyle LA, Hornick JL. Gastrointestinal stromal tumours: From KIT to succinate dehydrogenase. Histopathology 2014;64:53–67.
5. Ratner N, Miller SJ. A rasopathy gene commonly mutated in cancer: The neurofibromatosis type 1 tumour suppressor. Nat Rev Cancer 2015;15:290–301.
6. Neurofibromatosis. Conference Statement. National Institutes Of Health (Nih) Consensus Development Conference. Arch Neurol 1988;45:575–8.
7. Pantaleo MA, Nannini M, Corless CL, Heinrich MC. Quadruple wild-type (WT) GIST: Defining the subset of GIST that lacks abnormalities of KIT, PDGFRA, SDH, or RAS signaling pathways. Cancer Med 2015;4:101–3.
8. Miettinen M, Wang ZF, Sarlomo-Rikala M, Osuch C, Rutkowski P, Lasota J. Succinate dehydrogenase-deficient GISTs: A clinicopathologic, immunohistochemical, and molecular genetic study of 66 gastric GISTs with predilection to young age. Am J Surg Pathol 2011;35:1712–21.
9. Blay JY, Le Cesne A, Cassier PA, Ray-Coquard IL. Gastrointestinal stromal tumors (GIST): A rare entity, a tumor model for personalized therapy, and yet ten different molecular subtypes. Discov Med 2012;13:357–67.
10. Mcwhinney SR, Pasini B, Stratakis CA, International Carney Triad And Carney-Stratakis Syndrome Consortium. Familial gastrointestinal stromal tumors and germ-line mutations. N Engl J Med 2007;357:1054–6.
11. Pasini B, Mcwhinney SR, Bei T, Matyakhina L, Stergiopoulos S, Muchow M, et al. Clinical and molecular genetics of patients with the Carney-Stratakis syndrome and germline mutations of the genes coding for the succinate dehydrogenase subunits SDHB, SDHC, and SDHD. Eur J Hum Genet 2008;16:79–88.
12. Haller F, Moskalev EA, Faucz FR, Barthelmess S, Wiemann S, Bieg M, et al. Aberrant DNA hypermethylation of SDHC: A novel mechanism of tumor development in Carney triad. Endocr Relat Cancer 2014;21:567–77.
13. Killian JK, Miettinen M, Walker RL, Wang Y, Zhu YJ, Waterfall JJ, et al. Recurrent epimutation of SDHC in gastrointestinal stromal tumors. Sci Transl Med 2014;6:268ra177.
14. Ferner RE, Huson SM, Thomas N, Moss C, Willshaw H, Evans DG, et al. Guidelines for the diagnosis and management of individuals with neurofibromatosis 1. J Med Genet 2007;44:81–8.
15. Boyd KP, Korf BR, Theos A. Neurofibromatosis type 1. J Am Acad Dermatol 2009;61:1–14.
16. Jett K, Friedman JM. Clinical and genetic aspects of neurofibromatosis 1. Genet Med 2010;12:1–11.
17. Choi Y, Chan AP. PROVEAN web server: A tool to predict the functional effect of amino acid substitutions and indels. Bioinformatics 2015;31:2745–7.
18. Ng PC, Henikoff S. Sift: Predicting amino acid changes that affect protein function. Nucleic Acids Res 2003;31:3812–4.
19. Adzhubei IA, Schmidt S, Peshkin L, Ramensky VE, Gerasimova A, Bork P, et al. A method and server for predicting damaging missense mutations. Nat Methods 2010;7:248–9.
20. Reva B, Antipin Y, Sander C. Predicting the functional impact of protein mutations: Application to cancer genomics. Nucleic Acids Res 2011;39:E118.
21. Limongelli I, Marini S, Bellazzi R. PaPI: Pseudo amino acid composition to score human protein-coding variants. Bmc Bioinformatics 2015;16:123.
22. Desmet FO, Hamroun D, Lalande M, Collod-Beroud G, Claustres M, Beroud C. Human splicing finder: An online bioinformatics tool to predict splicing signals. Nucleic Acids Res 2009;37:E67.

Published OnlineFirst July 7, 2016; DOI: 10.1158/1078-0432.CCR-16-0152

23. Rossi S, Gasparotto D, Miceli R, Toffolatti L, Gallina G, Scaramel E, et al. KIT, PDGFRA, and BRAF mutational spectrum impacts on the natural history of imatinib-naive localized GIST: A population-based study. Am J Surg Pathol 2015;39:922–30.
24. Gill AJ, Benn DE, Chou A, Clarkson A, Muljono A, Meyer-Rochow GY, et al. Immunohistochemistry for SDHB triages genetic testing of SDHB, SDHC, and SDHD in paraganglioma-pheochromocytoma syndromes. Hum Pathol 2010;41:805–14.
25. Gill AJ, Chou A, Vilain R, Clarkson A, Lui M, Jin R, et al. Immunohistochemistry for SDHB divides gastrointestinal stromal tumors (GISTs) into 2 distinct types. Am J Surg Pathol 2010;34:636–44.
26. Boikos SA, Pappo AS, Killian JK, Laquaglia MP, Weldon CB, George S, et al. Molecular subtypes of KIT/PDGFRA wild-type gastrointestinal stromal tumors: a report from The National Institutes of Health Gastrointestinal Stromal Tumor Clinic. JAMA Oncol 2016Mar 24. [Epub ahead of print].
27. Doyle LA, Nelson D, Heinrich MC, Corless CL, Hornick JL. Loss of succinate dehydrogenase subunit B (SDHB) expression is limited to a distinctive subset of gastric wild-type gastrointestinal stromal tumours: A comprehensive genotype-phenotype correlation study. Histopathology 2012;61:801–9.
28. Gasparotto D, Rossi S, Campagna D, Scavina P, Tiziano FD, Marzotto A, et al. Imatinib-sensitizing KIT mutation in a Carney-Stratakis-associated GI stromal tumor. J Clin Oncol 2016;34:E99–103.
29. Schrader KA, Cheng DT, Joseph V, Prasad M, Walsh M, Zehir A, et al. Germline variants in targeted tumor sequencing using matched normal DNA. Jama Oncol 2016;2:104–11.
30. Krauthammer M, Kong Y, Bacchiocchi A, Evans P, Pornputtapong N, Wu C, et al. Exome sequencing identifies recurrent mutations in NF1 and rasopathy genes in sun-exposed melanomas. Nat Genet 2015;47:996–1002.
31. Hechtman JF, Zehir A, Mitchell T, Borsu L, Singer S, Tap W, et al. Novel oncogene and tumor suppressor mutations in KIT And PDGFRA wild type gastrointestinal stromal tumors revealed by next generation sequencing. Genes Chromosomes Cancer 2015;54:177–84.
32. Belinsky MG, Rink L, Cai KQ, Capuzzi SJ, Hoang Y, Chien J, et al. Somatic loss of function mutations in neurofibromin 1 and MYC associated factor x genes identified by exome-wide sequencing in a wild-type GIST case. Bmc Cancer 2015;15:887.
33. Ferner RE. Neurofibromatosis 1 and neurofibromatosis 2: A twenty first century perspective. Lancet Neurol 2007;6:340–51.
34. Messiaen L, Vogt J, Bengesser K, Fu C, Mikhail F, Serra E, et al. Mosaic type-1 NF1 microdeletions as a cause of both generalized and segmental neurofibromatosis type-1 (NF1). Hum Mutat 2011;32:213–9.
35. Zoller ME, Rembeck B, Oden A, Samuelsson M, Angervall L. Malignant and benign tumors in patients with neurofibromatosis type 1 in a defined Swedish population. Cancer 1997;79:2125–31.
36. Uusitalo E, Rantanen M, Kallionpää RA, Pöyhönen M, Leppävirta J, Ylä-Outinen H, et al. Distinctive cancer associations in patients with neurofibromatosis type 1. J Clin Oncol 2016;34:1978–86.
37. Andersson J, Sihto H, Meis-Kindblom JM, Joensuu H, Nupponen N, Kindblom LG. NF1-associated gastrointestinal stromal tumors have unique clinical, phenotypic, and genotypic characteristics. Am J Surg Pathol 2005;29:1170–6.
38. Miettinen M, Fetsch JF, Sobin LH, Lasota J. Gastrointestinal stromal tumors in patients with neurofibromatosis 1: A clinicopathologic and molecular genetic study of 45 cases. Am J Surg Pathol 2006;30:90–6.
39. Upadhyaya M, Huson SM, Davies M, Thomas N, Chuzhanova N, Giovannini S, et al. An absence of cutaneous neurofibromas associated with a 3-bp inframe deletion in exon 17 of the NF1 gene (C.2970-2972 delAAT): Evidence of a clinically significant NF1 genotype-phenotype correlation. Am J Hum Genet 2007;80:140–51.
40. Miettinen M, Sobin LH, Sarlomo-Rikala M. Immunohistochemical spectrum of GISTs at different sites and their differential diagnosis with a reference to CD117 (KIT). Mod Pathol 2000;13:1134–42.
41. Takazawa Y, Sakurai S, Sakuma Y, Ikeda T, Yamaguchi J, Hashizume Y, et al. Gastrointestinal stromal tumors of neurofibromatosis type I (Von Recklinghausen's disease). Am J Surg Pathol 2005;29:755–63.
42. Burgoyne AM, Somaiah N, Sicklick JK. Gastrointestinal stromal tumors in the setting of multiple tumor syndromes. Curr Opin Oncol 2014;26:408–14.
43. Agaimy A, Vassos N, Croner RS. Gastrointestinal manifestations of neurofibromatosis type 1 (Recklinghausen's disease): Clinicopathological spectrum with pathogenetic considerations. Int J Clin Exp Pathol 2012;5:852–62.
44. Mussi C, Schildhaus HU, Gronchi A, Wardelmann E, Hohenberger P. Therapeutic consequences from molecular biology for gastrointestinal stromal tumor patients affected by neurofibromatosis type 1. Clin Cancer Res 2008;14:4550–5.

Published OnlineFirst July 7, 2016; DOI: 10.1158/1078-0432.CCR-16-0152

AACR American Association for Cancer Research

Clinical Cancer Research

Quadruple-Negative GIST Is a Sentinel for Unrecognized Neurofibromatosis Type 1 Syndrome

Daniela Gasparotto, Sabrina Rossi, Maurizio Polano, et al.

Clin Cancer Res 2017;23:273-282. Published OnlineFirst July 7, 2016.

Modern Pathology (2017), 1–9

Neurofibromin C terminus-specific antibody (clone NFC) is a valuable tool for the identification of *NF1*-inactivated GISTs

Sabrina Rossi[1,8], Daniela Gasparotto[2,8], Matilde Cacciatore[1], Marta Sbaraglia[1], Alessia Mondello[2], Maurizio Polano[2], Alessandra Mandolesi[3], Alessandro Gronchi[4], David E Reuss[5,6], Andreas von Deimling[5,6], Roberta Maestro[2,9] and Angelo Paolo Dei Tos[1,7,9]

[1]Department of Pathology & Molecular Genetics, Treviso General Hospital, Treviso, Italy; [2]Oncogenetics and Functional Oncogenomics Unit, CRO Aviano National Cancer Institute, Aviano, Italy; [3]Department of Internal Medicine, Ospedali Riuniti di Ancona, Ancona, Italy; [4]Department of Surgery, Fondazione IRCCS Istituto Nazionale dei Tumori di Milano, Milano, Italy; [5]Department of Neuropathology, Institute of Pathology, University of Heidelberg, Heidelberg, Germany; [6]Clinical Cooperation Unit Neuropathology, German Cancer Consortium (DKTK), German Cancer Research Center (DKFZ), Heidelberg, Germany and [7]Department of Medicine, University of Padova School of Medicine, Padova, Italy

An increasing body of evidence supports the involvement of *NF1* mutations, constitutional or somatic, in the pathogenesis of gastrointestinal stromal tumors (GISTs). Due to the large size of the *NF1* locus, the existence of multiple pseudogenes and the wide spectrum of mechanisms of gene inactivation, the analysis of *NF1* gene status is still challenging for most laboratories. Here we sought to assess the efficacy of a recently developed neurofibromin-specific antibody (NFC) in detecting *NF1*-inactivated GISTs. NFC reactivity was analyzed in a series of 98 GISTs. Of these, 29 were '*NF1*-associated' (17 with ascertained *NF1* mutations and 12 arising in the context of clinically diagnosed Neurofibromatosis type 1 syndrome and thus considered *bona fine NF1* inactivated); 38 were '*NF1*-unrelated' (either wild-type or carrying non-pathogenic variants of *NF1*). Thirty-one additional GISTs with no available information on *NF1* gene status or with *NF1* gene variants of uncertain pathogenic significance were also included in the analysis. Cases were scored as NFC negative when, in the presence of NFC positive internal controls, no cytoplasmic staining was detected in the neoplastic cells. NFC immunoreactivity was lost in 24/29 (83%) *NF1*-associated GISTs as opposed to only 2/38 (5%) *NF1*-unrelated GISTs ($P = 3e-11$). NFC staining loss significantly correlated ($P = 0.007$) with the presence of biallelic *NF1* inactivation, due essentially to large deletions or truncating mutations. NFC reactivity was instead retained in two cases in which the *NF1* alteration was heterozygous and in one case where the pathogenic *NF1* variant, although homo/hemizygous, was a missense mutation predicted not to affect neurofibromin half-life. Overall this study provides evidence that NFC is a valuable tool for identifying *NF1*-inactivated GISTs, thus serving as a surrogate for molecular analysis.
Modern Pathology advance online publication, 1 September 2017; doi:10.1038/modpathol.2017.105

Neurofibromin, encoded by the *NF1* gene, is a GTPase-activating protein with tumor suppressor functions: neurofibromin binds and inhibits active GTP-bound Ras, preventing the downstream triggering of Ras effector pathways (MAPK and PI3K/Akt/mTOR). *NF1* gene inactivation is typically involved in the pathogenesis of tumors arising in the context of Neurofibromatosis type 1, most notably malignant peripheral nerve sheath tumors, neurofibromas, and optic pathway gliomas. However, recent evidence has broadened the spectrum of *NF1*-driven tumors and *NF1* mutations have been shown to contribute to the pathogenesis of over 10% sporadic tumors, including melanomas, glioblastomas, breast, ovarian and lung carcinomas, and sarcomas.[1–4]

Correspondence: Dr R Maestro, PhD, Oncogenetics and Functional Oncogenomics Unit, CRO Aviano National Cancer Institute, Via Gallini 2, Aviano 33081, Italy or Professor AP Dei Tos, MD, Department of Pathology & Molecular Genetics, Treviso General Hospital, Treviso 31100, Italy.
E-mail: maestro@cro.it or angelopaolo.deitos@aulss2.veneto.it
[8]S Rossi and D Gasparotto are co-first authors.
[9]R Maestro and AP Dei Tos are co-last authors
Received 19 April 2017; revised 30 June 2017; accepted 30 June 2017; published online 1 September 2017

We have recently reported that *NF1* is a driver mutation in a significant fraction of gastrointestinal stromal tumors (GISTs).[5] GIST is the most frequent mesenchymal neoplasm of the digestive tract. The vast majority of GISTs (about 85%) are typically driven by activating mutations of receptor tyrosine kinases, namely *KIT* and *PDGFRA*. *BRAF* or *HRAS* mutations have been reported in a few cases.[6,7] All these alterations result in the constitutive activation of MAPK and PI3K/Akt/mTOR pathways. About 5% of GISTs feature inactivation of components of the mitochondrial succinate dehydrogenase complex (*SDH*) and are typically associated with syndromic conditions (Carney Stratakis and Carney Triad). The remaining fraction of GISTs (a.k.a. quadruple-negative GISTs, about 10%) were essentially considered to be 'driver mutation unknown' until very recent literature highlighted that *NF1* mutations play a greater role in GIST pathogenesis than commonly thought.[4,5,8] *NF1* mutations were historically considered to be confined to GISTs arising in the context of Neurofibromatosis type 1.[7,9] We instead demonstrated that *NF1* mutations, be they constitutional or somatic, occur in a large proportion of 'apparently sporadic' quadruple-negative GISTs.[5] The presence of *NF1* mutations in GISTs has important diagnostic and predictive implications for patient management. Detection of an *NF1*-mutated GIST may be the sentinel of an unrecognized Neurofibromatosis type 1 condition, with obvious implications for the patient and his/her family. On the other hand, unlike receptor tyrosine kinase-mutated GISTs, which generally respond to kinase inhibitors, *NF1*-mutated GISTs are imatinib resistant.[9,10] Hence, the detection of *NF1* inactivation is crucial for proper clinical management of GIST patients.

The analysis of *NF1* gene status is problematic for most laboratories and the diagnosis of Neurofibromatosis type 1 is still essentially based on clinical findings. The large size of the *NF1* locus (58 exons and very large introns), the existence of multiple pseudogenes and the wide spectrum of mechanisms of gene inactivation (from missense mutations to large deletions, translocations and possibly epigenetic silencing), has long prevented comprehensive molecular testing of *NF1* and this investigation is still limited to a few laboratories equipped with massive parallel sequencing (next generation), comparative genomic hybridization technologies and multiplex ligation-dependent probe amplification approaches.[1,11]

Antibodies have proven to be reliable surrogates for gene alteration analysis in different contexts. For instance, HER2 staining is used to identify *HER2*-amplified breast cancers; anti-MDM2 antibodies are used to identify *MDM2*-amplified liposarcomas; ALK immunoreactivity is indicative of *ALK* rearrangements;[12] loss of SDHB staining is considered indicative of *SDHx* gene inactivation,[13] and VE1 antibody is a good surrogate for *BRAF* V600E mutation detection, also in the context of GISTs.[14–16]

We recently generated an antibody, NFC, directed against the last 281 amino acids of neurofibromin.[17] This region is commonly lost in *NF1*-inactivated tumors, as the vast majority of *NF1* mutations are deletions or give rise to truncated proteins.[1] NFC has demonstrated high sensitivity and specificity in distinguishing *NF1*-associated malignant peripheral nerve sheath tumors from other spindle cell neoplasms.[17,18]

Here we sought to explore the reliability of NFC staining in identifying *NF1*-associated GISTs. To this end, we screened a well-characterized series of GISTs and correlated NFC reactivity with *NF1* mutation data.

Materials and methods

Tumor Samples

Clinicopathological and molecular features of the analyzed tumor series are summarized in Table 1. The study was carried out on 98 formalin-fixed paraffin-embedded tumors retrieved from the pathological files of the collaborating institutions or submitted for consultation to one of the authors (APDT). The tumors—93 GISTs and 5 microGISTs (mGISTs, size ≤ 1 cm)—were from 89 patients (multiple tumors were analyzed for six patients). Twelve of these patients had a clinical diagnosis of Neurofibromatosis type 1. Informed consent was obtained from all living individuals.

Paraffin block age ranged from 6 to 254 months (median 48 months). All samples were freshly cut prior to staining.

All 98 cases included in the study were profiled for *KIT*, *PDGFRA*, *BRAF*, or *SDH* gene status; one quadruple-negative GIST carried an *ETV6–NTRK3* gene fusion.[19] The *NF1* gene status was ascertained in 56 samples: *NF1* pathogenic mutations were detected in 17 tumors, all of them quadruple-negative; three cases—two *KIT*-mutated tumors (#38, 39) and one quadruple-negative GIST (# 98)—bore non-pathogenic mutations and a genetic variant of uncertain pathogenic significance, respectively; 36 tumors were *NF1* wild-type.

The nature of the *NF1* mutations was assessed in 19/20 cases: the mutation was somatic in 4 GISTs (#5, #8, #10, #17) and constitutional in 15 (13 pathogenic, 1 non-pathogenic, and 1 variant of uncertain significance).

The five mGISTs included in the study were from patients with a diagnosis of Neurofibromatosis type 1.

The remaining 42 cases were not analyzed for *NF1* status. These included 30 sporadic GISTs and 12 GISTs that were considered *bona fide NF1* inactivated, having arisen in the context of clinically diagnosed Neurofibromatosis type 1.

Overall, from a molecular standpoint, our series was composed of three major groups: '*NF1*-associated'

Table 1 Clinicopathological and molecular characteristics of the series

Sample and patient characteristics									Driver	NF1 mutation_1				NF1 mutation_2					NFC reactivity	
Sample #	Tumor features	PATIENT #	AGE	SEX	NF-Type 1 (Clinical diagNosis)	SITE	SIZE (cm)	MI	Driver gene: KIT, PDGFRA, BRAF, SDH or NF1	Mutation	Origin	Variant Frequency	Protein change	Mutation	Origin	Variant Frequency	Protein change	NF1 biallelic Inactivation	NFC pattern	NFC staining intensity
1	GIST	P1	67	F	Y	Sm Int	3.0	2	NF1	exon 3 del	C	42	?	c. 1398_1399insA	S	34	p.Thr467AsnfsTer3	Y	CL	
2	GIST	P1	67	F	Y	Sm Int	1.2	0	NF1	nd									CL	
3	GIST	P2	60	F	N	Sm Int	2.5	2	NF1	c.1105C>T	C	51	p.Gln369Ter	c.6380delT	S	35	p.Asn2128IlefsTer22	Y	CL	
4	GIST	P3	26	M	Y	Sm Int	5.0	10	NF1	c.7189+2T>G	C	50	?	c.1576delA	S	46	p.Ile526LeufsTer30	Y	CL	
5	GIST	P4	59	M	N	Sm Int	1.5	0	NF1	c.1641+1G>T	S	36	?	c.2514delC	S	34	p.Asn839ThrfsTer2	Y	CL	
6	GIST	P5	73	F	N	Perit	16.0	30	NF1	c.1658A>G	C	95	p.His553Arg	NF1 mutation_1 in homozygosity/hemizygosity				Y	R	W
7	GIST	P6	56	M	Y	Stom	3.2	8	NF1	c.2272_2273delAG	C	89	p.Arg758SerfsTer9	NF1 mutation_1 in homozygosity/hemizygosity				Y	CL	
8	GIST	P7	86	F	N	Sm Int	8.0	8	NF1	c.2511G>A	S	50	p.Trp837Ter	c.5005delT	S	51	p. Phe1669LeufsTer28	Y	CL	
9	GIST	P8	31	F	N	Sm Int	9.0	83	NF1	c.4600C>T	C	89	p.Arg1534Ter	NF1 mutation_1 in homozygosity/hemizygosity				Y	CL	
10	GIST	P9	36	M	N	Perit	11.0	10	NF1	c.5430_5431insA	S	72	p.Thr1811AsnfsTer8	NF1 mutation_1 in homozygosity/hemizygosity				Y	CL	
11	GIST	P10	61	F	Y	Duod	4.0	6	NF1	c.1754_1757delTAAC	C	57	p.Thr586ValfsTer18					N	PL	W
12	mGIST	P10	61	F	Y	Sm Int	0.4	0	NF1	c.1754_1757delTAAC	C	57	p.Thr586ValfsTer18					N	PL	W
13	GIST	P11	73	F	N	Duod	8.0	18	NF1	exon 2-28 del	C	>80	?	NF1 mutation_1 in homozygosity/hemizygosity				Y	CL	
14	GIST	P12	53	M	Y	Sm Int	1.4	2	NF1	c.574C>T	C	53	p.Arg192Ter	c.1805delA	S	29	p.Ile603TyrfsTer2	Y	CL	
15	GIST	P12	53	M	Y	Sm Int	3.0	3	NF1	c.574C>T	C	63	p.Arg192Ter	c.3974+2T>A	S	23	?	Y	CL	
16	mGIST	P12	53	M	Y	Sm Int	0.8	0	NF1	nd									CL	
17	GIST	P13	71	F	N	Sm Int	1.5	0	NF1	c.2510G>A	S	33	p.Trp837Ter					N	R	M
18	GIST	P14	72	F	Y	Sm Int	1.2	0	NF1	c.7285delT	C	50	p.Phe2429LeufsTer3	c.5228_5229delCT	S	26	p.Leu1744GlnfsTer12	Y	PL	M
19	mGIST	P14	72	F	Y	Sm Int	0.4	0	NF1	c.7285delT	C	49	p.Phe2429LeufsTer3					N	R	W
20	mGIST	P14	72	F	Y	Sm Int	0.3	0	NF1	nd									PL	W
21	GIST	P15	46	M	Y	Sm Int	3.5		NF1 *(bona fide)*	nd									CL	
22	GIST	P16	42	F	Y	Sm Int	1.3	0	NF1 *(bona fide)*	nd									CL	
23	GIST	P16	42	F	Y	Sm Int	2.0	0	NF1 *(bona fide)*	nd									CL	
24	GIST	P17	55	F	Y	Lg Int	>2		NF1 *(bona fide)*	nd									CL	
25	GIST	P18	46	F	Y	Sm Int	>2		NF1 *(bona fide)*	nd									R	M
26	GIST	P19	65	M	Y	Duod	1.5	0	NF1 *(bona fide)*	nd									R	W
27	GIST	P19	65	M	Y	Duod	3.0	1	NF1 *(bona fide)*	nd									PL	W
28	mGIST	P19	65	M	Y	Duod	0.7	0	NF1 *(bona fide)*	nd									PL	W
29	GIST	P20	52	M	Y	Sm Int	5.0	1	NF1 *(bona fide)*	nd									PL	W
30	GIST	P21	31	F	N	Sm Int	3.2	3	unknown	wild-type									CL	
31	GIST	P22	53	M	N	RetroP	8.0	20	unknown	wild-type									R	M
32	GIST	P23	77	F	N	Stom	15.0	29	unknown	wild-type									CL	
33	GIST	P24	68	M	N	Stom	5.5	1	PDGFRA	wild-type									R	M
34	GIST	P25	71	M	N	Stom	5.2	3	PDGFRA	wild-type									R	M
35	GIST	P26	71	F	N	Stom	1.4	1	PDGFRA	wild-type									R	W
36	GIST	P27	81	F	N	Stom	12.0	18	PDGFRA	wild-type									R	S
37	GIST	P28	50	F	N	Stom	3.5	0	PDGFRA	wild-type									R	M
38	GIST	P29	41	M	N	Sm Int	1.9	1	KIT	non-path c.1367C>T	U	48	non-path p.Ala456Val					N	R	M
39	GIST	P30	64	M	N	Stom	4.5	12	KIT	non-path c.5026G>A	C	51	non-path p.Ala1676Thr					N	R	S
40	GIST	P31	73	M	N	Stom	2.0	2	KIT	wild-type									R	S
41	GIST	P32	72	M	N	Sm Int	8.0	12	KIT	wild-type									R	W
42	GIST	P33	74	F	N	Sm Int	9.5	20	KIT	wild-type									R	M
43	GIST	P34	77	F	N	Stom	3.5	2	KIT	wild-type									R	M
44	GIST	P35	43	M	N	Stom	5.0	5	KIT	wild-type									R	W
45	GIST	P36	72	M	N	Sm Int	5.5	1	KIT	wild-type									R	W
46	GIST	P37	75	M	N	Stom	4.0	23	KIT	wild-type									R	S
47	GIST	P38	63	F	N	Stom	6.5	5	KIT	wild-type									R	S
48	GIST	P39	39	F	N	Sm Int	2.0	10	KIT	wild-type									R	S
49	GIST	P40	41	M	N	Sm Int	5.0	7	KIT	wild-type									R	S
50	GIST	P41	70	F	N	Stom	6.0	73	KIT	wild-type									R	M
51	GIST	P42	75	F	N	Esoph	6.0	1	KIT	wild-type									R	W
52	GIST	P43	81	F	N	Stom	4.0	6	KIT	wild-type									R	W
53	GIST	P44	69	F	N	Stom	14.0	10	KIT	wild-type									R	S
54	GIST	P45	76	M	N	Stom	7.0	2	KIT	wild-type									R	M
55	GIST	P46	55	M	N	Stom	16.0	32	KIT	wild-type									R	W
56	GIST	P47	75	M	N	Sm Int	3.5	2	KIT	wild-type									R	W
57	GIST	P48	55	M	N	Stom	3.5	34	KIT	wild-type									R	S
58	GIST	P49	81	F	N	Stom	5.0	4	KIT	wild-type									R	W
59	GIST	P50	36	M	N	Sm Int	6.0	0	KIT	wild-type									R	M
60	GIST	P51	52	M	N	Sm Int	2.0	0	KIT	wild-type									R	M
61	GIST	P52	80	F	N	Sm Int	3.0	9	KIT	wild-type									R	M
62	GIST	P53	82	F	N	Sm Int	2.6	1	KIT	wild-type									R	M
63	GIST	P54	63	M	N	Sm Int	8.0	8	KIT	wild-type									R	M
64	GIST	P55	44	M	N	Rect	5.0	34	ETV6-NTRK3	wild-type									R	S
65	GIST	P56	88	F	N	Sm Int	1.8	1	BRAF	wild-type									R	S
66	GIST	P57	42	F	N	Sm Int	3.8	3	BRAF	wild-type									R	M
67	GIST	P58	65	F	N	Sm Int	5.4	12	BRAF	wild-type									R	S
68	GIST	P59	60	F	N	Sm Int	>2		KIT	nd									R	S
69	GIST	P60	81	M	N	Perit	>2		PDGFRA	nd									R	S
70	GIST	P61	76	F	N	Stom	>2		PDGFRA	nd									R	M
71	GIST	P62	85	F	N	Lg Int	20.0	10	KIT	nd									R	S
72	GIST	P63	76	M	N	Stom	1.8	1	PDGFRA	nd									R	W
73	GIST	P64	74	M	N	Stom	1.8	1	PDGFRA	nd									R	S
74	GIST	P65	45	F	N	Rect	>2		KIT	nd									R	S
75	GIST	P66	52	F	N	Sm Int	11.0	9	KIT	nd									R	M
76	GIST	P67	81	M	N	Stom	4.5		PDGFRA	nd									R	S
77	GIST	P68	69	M	N	Stom	10.5	3	PDGFRA	nd									R	M
78	GIST	P69	68	M	N	Stom	>2		KIT	nd									R	M
79	GIST	P70	62	M	N	Th Wall	>2		KIT	nd									R	M
80	GIST	P71	37	M	N	Rect	7.0		KIT	nd									R	W
81	GIST	P72	64	M	N	Stom	14.0	4	KIT	nd									R	S
82	GIST	P73	63	F	N	Sm Int	10.4	10	KIT	nd									R	M
83	GIST	P74	68	M	N	Stom	6.3	6	PDGFRA	nd									R	S
84	GIST	P75	50	M	N	Sm Int	>2		KIT	nd									R	S
85	GIST	P76	74	M	N	Perit	>2		PDGFRA	nd									R	S
86	GIST	P77	70	M	N	Duod	7.0	8	KIT	nd									R	M
87	GIST	P78	72	F	N	Stom	8.5	2	KIT	nd									R	S
88	GIST	P79	67	M	N	Stom	9.5	8	KIT	nd									R	M
89	GIST	P80	50	M	N	Sm Int	11.0	11	KIT	nd									R	S
90	GIST	P81	52	M	N	Sm Int	8.0	9	KIT	nd									R	W
91	GIST	P82	47	M	N	Stom	6.0	17	KIT	nd									R	S
92	GIST	P83	74	M	N	Stom	>2		PDGFRA	nd									R	S
93	GIST	P84	66	M	N	Perit	>2		KIT	nd									R	S
94	GIST	P85	47	F	N	Sm Int	10.5	1	KIT	nd									R	M
95	GIST	P86	63	F	N	Liver	>2		KIT	nd									R	S
96	GIST	P87	75	F	N	Stom	10.0	1	KIT	nd									R	S
97	GIST	P88	75	M	N	Perit	>2		KIT	nd									R	M
98	GIST	P89	42	F	N	Lg Int	5.0	39	unknown	unc-sign c.4120C>T	C	50	unc-sign p.His1374Tyr					N	R	M

Abbreviations: CL, complete loss; Duod, duodenum; Esoph, esophagus; Lg Int, large intestine; M, moderate staining intensity; N, No; ND, NF1 mutation analysis not done; non-path, non-pathogenic NF1 variants; Perit, peritoneum; PL, partial loss; R, retained; Rect, rectum; RetroP, retroperituneum; S, strong staining intensity; Sm Int, small intestine; Stom, stomach; Th Wall, thoracic wall; U, unspecified; unc-sign, NF1 variant of uncertain pathogenic significance; W, weak staining intensity; Y, Yes.
Brackets indicate multiple tumors of the same patients.

Table 2 NFC reactivity according to NF1 association

NF1 association	*Driver mutation (number of samples)*	*Evidence*	*NFC reactivity*	*NFC pattern of loss*	*Number of cases*
NF1-associated	Bona fide NF1 (12)	Clinical diagnosis of neurofibromatosis type 1	10 Loss	6 Complete, 4 partial	29
			2 Retention	No loss	
	NF1 (17)	Constitutional *NF1* pathogenic mutations *(13 cases)*	11 Loss	8 Complete, 3 partial	
			2 Retention	No loss	
		Somatic *NF1* pathogenic mutations *(4 cases)*	3 Loss	3 Complete	
			1 Retention	No loss	
NF1-unrelated	KIT (26) PDGFRA (5) BRAF (3) ETV6-NTRK3 (1) Unknown (3)	*NF1* wild-type or with non-pathogenic *NF1* variants No clinical evidence of neurofibromatosis type 1	2 Loss	2 Complete	38
			36 Retention	No loss	
Undetermined	KIT (21) PDGFRA (9) Unknown (1)	No information on *NF1* gene status or *NF1* variants of uncertain pathogenic significance No clinical evidence of neurofibromatosis type 1	31 Retention	No loss	31

tumors (29 cases), including the 17 tumors carrying *NF1* pathogenic mutations, together with the 12 GISTs arising in the context of clinically diagnosed Neurofibromatosis type 1; '*NF1*-unrelated' tumors, consisting of the 38 cases with no or non-pathogenic *NF1* mutations; '*NF1*-undetermined' cases (31 cases), including the sporadic GISTs with no available information on *NF1* status and the GIST (# 98) carrying an *NF1* variant of uncertain pathogenic significance (Table 2).

Irrespective of whether the origin of *NF1* mutation was constitutional or somatic, the small intestine was the prevalent site in *NF1*-associated GISTs (20/29 cases), as different from the *NF1*-unrelated tumors (16/38 cases) ($P = 0.047$), where gastric lesions were instead more common (19/38) ($P = 3e-5$) (Table 1), in agreement with previous reports.[5,20,21]

Immunohistochemistry

The NFC monoclonal antibody was used to assess neurofibromin protein expression by immunohistochemistry. This antibody was raised in mice by immunization with a recombinant protein corresponding to the C terminus of human neurofibromin (last 281 amino acids), a region commonly lost in *NF1*-inactivated tumors.[17] NFC demonstrated high sensitivity and specificity in the identification of *NF1*-associated malignant peripheral nerve sheath tumors.[17]

NFC immunostaining was performed on whole sections of the 29 *NF1*-associated tumors listed in Table 2 plus the case carrying an *NF1* variant of uncertain significance. Tissue microarrays were implemented for the remaining cases. Each tumor was represented by three 2-mm cores.

Freshly cut 4 μm sections were first dried at 60 °C for 30 min and then stained using an automated immunostainer (Dako AutostainerLink 48). The staining was preceded by heat-induced antigen retrieval (98 °C, waterbath) carried out in citrate buffer, pH 6.1 for 40 min (EnVision FLEX Target Retrieval Solution, low pH). The DAKO staining procedure included 5 min' incubation with FLEX Peroxidase Block, 1 h of incubation with 1:4 diluted NFC hybridoma supernatant, 15 min incubation with EnVision FLEX+ Mouse LINKER (Dako), 20 min incubation with the labeled polymer (HT/HRP), and 10 min incubation with a substrate chromogen (FLEX DAB+Sub Chromo). All staining steps were carried out at room temperature.

NFC expression was considered lost when no cytoplasmic staining was seen in the neoplastic cells but appropriate internal controls (fibroblasts, ganglion cells, plasma cells, endothelium, smooth muscle) reacted positively. NFC loss was regarded as complete when the neoplastic cells were homogeneously negative, and partial when the staining was heterogeneous with limited tumor areas retaining NFC expression. NFC expression was considered to be maintained when tumor cells were homogeneously positive. Staining intensity (weak, moderate, strong) was recorded.

Molecular Analysis

For the purposes of molecular analysis, areas enriched in tumor cells were marked by the pathologist on tissue slides. DNA was extracted with the EZ1 biorobot (Qiagen) or QIAamp DNA FFPE Tissue kit (Qiagen). Massive parallel sequencing libraries were prepared with a TruSeq Custom Amplicon v1.5 panel (Illumina), run on MiSeq (Illumina), and analyzed as previously described.[5] *NF1* mutations were validated by Sanger sequencing (Reference *NF1* gene sequence: NM_001042492.2; Reference neurofibromin protein sequence: NP_001035957.1). Regions with low coverage at massive parallel sequencing analysis were also

double checked by Sanger sequencing on an ABI PRISM 3100 Genetic Analyzer (Applied Biosystems). Only variants with frequencies >20% were considered.

Mutations were considered heterozygous when the frequency was in the 20–60% range; homo/hemizygous when it was >70%. *NF1* biallelic inactivation was defined by the presence of a homo/hemizygous mutation or by two distinct heterozygous *NF1* mutations in the same tumor. Where available, matched normal DNA was analyzed to determine whether the mutation detected in the tumor was constitutional or somatic.

The Human Gene Mutation Database (http://www.hgmd.cf.ac.uk) and ClinVar (https://www.ncbi.nlm.nih.gov/clinvar) were interrogated to search for published associations with the Neurofibromatosis type 1 syndrome of the identified mutations. In addition, Provean (http://provean.jcvi.org), SIFT (http://sift.bii.a-star.edu.sg), PolyPhen2 (genetics.bwh.harvard.edu/pph2), MutationAssessor (http://mutationassessor.org/), and PaPI (http://papi.unipv.it) tools were used to predict the effect of non-synonymous variants. The Human Splicing Finder software (www.umd.be/HSF3) was used to evaluate splice site mutations. The ExPASy ProtParam tool (http://web.expasy.org/protparam/) was implemented to assess the impact of single amino-acid variations on protein half-life.

Statistical Analysis

Fisher's exact test (two-tailed) was used to compare categorical variables.

Results

The results of NFC immunostaining are summarized in Tables 1 and 2. Representative samples are shown in Figure 1. Clear-cut positive internal controls were always present in all analyzed cases.

NFC staining was cytoplasmic and granular in quality in both neoplastic and non-neoplastic/positive control cells. Ganglion cells and nerves, followed by plasma cells and fibroblasts, displayed the strongest reactivity. Endothelial cells showed highly variable staining intensity (from moderate to weak). Regarding the gastric mucosa, NFC reactivity was positive in the glands, usually with moderate intensity; the foveolae were instead negative. NFC stained the intestinal mucosa homogeneously but with variable intensity. NFC reactivity in the smooth muscle cells of the *muscularis propria* was usually weak.

Loss of NFC immunostaining was observed in 26 of the 98 analyzed tumors, specifically in 24/29 (83%) *NF1*-associated and 2/38 (5%) *NF1*-unrelated GISTs ($P = 3e-11$). Among the 24 *NF1*-associated tumors displaying loss of NFC reactivity (20 GISTs and 4 mGISTs), 17 samples showed complete loss (16 GISTs and 1 mGISTs) and 7 partial loss (4 GISTs and 3 mGISTs) (Figures 1a–d). Specifically, NFC deficiency was detected in 11/13 tumors with constitutional pathogenic *NF1* mutations; 10/12 tumors arising in clinically diagnosed Neurofibromatosis type 1 patients; and 3/4 tumors with somatic pathogenic *NF1* mutations.

Of the *NF1*-unrelated tumors, loss of NFC reactivity (complete loss) was observed in only 2/38 GISTs (#30 and #32 in Table 1; Figure 1e). Both these tumors were positive for CD117 and DOG1. One was a low-risk GIST with mixed morphology arising in the small intestine; the other was a localized high-risk GIST with spindle morphology occurring in the stomach. These patients (a 31-year-old woman and a 77-year-old lady), who presented no diagnostic signs of Neurofibromatosis type 1, did not receive any adjuvant therapy and were disease free at the last follow-up (13 and 25 months, respectively). Due to the absence of mutations in *KIT*, *PDGFRA*, RAS (H/K/N), *BRAF*, *SDH*, and *NF1* genes, these two GISTs were classified as 'driver mutation unknown'.

Loss of NFC reactivity correlated with biallelic inactivation of *NF1* ($P = 0.007$), due to either large deletions or truncating mutations.

NF1 gene status was known for three of the five *NF1*-associated tumors retaining NFC reactivity: sample #6 was a GIST with weak NFC staining intensity carrying a homo/hemizygous missense mutation (His553Arg) (Figure 1f). According to the ExPASy ProtParam tool, this variation does not significantly impact on protein turnover. The other two samples, featuring weak (#17) or moderate (#19) NFC reactivity, were both small tumors (size <1.5 cm) that retained a wild-type *NF1* allele besides the one carrying a truncating mutation.

Another GIST (#98) carried the heterozygous *NF1* mutation His1374Tyr. This missense variant was classified by ClinVar to be of uncertain pathogenic significance, which is why this GIST was included in the group of tumors with an unknown driver gene and undetermined *NF1* association. In this case, too, the tumor retained a wild-type allele and maintained NFC reactivity.

The NFC reactivity retained in 36/38 *NF1* wild-type tumors was strong (12 samples) or moderate (15 samples) in most cases (Figures 1g and h). Weak staining was detected in 9 samples that were relatively old (≥4 years), indicating that pre-analytical factors can influence NFC performance, as previously described.[17]

No information on *NF1* gene status was available in 30 samples. This set included 21 *KIT*- and 9 *PDGFRA*-driven GISTs. All these tumors retained NFC reactivity (strong in 17 samples, moderate in 11 and weak in 2).

Discussion

We have recently demonstrated that *NF1* mutations play a prominent role in the pathogenesis of

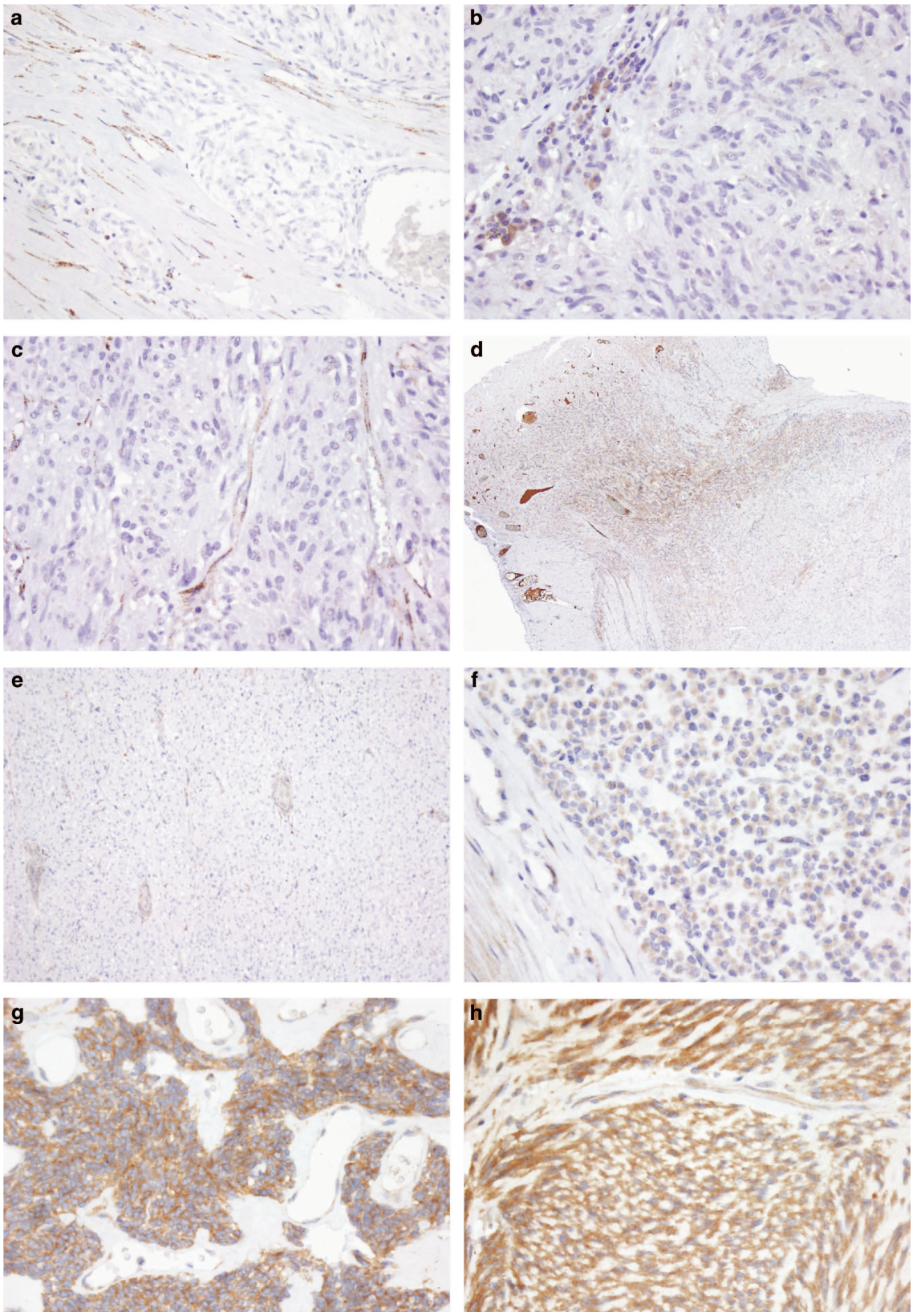
a
b
c
d
e
f
g
h

apparently 'sporadic' GISTs.[5] Specifically, we have reported that about 60% of so-called quadruple-negative GISTs (GISTs lacking *KIT*, *PDGFRA*, *BRAF*, and *SDH* mutations; 10% of all GISTs) carry *NF1* mutations that are constitutional in most cases. Our work has thus demonstrated that a significant fraction of quadruple-negative GISTs arise in the context of unrecognized Neurofibromatosis type 1 syndrome. The identification of *NF1*-driven GISTs has important clinical implications, both in terms of patient and family surveillance, due to their cancer-prone condition; and in terms of treatment strategies, considering the poor sensitivity to imatinib of *NF1*-related tumors.[9,10] In this regard, the promising results recently obtained with MEK inhibitors in the treatment of unresectable *NF1*-associated plexiform neurofibromas[22] open novel therapeutic opportunities for *NF1*-associated GISTs.

Unfortunately, the detection of *NF1* mutations, be they constitutional or somatic, is challenging due to the large size of the gene and the numerous mechanisms of inactivation.[1,11]

On these grounds, we sought to explore the efficacy of an immunohistochemical approach to identifying *NF1*-mutated GISTs. To this end, we collected a series of *NF1*-associated GISTs (including both GISTs and mGISTs arising in the context of clinically diagnosed Neurofibromatosis type 1 and *NF1*-mutated tumors submitted to the pathologist as 'sporadic') and *NF1*-unrelated tumors, and interrogated the cohort with the NFC antibody, a custom-raised antibody directed against the C terminus of neurofibromin. This antibody has previously been shown to differentiate malignant peripheral nerve sheath tumors, typically *NF1*-associated neoplasms, from other *NF1*-unrelated mimics.[17,18]

The results of our analysis can be summarized as follows: the vast majority (83%) of the tested *NF1*-associated GISTs/mGISTs displayed complete or partial loss of NFC reactivity. Staining successfully identified 12 of the 13 tumors carrying homo/hemizygous *NF1* gene inactivation due to large deletions or truncating mutations, irrespective of whether the alteration was of somatic or constitutional origin. There was one exception: a case (#6) bearing a homo/hemizygous N-terminal His553Arg pathogenic missense mutation. Said mutation was predicted by ProtParam to not significantly impact on neurofibromin turnover. This finding corroborates previous observations that NFC reactivity is likely preserved by stable neurofibromin variants.[17]

The inability to reveal missense mutations is an intrinsic drawback of antibodies designed to distinguish full length *vs* truncated proteins (eg, antibodies against X-linked alpha-thalassemia/mental retardation syndrome, ATRX).[23,24] However, $<10\%$ of *NF1* pathogenic mutations reported in the ClinVar database are missense mutations.[25]

NFC staining was retained not only in the two GISTs carrying non-pathogenic missense mutations (#38 and #39), but also in the two tumors (#17, #19) that retained a wild-type *NF1* allele, while carrying truncating mutations. This suggests that the amount of neurofibromin encoded by a single wild-type allele is sufficient to yield NFC reactivity.

In *NF1*-unrelated GISTs, NFC reactivity was retained in all but two tumors (95%). Notably, these two tumors were also negative for canonical *KIT*, *PDGFRA*, *BRAF*, and *SDHx* mutations. Despite the lack of *NF1* mutations, their negativity for NFC may underlie the existence of alternative mechanisms of *NF1* inactivation. For instance, it has been demonstrated that enhanced proteasomal destruction accounts for *NF1* loss in glioblastomas.[26,27] Thus, *NF1* could play an even greater role in the pathogenesis of GISTs than inferred by gene mutation analysis.[5]

As regards the pattern of staining, NFC loss was complete in most cases (17 cases). Partial loss was observed in seven *NF1*-associated tumors in which NFC reactivity was retained in focal areas. Partial loss has previously been reported to occur in malignant peripheral nerve sheath tumors[17] and could be ascribed to tumor heterogeneity. Intriguingly, partial loss was more common among micro-GISTs—considered to be *bona fide* GIST precursors[6,28] - than among overt GISTs. This suggests that full inactivation of *NF1* contributes to micro-GIST progression to overt GIST.

From a technical standpoint, although our series consisted of archival material, a clear-cut diffuse staining pattern of remarkable intensity was observed in the majority of NFC-positive cases, while weak reactivity was essentially observed in older samples (≥ 4 years).

As previously discussed,[17] similarly to other tumor suppressors, the interpretation of neurofibromin staining also relies on robust internal positive controls. Loss of staining for INI1, ATRX, SDHB, and SDHA, which are ubiquitously expressed, is not usually an issue as internal positive controls are easy to find.[12,13,23,24,29] Neurofibromin has been reported

Figure 1 (**a**) Case #9: *NF1*-associated GIST showing complete NFC loss. Fibroblasts were used as internal positive controls (magnification ×20). (**b**) Case #1: *NF1*-associated GIST showing complete NFC loss. Inflammatory cells served as internal positive controls (magnification ×40). (**c**) Case # 22: *NF1*-associated GIST showing complete NFC loss. Weak reactivity is present in the endothelium (positive control) (magnification ×40). (**d**) Case #28: *NF1*-associated microGIST showing partial loss of NFC (magnification ×10). (**e**) Case #30: complete NFC loss in an *NF1* wild-type GIST. This case was considered as 'driver gene unknown', being wild-type not only for *NF1* but also for *KIT, PDGFRA, RAS (H/K/N), BRAF*, and *SDHx*. Normal vessels served as internal positive controls (magnification ×20). (**f**) Case #6: *NF1*-associated GIST showing weak NFC reactivity. This case carried a homo/hemizygous missense mutation at the N terminus (His553Arg) (magnification ×40). (**g**, **h**) Two *NF1* 'wild-type'/*KIT*-driven GISTs (#46, #57) showing strong NFC reactivity (magnification ×40).

to be expressed at high levels in all fetal rat tissues, but is essentially confined to the central and peripheral nervous systems postnatally.[30,31] Accordingly, we observed strong NFC reactivity in ganglion cells and in the myenteric plexus; fibroblasts and inflammatory cells could also be positive, thus serving as additional internal controls. By contrast, the endothelium tended to display weak NFC staining, which could be overlooked at low power.

Overall our results provide evidence that NFC staining is a simple, rapid, and cost effective strategy for identifying *NF1*-inactivated GISTs, thus constituting a surrogate for molecular analysis. In addition, this study adds further support to the relevance of *NF1* in the inception and progression of GISTs.

Acknowledgments

This work was supported by a CRO Intramural Grant and by the Italian Ministry of Health (RF-2011-02348953). We are grateful to M. Mafra, *P.* Iuzzolino, A. Rizzo for their support and suggestions.

Disclosure/conflict of interest

AG and APDT have received honoraria and participated in Compensated Advisory Boards for Novartis and Pfizer. AG has also participated in Compensated Advisory Boards for Bayer. All remaining authors have declared no conflict of interest.

References

1 Ratner N, Miller SJ. A RASopathy gene commonly mutated in cancer: the neurofibromatosis type 1 tumour suppressor. Nat Rev Cancer 2015;15:290–301.
2 Krauthammer M, Kong Y, Bacchiocchi A, *et al.* Exome sequencing identifies recurrent mutations in NF1 and RASopathy genes in sun-exposed melanomas. Nat Genet 2015;47:996–1002.
3 Hechtman JF, Zehir A, Mitchell T, *et al.* Novel oncogene and tumor suppressor mutations in KIT and PDGFRA wild type gastrointestinal stromal tumors revealed by next generation sequencing. Genes Chromosomes Cancer 2015;54:177–184.
4 Boikos SA, Pappo AS, Killian JK, *et al.* Molecular subtypes of KIT/PDGFRA wild-type gastrointestinal stromal tumors: a report from the National Institutes of Health Gastrointestinal Stromal Tumor Clinic. JAMA Oncol 2016;2:922–928.
5 Gasparotto D, Rossi S, Polano M, *et al.* Quadruple-negative GIST is a sentinel for unrecognized neurofibromatosis type 1 syndrome. Clin Cancer Res 2017;23:273–282.
6 Corless CL. Gastrointestinal stromal tumors: what do we know now? Mod Pathol 2014;27(Suppl 1):S1–16.
7 Doyle LA, Hornick JL. Gastrointestinal stromal tumours: from KIT to succinate dehydrogenase. Histopathology 2014;64:53–67.
8 Shi E, Chmielecki J, Tang CM, *et al.* FGFR1 and NTRK3 actionable alterations in "Wild-Type" gastrointestinal stromal tumors. J Transl Med 2016;14:339.
9 Miettinen M, Fetsch JF, Sobin LH, *et al.* Gastrointestinal stromal tumors in patients with neurofibromatosis 1: a clinicopathologic and molecular genetic study of 45 cases. Am J Surg Pathol 2006;30:90–96.
10 Mussi C, Schildhaus HU, Gronchi A, *et al.* Therapeutic consequences from molecular biology for gastrointestinal stromal tumor patients affected by neurofibromatosis type 1. Clin Cancer Res 2008;14:4550–4555.
11 Paschou M, Doxakis E. Neurofibromin 1 is a miRNA target in neurons. PLoS ONE 2012;7:e46773.
12 Chan JK, Ip YT, Cheuk W. The utility of immunohistochemistry for providing genetic information on tumors. Int J Surg Pathol 2013;21:455–475.
13 Doyle LA, Nelson D, Heinrich MC, *et al.* Loss of succinate dehydrogenase subunit B (SDHB) expression is limited to a distinctive subset of gastric wild-type gastrointestinal stromal tumours: a comprehensive genotype-phenotype correlation study. Histopathology 2012;61:801–809.
14 Patil DT, Ma S, Konishi M, *et al.* Utility of BRAF V600E mutation-specific immunohistochemistry in detecting BRAF V600E-mutated gastrointestinal stromal tumors. Am J Clin Pathol 2015;144:782–789.
15 Ritterhouse LL, Barletta JA. BRAF V600E mutation-specific antibody: a review. Semin Diagn Pathol 2015;32:400–408.
16 Rossi S, Sbaraglia M, Dell'Orto MC, *et al.* Concomitant KIT/BRAF and PDGFRA/BRAF mutations are rare events in gastrointestinal stromal tumors. Oncotarget 2016;7:30109–30118.
17 Reuss DE, Habel A, Hagenlocher C, *et al.* Neurofibromin specific antibody differentiates malignant peripheral nerve sheath tumors (MPNST) from other spindle cell neoplasms. Acta Neuropathol 2014;127:565–572.
18 Röhrich M, Koelsche C, Schrimpf D, *et al.* Methylation-based classification of benign and malignant peripheral nerve sheath tumors. Acta Neuropathol 2016;131:877–887.
19 Brenca M, Rossi S, Polano M, *et al.* Transcriptome sequencing identifies ETV6-NTRK3 as a gene fusion involved in GIST. J Pathol 2016;238:543–549.
20 Andersson J, Sihto H, Meis-Kindblom JM, *et al.* NF1-associated gastrointestinal stromal tumors have unique clinical, phenotypic, and genotypic characteristics. Am J Surg Pathol 2005;29:1170–1176.
21 Agaimy A, Vassos N, Croner RS. Gastrointestinal manifestations of neurofibromatosis type 1 (Recklinghausen's disease): clinicopathological spectrum with pathogenetic considerations. Int J Clin Exp Pathol 2012;5:852–862.
22 Dombi E, Baldwin A, Marcus LJ, *et al.* Activity of selumetinib in neurofibromatosis type 1-related plexiform neurofibromas. N Engl J Med 2016;375:2550–2560.
23 Liu XY, Gerges N, Korshunov A, *et al.* Frequent ATRX mutations and loss of expression in adult diffuse astrocytic tumors carrying IDH1/IDH2 and TP53 mutations. Acta Neuropathol 2012;124:615–625.
24 Wiestler B, Capper D, Holland-Letz T, *et al.* ATRX loss refines the classification of anaplastic gliomas and identifies a subgroup of IDH mutant astrocytic tumors with better prognosis. Acta Neuropathol 2013;126:443–451.

25 Laycock-van Spyk S, Thomas N, Cooper DN, *et al.* Neurofibromatosis type 1-associated tumours: their somatic mutational spectrum and pathogenesis. Hum Genomics 2011;5:623–690.
26 McGillicuddy LT, Fromm JA, Hollstein PE, *et al.* Proteasomal and genetic inactivation of the NF1 tumor suppressor in gliomagenesis. Cancer Cell 2009;16: 44–54.
27 Hollstein PE, Cichowski K. Identifying the ubiquitin ligase complex that regulates the NF1 tumor suppressor and Ras. Cancer Discov 2013;3:880–893.
28 Rossi S, Gasparotto D, Toffolatti L, *et al.* Molecular and clinicopathologic characterization of gastrointestinal stromal tumors (GISTs) of small size. Am J Surg Pathol 2010;34:1480–1491.
29 Wagner AJ, Remillard SP, Zhang YX, *et al.* Loss of expression of SDHA predicts SDHA mutations in gastrointestinal stromal tumors. Mod Pathol 2013;26:289–294.
30 Daston MM, Ratner N. Neurofibromin, a predominantly neuronal GTPase activating protein in the adult, is ubiquitously expressed during development. Dev Dyn 1992;195:216–226.
31 Daston MM, Scrable H, Nordlund M, *et al.* The protein product of the neurofibromatosis type 1 gene is expressed at highest abundance in neurons, Schwann cells, and oligodendrocytes. Neuron 1992;8:415–428.

8. Acknowledgments

This study was supported by Associazione Italiana Ricerca sul Cancro (AIRC), the Italian Ministry of Health and a CRO 5 × 1000 Intramural Grant.

This work was possible thank to the valuable contribution of: Dr. Prof. Angelo P. Dei Tos (University of Padova, Italy); Dr. Silvana Pilotti, Dr. Alessandro Gronchi and Dr Elena Tamborini (IRCCS Istituto Nazionale Tumori, Milan, Italy); Dr. Sabrina Rossi (Pediatric Hospital Bambino Gesù, Rome, Italy); Dr. Marta Sbaraglia, Dr. Matilde Cacciatore, Dr. Marco Massani, Dr. Stefano Lamon, Dr. Elisabetta Frate (Treviso General Hospital, Italy); Dr. Raffaella Bracci and Alessandra Mandolesi (Ospedali Riuniti, Ancona, Italy); Dr. David E. Reuss and DrAndreas von Deimling (University of Heidelberg, Heidelberg, Germany); Dr Jerin Agai (Vipiteno General Hospital, Vipiteno Sterzing, Italy); Dr. Franco Stanzial and Dr. Guido Mazzoleni (Bolzano General Hospital, Bolzano, Italy).

I would like to thank my supervisor Dr. Roberta Maestro for her support and scientific advice and all members of my research group Dr. Daniela Gasparotto, Dr. Maurizio Polano, Dr. Erica Lorenzetto, Dr. Federica Nardi and Dr. Davide Baldazzi for their experimental contribution.